AFIT/GGC/EE/77-5
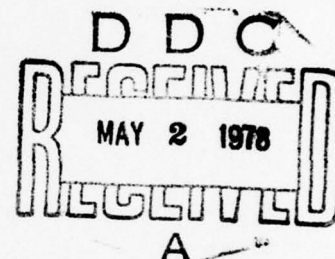
AFIT/GGC/EE/77-5

AD No.
ODC FILE COPY

AN INVESTIGATION OF THE TRACKING PERFORMANCE

OF THE FIRE FLY MANUAL DIRECTOR GUNSIGHT

FOR AIR-TO-AIR GUNNERY

9 Master's THESIS

AFIT/GGC/EE/77-5   David L. Frostman
                         Capt   USAF

6 AN INVESTIGATION OF THE TRACKING PERFORMANCE
OF THE FIRE FLY MANUAL DIRECTOR GUNSIGHT
FOR AIR-TO-AIR GUNNERY,

9 Master's THESIS,

Presented to the Faculty of the School of Engineering

of the Air Force Institute of Technology

Air University

in Partial Fulfillment of the

Requirements for the Degree of

Master of Science in Electrical Engineering

12 178 p.

by

10 David L. Frostman, B.S.E.E., M.S.B.A.

Capt   USAF

Graduate Guidance and Control

11 December 1977

Preface

This thesis effort was undertaken with two specific objectives in mind. The first objective was to satisfy the requirements of the AFIT program. The second was to utilize the thesis as a learning experience to tie together some of the concepts which were presented in the course work and to develop a systematic approach to solving a realistic problem. This thesis report represents the fulfillment of both of these objectives.

Contents

Contents

List of Figures

List of Figures (cont'd)

List of Figures (cont'd)

List of Tables

List of Tables (cont'd)

List of Symbols

$\bar{A}$	Attacker acceleration vector
$\bar{A}_b$	Attacker specific force vector
A_{bu}, A_{bv}, A_{bw}	Components of the attacker specific force vector expressed in terms of body-fixed coordinates
A_o	Angle-off of target heading with respect to the attacker
$\bar{A}_r$	Relative acceleration vector between target and attacker
A_{ru}, A_{rv}, A_{rw}	Components of relative acceleration vector expressed in terms of body-fixed coordinates
$\bar{A}_t$	Target acceleration vector
b	Reference wingspan
$(BL)_T$	Tank buttock line; the distance, measured in the $\bar{u}\bar{w}$ plane, between the aircraft water line and the centerline of the external fuel tanks
c	Mean aerodynamic chord
C_1, C_2	Constants used to account for second order effects in the bullet time-of-flight calculation
D_f	Magnitude of the future range vector
$DZ_{\dot{e}_{LV}}$	Longitudinal pilot model deadzone on elevation tracking error rate
$DZ_{\dot{e}_{LW}}$	Lateral pilot model deadzone on traverse tracking error rate
DZ_φ	Lateral pilot model deadzone on differential bank angle
E_{LG}	Angle between the aircraft $\bar{u}$ axis and the axis of the gun
e_{LV}	Elevation tracking error, in radians

e_{LW} Traverse tracking error, in radians

F_{LAT} Lateral pilot model stick force

F_{LON} Longitudinal pilot model stick force

F_{RUD} Lateral pilot model rudder pedal force

F_x, F_y, F_z Components of aerodynamic force applied along $\bar{u}$, $\bar{v}$, and $\bar{w}$ body axes

F_{x_T}, F_{y_T}, F_{z_T} Thrust force components applied along body axes

$\bar{g}$ Gravity vector

g_x, g_y, g_z Components of the gravity vector along body axes

I_x, I_y, I_z Moments of inertia along body axes

I_{xz} Product of inertia in the $\bar{u}\bar{w}$ plane

K_{AIL} Lateral pilot model transmission gain

K_{CO} Crossover gain; the gain at which the complex poles of the closed loop longitudinal system due to the aircraft short period dynamics pass from the left half s-plane to the right half s-plane

K_L Longitudinal pilot model gain parameter which determines the amplitude of the low frequency component in the elevation tracking error

k_o Ballistic coefficient

K_P F-106 flight control system feedback gain on roll rate

K_{PE} Longitudinal pilot model transmission gain

K_q F-106 flight control system feedback gain on pitch rate

K_R — Longitudinal pilot model gain parameter which affects the amplitude of the high frequency component of elevation tracking error

K_{RTR} — Lateral pilot model gain parameter which affects amplitude and frequency of the traverse error

K_{RUD} — Lateral pilot model rudder pedal gain

K_φ — Lateral pilot model differential bank angle feedback gain

K_{δ_A} — Differential elevon-to-rudder crossfeed gain

L — Total rolling moment

M — Total pitching moment

m — Aircraft mass

N — Total yawing moment

(NP) — Aircraft neutral point

P — Roll angular velocity

Q, q — Pitch angular velocity

$\bar{q}$ — Dynamic pressure

R — Range magnitude; yaw angular velocity

$\bar{R}_{ba}$ — Range vector from bullet release point to bullet impact point

$\bar{R}_r$ — Present required range vector to obtain a hit

R_{ru}, R_{rv}, R_{rw} — Components of required range vector expressed in terms of body-fixed axes

R_{tv}, R_{tw} — Components of present range vector in body axes

S — Wing reference area

T — Thrust magnitude

List of Symbols (cont'd)

T_f — Bullet time-of-flight

$\bar{u}, \bar{v}, \bar{w}$ — Body-fixed coordinate system; $\bar{u}$ out the nose of the aircraft, $\bar{v}$ out the right wing, $\bar{w}$ nominally down

U — $\bar{u}$ body axis component of translational velocity

V — $\bar{v}$ body axis component of translational velocity

$\bar{V}_a$ — Attacker velocity vector

$\bar{V}_m$ — Bullet muzzle velocity vector

$\bar{V}_r$ — Relative velocity vector between attacker and target

V_{ru}, V_{rv}, V_{rw} — Relative velocity components in body axes

$\bar{V}_t$ — Target velocity vector

$\bar{V}_T$ — Total aircraft velocity vector

V_T — Magnitude of total aircraft velocity vector

W — $\bar{w}$ body axis component of translational velocity

X — Total external force applied along the $\bar{u}$ body axis

X_{cg} — Distance, measured in the $\bar{u}$ direction, from the wing leading edge at the wing root, to the aircraft center of gravity

x_o — Distance, measured in the $\bar{u}$ direction, between the aircraft center of gravity and the origin of the thrust vector

Y — Total external force applied along the $\bar{v}$ body axis

$(Y_{ref} - Y_{cg})$ — cg moment arm in the $\bar{v}$ direction

Z — Total external force applied along the $\bar{w}$ body axis

z_o — Distance, measured in the $\bar{w}$ direction, between the aircraft center of gravity and the origin of the thrust vector

$(Z_{ref} - Z_{cg})$ — cg moment arm in the $\bar{w}$ direction

α — Aerodynamic angle-of-attack

β — Sideslip angle

δ_A — Aileron deflection

δ_E — Elevator deflection

δ_R — Rudder deflection

ϵ_T — Angle between the $\bar{u}$ body axis and the direction of the thrust vector

ζ_n — Damping parameter in low pass filter of longitudinal pilot model

Θ — Pitch angle

λ — Gunnery lead angle

ρ/ρ_o — Relative air density ratio

τ_E, τ_T — Time constants which represent pilot's response delay

τ_q — Pitch damper washout circuit time constant

Φ, φ — Roll angle

Ψ — Yaw angle

$\bar{\omega}$ — Total aircraft angular velocity

ω_n — Natural frequency parameter of low pass filter in longitudinal pilot model

ω_t — Target turn rate

C_D Total drag coefficient

C_L Total lift coefficient

C_{L_o} Lift coefficient at $\alpha = 0$

C_{L_α} Lift curve slope

$C_{L_{o_T}}$ Lift coefficient at $\alpha = 0$ due to tanks

$C_{L_{\alpha_T}}$ Lift curve slope due to tanks

$C_{L_{\delta_E}}$ Change in lift coefficient due to elevator deflection

C_{ℓ_β} Change in rolling moment coefficient for a change in sideslip

C_{ℓ_P} Change in rolling moment coefficient due to roll rate

C_{ℓ_R} Change in rolling moment coefficient due to yaw rate

$C_{\ell_{\delta_R}}$ Change in rolling moment coefficient due to rudder deflection

$C_{\ell_{\delta_A}}$ Change in rolling moment coefficient due to aileron deflection

$C_{\ell_{\beta_\alpha}}$ Change in C_{ℓ_β} for a change in α

$C_{\ell_{\beta_{\alpha^2}}}$ Second order effect of α on C_{ℓ_β}

$C_{\ell_{\beta|\beta|}}$ Change in C_{ℓ_β} for a change in $|\beta|$

$C_{\ell_{\beta_T}}$ Change in C_{ℓ_β} due to tanks

$C_{\ell_{P_\alpha}}$ — Change in C_{ℓ_P} for a change in α

$C_{\ell_{P_\alpha}2}$ — Second order effect of α on C_{ℓ_P}

$C_{\ell_{R_\alpha}}$ — Change in C_{ℓ_R} for a change in α

C_{m_o} — Pitching moment coefficient at $\alpha=0$

C_{m_q} — Change in pitching moment coefficient for a change in q

$C_{m_{\delta_E}}$ — Change in pitching moment coefficient for a change in elevator deflection

$C_{m_{o_T}}$ — Pitching moment coefficient at $\alpha=0$ due to tanks

$C_{m_{\alpha_T}}$ — Change in C_{m_α} due to tanks

C_{n_β} — Change in yawing moment coefficient for a change in sideslip

C_{n_P} — Change in yawing moment coefficient for a change in roll rate

C_{n_R} — Change in yawing moment coefficient for a change in yaw rate

$C_{n_{\delta_R}}$ — Change in yawing moment coefficient for a change in rudder deflection

$C_{n_{\delta_A}}$ — Change in yawing moment coefficient for a change in aileron deflection

$C_{n_{\beta_\alpha}}$ — Change in C_{n_β} for a change in α

$C_{n_{\beta_\alpha}2}$ — Second order effect of α on C_{n_β}

$C_{n_{\beta}|\beta|}$ Change in $C_{n_{\beta}}$ for a change in $|\beta|$

$\Delta C_{n_{\beta}}$ Incremental change in $C_{n_{\beta}}$

$C_{n_{\beta_T}}$ Change in $C_{n_{\beta}}$ due to tanks

$C_{n_{\delta_A}\alpha}$ Change in $C_{n_{\delta_A}}$ for a change in α

$C_{n_{\delta_A}\delta_E}$ Change in $C_{n_{\delta_A}}$ for a change in δ_E

$C_{y_{\beta}}$ Change in side force coefficient for a change in sideslip angle

C_{y_P} Change in side force coefficient for a change in roll rate

C_{y_R} Change in side force coefficient for a change in yaw rate

$C_{y_{\delta_R}}$ Change in side force coefficient for a change in rudder deflection

$C_{y_{\delta_A}}$ Change in side force coefficient for a change in aileron deflection

$C_{y_{\beta_\alpha}}$ Change in $C_{y_{\beta}}$ for a change in α

$C_{y_{\beta_\alpha}2}$ Second order effect of α on $C_{y_{\beta}}$

$C_{y_{\beta}|\beta|}$ Change in $C_{y_{\beta}}$ for a change in $|\beta|$

$C_{y_{\alpha_T}}$ Change in $C_{y_{\alpha}}$ due to tanks

$C_{y_{\beta_T}}$ Change in $C_{y_{\beta}}$ due to tanks

Abstract

The tracking performance of the Fire Fly manual director gunsight is evaluated during the terminal phase of air-to-air gunnery using the F-106 aircraft as the test bed. A digital simulation of the closed loop tracking task is performed using the EASY Dynamic Analysis programs developed by Boeing Computer Services, Inc. The multi-axis analytical pilot model, developed for the Terminal Aerial Weapon Delivery Simulation (TAWDS) program by McDonnell Aircraft Company, is adapted for use in the F-106/Fire Fly gunsight simulation. A set of nominal pilot model parameter values, determined by root locus analysis, is used in simulating the tracking performance of the Fire Fly gunsight against targets in constant altitude, constant airspeed, constant rate turns at bank angles of 30, 60, and 70 degrees. The tracking error responses are found to have characteristics similar to those observed in the tracking responses obtained from man-in-the-loop simulation studies conducted by McDonnell Aircraft Company. The dependence of the tracking error responses on the pilot model parameter values is demonstrated by simulation runs in which several pilot model parameter values are varied.

AN INVESTIGATION OF THE TRACKING PERFORMANCE

OF THE FIRE FLY MANUAL DIRECTOR GUNSIGHT

FOR AIR-TO-AIR GUNNERY

I. Introduction

Background

Since World War I, the air-to-air gun has been one of
the fighter pilot's primary weapons in aerial combat. Present
guns are capable of unleashing a lethal amount of firepower
somewhere out in front of the aircraft. The question of how
best to control and use that firepower with some type of fire
control system is currently the subject of considerable
research and development effort. The development of gunfire
technology was essentially dormant from 1954-1964 as a result
of the emphasis on the development of air-to-air missile
technology. However, recent experience in fighter/fighter
engagements worldwide indicates that where sophisticated
air-to-air missile systems prevent disengagement from an
encounter, the outcome will probably be decided by a gunnery
duel (Ref 1: Chap. II, p. 1).

Air-to-air combat between present day jet aircraft may
be initiated at any altitude between sea level and 50,000 feet,
and at airspeeds between 150 knots and Mach 2+ (Ref 2: 5).
Aerial combat may also occur between aircraft of diverse

capabilities and multi-plane engagements are common. These factors further complicate the already difficult problem of effective fire control.

The role of the pilot in the operation of present fire control systems is crucial. In most systems, the pilot is responsible, at least in part, for precision tracking and selection of the appropriate weapon (missile, rocket, gun) to be used. In addition, the pilot must decide when to engage or disengage an enemy. He must monitor the performance of his own aircraft and he must continuously be aware of the threat environment. These responsibilities produce a critically high pilot workload.

This thesis is concerned with the evaluation of the manual director gunsight portion of an integrated automatic flight control and fire control system which is specifically designed to alleviate pilot workload in the air-to-air combat environment. The particular system, called Fire Fly, was developed by the Aircraft Equipment Division of General Electric Company. The Fire Fly system is being tested in a joint program conducted by the Air Force Flight Dynamics Laboratory and the Air Force Avionics Laboratory, using the F-106 as the test bed aircraft. The overall goal of the Fire Fly system is to provide integrated automatic flight control and fire control by allowing the pilot to select from a range of control options. By selecting the option he desires, the pilot can allow the Fire Fly fire control system to automatically control the aircraft flight control system

for precision tracking during aerial combat. The available range of control options extends from full manual control by the pilot to full automatic control by the Fire Fly system. The primary objectives of the Fire Fly system are to provide improved precision tracking and to reduce pilot workload during aerial combat.

To provide the reader with some basic insights into the fire control problem and its solution, the following paragraphs briefly discuss the basic fire control problem and the two general types of gunsight system which can be used to aid the pilot in the precision tracking task.

Stated concisely, the fire control problem for air-to-air gunnery is: fire a bullet from an attacking aircraft at a target aircraft so as to score a hit on that target. To score a hit, the solution to the fire control problem must be obtained and displayed to the pilot in a meaningful and easily used form. The manner in which the solution is obtained is a function of the type of gunsight system used (Ref 3: Chap. I, p. 1).

In the highly dynamic environment of air-to-air combat, the attacker can seldom point his gun directly at the target to achieve a hit. To obtain a hit, the attacker must displace the gun direction from the target by a lead angle. This lead angle is a function of the range between the attacker and the target, the angular rate of the line-of-sight from the attacker to the target, target motion, and bullet ballistics. The purpose of the gunsight is to provide a measure of aiming

error so appropriate firing or corrective control can be effected (Ref 4: 1).

All air-to-air gunsight systems direct the attacker gunfire by directing the attacking pilot to fly his aircraft, and hence the gun, to a particular position with respect to the target. This task is accomplished by the gunsight system, which displays a dot of light or pipper on a Head Up Display (HUD) in front of the pilot. The pilot then superimposes the pipper on the target by maneuvering his aircraft (Ref 3: Chap. VI, p. 1).

There are two basic classes of gunsight system for air-to-air gunnery: the disturbed reticle gunsight and the director gunsight. The two classes differ in the manner in which the angular rate of the line-of-sight from the attacker to the target is measured. In the disturbed reticle system, the lead angle is computed using own aircraft angular rate as the primary input. If the pilot is tracking the target so that the pipper remains on the target, then own aircraft body rate is equal to the line-of-sight rate. Thus, the pilot must keep the pipper on the target, which can be dynamically difficult because the effect of feeding back own aircraft angle rates to the sight is destabilizing (Ref 5: 13-14). The commonly used Lead Computing Optical Sight (LCOS) is an example of a disturbed reticle sight.

The director gunsight uses line-of-sight rate as its major input. An angle tracking radar or an electro-optical tracker is used, in conjunction with a Kalman filter, to

estimate the angular rate of the line-of-sight and the target acceleration based on past history of target trajectory (Ref 2: 8-9). Although the director system is more complex and expensive than the disturbed reticle system, it offers distinct advantages for air-to-air combat. The director gunsight provides a direct measure of gun error for the pilot to null. Also, since the lead angle computation does not depend on own aircraft motion, except for disturbance errors, the pilot's control task is not complicated by sight dynamics. In addition, if angular rate measurement noise is sufficiently attenuated by filtering, the director system provides improved steering stability in the tracking task (Ref 5: 19).

The Fire Fly system employs a director gunsight system which utilizes an Ascot electro-optical tracker and a Kalman filter algorithm for estimation of the target state.

Purpose

The purpose of this thesis effort was to examine the tracking performance of the Fire Fly manual director gunsight during the terminal phase of air-to-air combat. The evaluation was conducted using a digital computer simulation. The simulation introduced two secondary, but important, objectives. First, through the development of the digital computer model and establishment of appropriate simulation techniques, the author established the usefulness of the ECS Transient Analysis Integrated Computer Program (EASY), which was developed by Boeing Computer Services, Inc., for

analyzing dynamic, nonlinear weapon systems. Second, the author adapted the analytic multi-axis pilot model, which was developed in the Terminal Aerial Weapon Delivery Simulation (TAWDS) program, for use in the F-106/Fire Fly gunsight simulation.

Scope

Although the Fire Fly system is designed for use in air-to-air gunnery, air-to-ground gunnery, and dive bombing, this thesis was limited to an investigation of the air-to-air gunnery mission. Specifically, the Fire Fly gunsight system was evaluated only in the manual mode. That is, the tracking errors were presented to the pilot model, which, in turn, commanded the aircraft flight control system. The evaluation assumed continuous lock-on of the tracker and perfect estimation of the target state. Initial conditions were specified to put the attacker at an altitude of 10,000 feet and a speed of Mach .8. Target maneuvers consisted of constant altitude, constant airspeed, constant rate turns. The initial position of the attacker with respect to the target was specified so as to put the attacker near a gun solution. The attacker was assumed to have sufficient available thrust to maintain airspeed throughout the tracking maneuver.

The digital computer model of the F-106 aircraft and applicable aerodynamic data were provided by the Air Force Flight Dynamics Laboratory. The digital computer pilot model was adapted from the pilot model used in the Terminal Aerial

6

Weapon Delivery Simulation (TAWDS) programs (Ref 6: 65-119).

Overview

In the next chapter the Fire Fly system is discussed. The performance objectives of the Fire Fly system are presented from the standpoint of the integrated flight control/ fire control philosophy. The weapon delivery and gunnery equations are derived, and expressions are developed for elevation and traverse tracking errors which are to be displayed to the pilot. In addition, a brief discussion of the Kalman filter is provided from the viewpoint of the information that the Kalman filter provides to the gunsight.

Chapter Three discusses the F-106 aircraft and presents the six degree of freedom equations of motion which describe the aircraft. In addition, the longitudinal and lateral-directional flight control systems are presented and discussed. In Chapter Four, the pilot model is discussed. The generic model, which was developed for the F-4 aircraft in the TAWDS program, is presented, and the components of the model are discussed. The specific model used for the F-106 is presented, and justification for the particular choice of parameter values is given.

Chapter Five presents the results of the digital computer simulation. The tracking performance of the closed loop system is evaluated against targets in straight and level flight, and in constant altitude, constant airspeed, constant rate turns at bank angles of 30, 60, and 70 degrees. Time history

plots of elevation and traverse tracking errors are presented.
Plots of corresponding longitudinal and lateral pilot stick
forces are also presented. The changes in tracking performance
which result from changing the nominal pilot model parameter
values are also discussed. Chapter Six concludes that the
Fire Fly manual director gunsight system is capable of
tracking the targets simulated and that the EASY computer
program is useful for modeling and analyzing dynamic,
closed loop weapon systems. In addition, the TAWDS pilot
model can be adapted for use in the EASY computer simulation
of the F-106/Fire Fly gunsight system. Evaluation of the
Fire Fly gunsight tracking performance against dynamically
maneuvering targets is recommended as is validation of the
digital pilot model by comparison with F-106/Fire Fly
man-in-the-loop simulation information.

Appendix A presents a listing of the EASY computer model
used in the simulation. The flow of the model is discussed
as are specific modeling and simulation techniques. Appendix
B contains the specific aerodynamic data used in the simulation.

II. The Fire Fly System

General

The general Fire Fly system is discussed in this chapter to give the reader an insight into the type of fire control system which is being considered for implementation in future aircraft weapon systems. The Fire Fly system incorporates the concept of integrated flight control/fire control by providing automatic aircraft control to aid the pilot in the weapon delivery task. The system was designed to be used for air-to-air gunnery, air-to-ground gunnery, and conventional dive bombing. The pilot has the capability to select a variable amount of automatic control authority. In the manual mode, the pilot performs all aircraft control functions. By appropriately selecting authority limits for the Fire Fly system, the pilot relinquishes a specified degree of responsibility for precision tracking control to the automatic system. Within the assigned authority limits, the Fire Fly computer provides appropriate tracking control commands to the aircraft control augmentation system.

A general block diagram of the Fire Fly system is shown in Figure 1. The tracking system provides target information to the Fire Fly computer. The computer uses this information to estimate the target state. Aircraft sensors provide information about own aircraft state which the computer compares to the target state estimate to generate the target relative state. The target relative state information is used in the

9
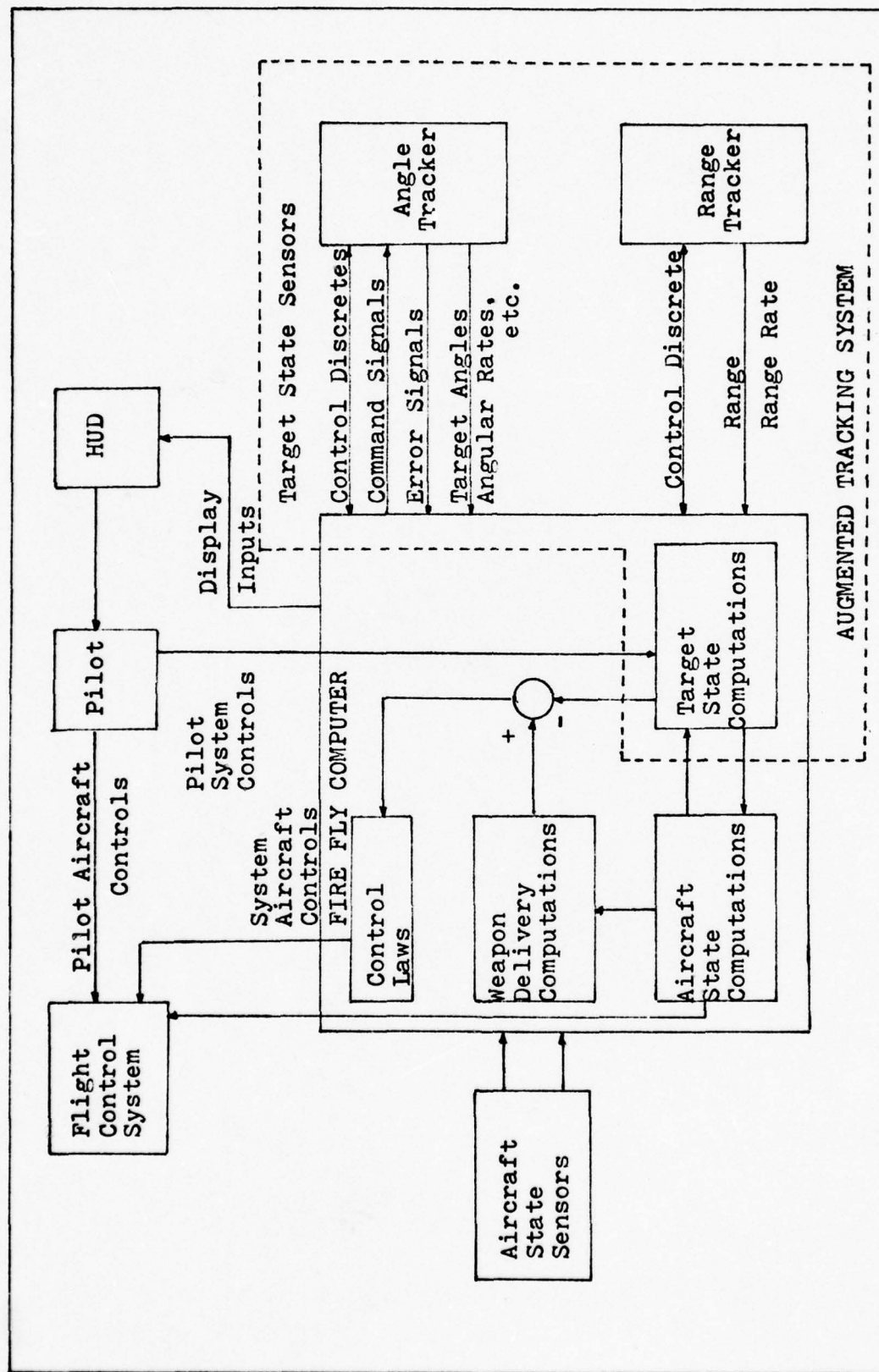
Figure 1. Fire Fly System Block Diagram (Adapted from Ref 1; Chap. III, p. 35)

weapon delivery calculations to compute the correct gun solution. The correct angles are then compared to the actual gun position relative to the target to generate error signals. These error signals are displayed to the pilot on a HUD (Ref 1: Chap. III, p. 34). In the manual mode of operation, the pilot attempts to null the errors by maneuvering the aircraft. When the Fire Fly system is given automatic control authority, the error signals are also fed to the Fire Fly control laws which generate commands to drive the control augmentation system. The Fire Fly control law commands replace pilot tracking control commands up to the authority limits selected by the pilot. Figure 2 depicts the flow of information in the Fire Fly computer.

Since the investigation reported herein concerns only the manual mode of operation, the pilot must maneuver the aircraft to null the gunnery errors. Furthermore, since continuous tracker lock-on and perfect estimation of the target state and own aircraft state are assumed, target relative state information is presented directly to the weapon delivery equations. This information is subject to a time delay which represents the time required for the filter to process target and own aircraft state information.

In the case where the target is dynamically maneuvering, the delay for filter processing will depend on the number of iterations required for the filter to attain good estimates of the target state. However, for the cases considered in this thesis, where the target acceleration is constant

11
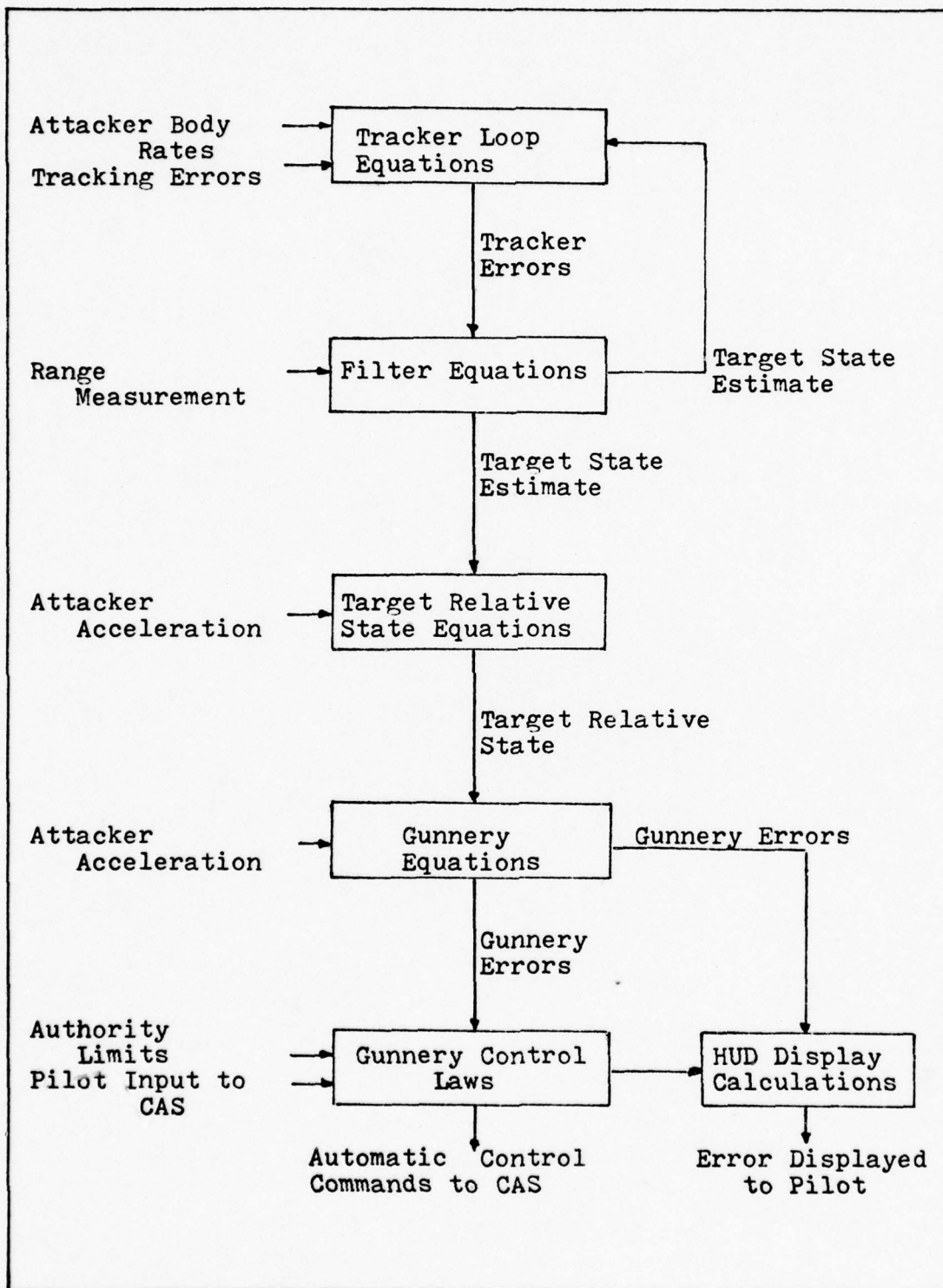
Figure 2. Fire Fly Computer Software Flow Diagram

throughout each simulation run, the time delay is due only to the actual information processing time. Since the Kalman filter has an iteration interval of 1/30 second (Ref 7: 45), the effects of the information processing delay are negligible, as the simulation results in Chapter Five indicate.

Figure 3 depicts a simplified block diagram of the closed loop tracking task. The next section develops the weapon delivery and gunnery equations and derives expressions for the elevation and traverse tracking errors which are displayed to the pilot.

Weapon Delivery Equations

The weapon delivery equations use target relative state information and measured attacker parameters to calculate the gunnery errors. Figure 4 depicts the air-to-air gunnery situation.

The relationships shown in Figure 4 are strictly valid only if the target acceleration is constant. If the target acceleration is time-varying, the relationships depicted in Figure 4 represent an approximation to second order. For the development of the weapon delivery equations in this chapter the second order approximation is assumed to be valid.

Referring to Figure 4, $\bar{R}_r$ represents the present required range vector for a hit, as measured from the attacker to the target. $\bar{R}_{ba}$ represents the range vector from bullet release point to bullet impact point. $\bar{V}_a$ is the attacker velocity vector relative to the airmass, and $\bar{V}_m$ is the gun muzzle

13
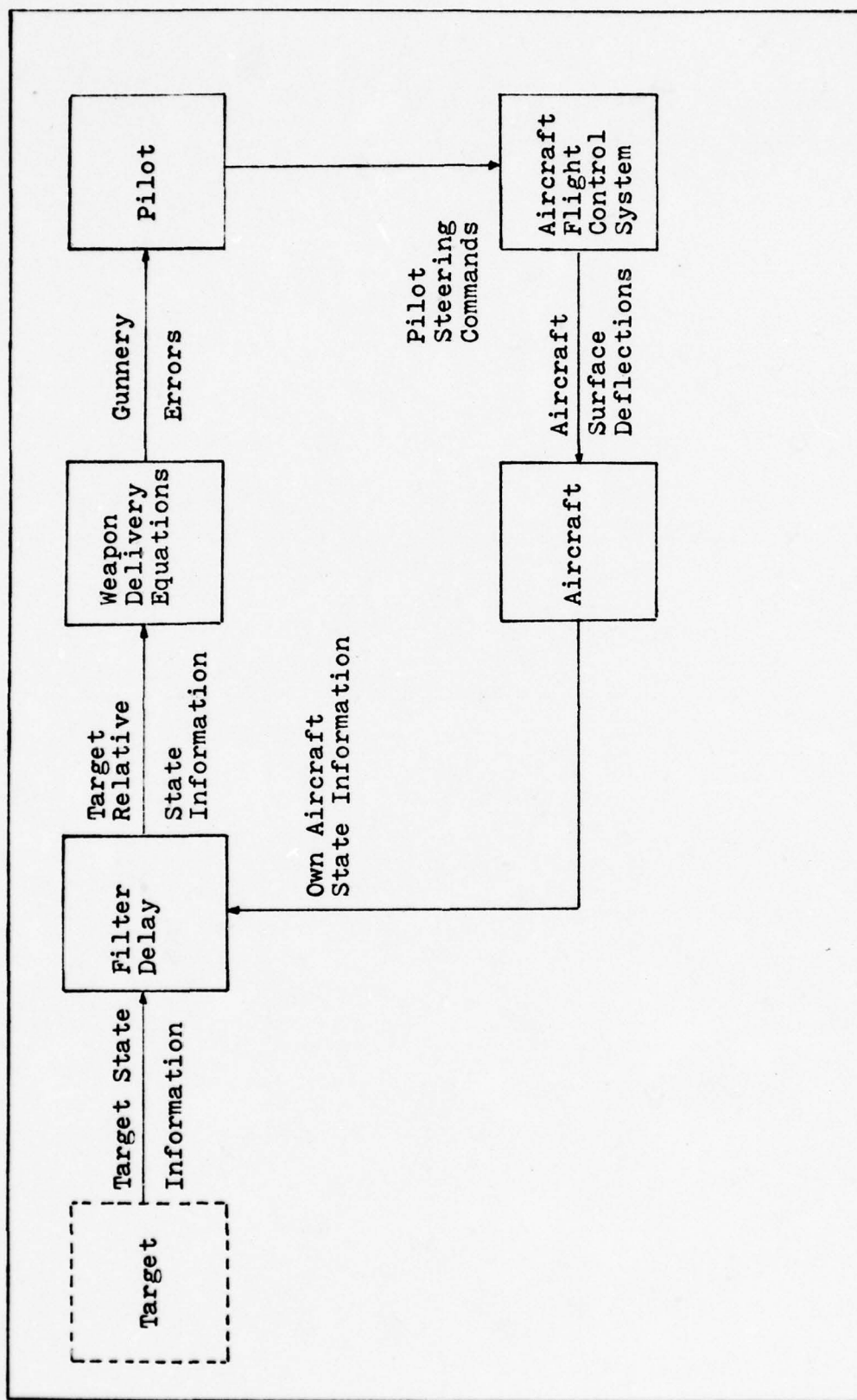
Figure 3. Simplified Closed Loop Tracking Task
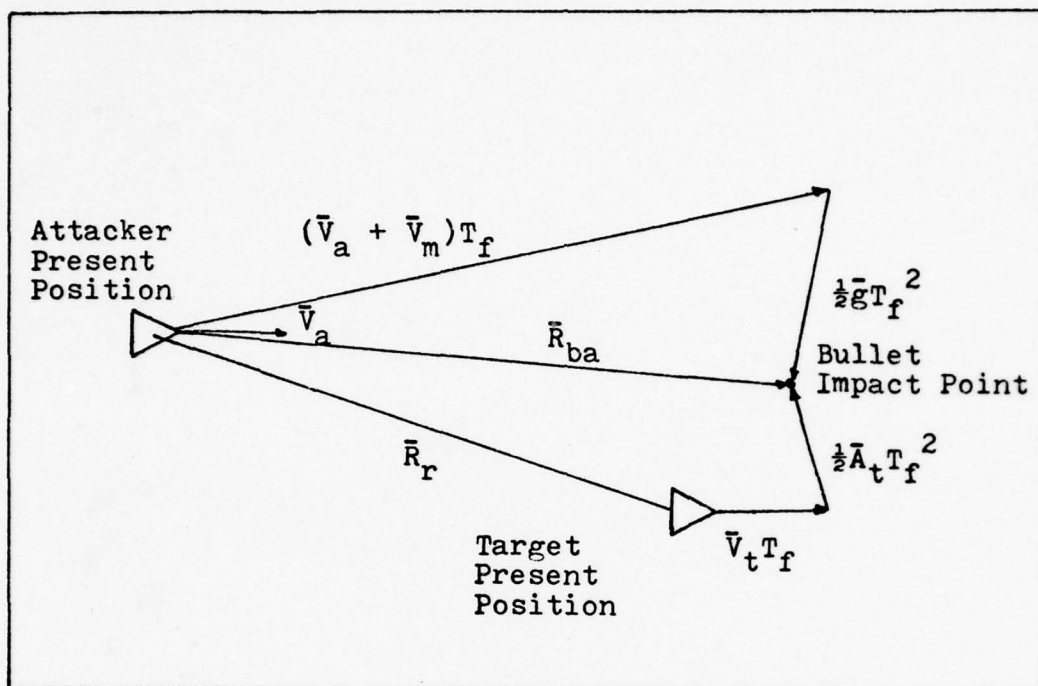
Figure 4. The Air-to-Air Gunnery Situation

velocity vector. $\bar{V}_t$ is the target velocity vector relative
to the airmass, and $\bar{A}_t$ is the target inertial acceleration
vector. T_f is the bullet time-of-flight and $\bar{g}$ is the gravity
vector. The present required range vector from the attacker
to the target is given by

$$\bar{R}_r = \bar{R}_{ba} - \bar{V}_t T_f - \tfrac{1}{2}\bar{A}_t T_f^2 \tag{1}$$

The range vector which represents the position of the bullet
after one time-of-flight is given by

$$\bar{R}_{ba} = [D_f/(V_a + V_m)] \, (\bar{V}_a + \bar{V}_m) + \tfrac{1}{2}\bar{g} T_f^2 \tag{2}$$

where D_f is the magnitude of $\bar{R}_{ba}$.

15

Substituting Eq (2) into Eq (1) yields

$$\bar{R}_r = [D_f/(V_a + V_m)](\bar{V}_a + \bar{V}_m) - \bar{V}_t T_f - \tfrac{1}{2}(\bar{A}_t - \bar{g})T_f^2 \quad (3)$$

The target velocity vector and the target acceleration vector are given by

$$\bar{V}_t = \bar{V}_r + \bar{V}_a \qquad (4)$$

$$\bar{A}_t = \bar{A}_r + \bar{A} \qquad (5)$$

where $\bar{V}_r$ is the target relative velocity vector, $\bar{A}_r$ is the target relative acceleration vector, and $\bar{A}$ is the attacker acceleration vector. The attacker acceleration vector can be expressed as

$$\bar{A} = \bar{A}_b + \bar{g} \qquad (6)$$

where $\bar{A}_b$ is the attacker specific force vector, measured by the outputs of body-mounted accelerometers. Substituting Eq (6) into Eq (5) yields

$$\bar{A}_t = \bar{A}_r + \bar{A}_b + \bar{g} \qquad (7)$$

Substituting Eqs (4) and (7) into Eq (3) yields the range vector required for a hit as

$$\bar{R}_r = [D_f/(V_a + V_m)]\bar{V}_m + [D_f/(V_a + V_m) - T_f]\bar{V}_a - \bar{V}_r T_f$$

$$- \tfrac{1}{2}(\bar{A}_t + \bar{A}_r)T_f^2 \qquad (8)$$

The ballistics relationship between bullet time-of-flight and future range is

$$T_f = D_f/(V_a + V_m - k_o\rho/\rho_o D_f\sqrt{V_a + V_m}) \tag{9}$$

where k_o is the ballistic coefficient and ρ/ρ_o is relative air density (Ref 1: Chap. III, p. 55).

Letting

$$C_b = k_o\rho/\rho_o\sqrt{V_a + V_m} \tag{10}$$

and substituting in Eq (9) yields

$$T_f = D_f/(V_a + V_m - C_bD_f) \tag{11}$$

Solving Eq (11) for D_f in terms of T_f yields

$$D_f = (V_a + V_m)T_f/(1 + C_bT_f) \tag{12}$$

Letting

$$K_b = 1/(1 + C_bT_f) \tag{13}$$

and substituting Eq (13) into Eq (12) yields

$$D_f = K_b(V_a + V_m)T_f \tag{14}$$

Substituting Eq (14) into Eq (8) yields the range vector required for a hit as

$$\bar{R}_r = K_bT_f\bar{V}_m - K_bC_bT_f{}^2\bar{V}_a - T_f\bar{V}_r - \tfrac{1}{2}(\bar{A}_b + \bar{A}_r)T_f{}^2 \tag{15}$$

17
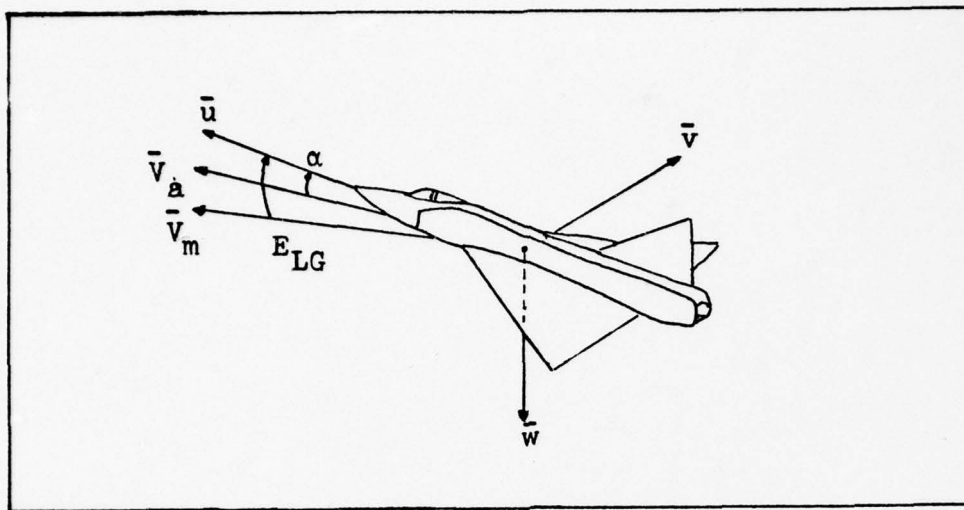
Figure 5. Body-Fixed Coordinate System

Eq (15) represents the physical vector relationships between the attacker and the target with respect to inertial space. To facilitate the use of these relationships for displaying information to the pilot, the inertial vector quantities in Eq (15) are coordinatized in terms of an axis system fixed in the body of the attacking aircraft. Figure 5 depicts a body-fixed coordinate system, $\bar{u}\bar{v}\bar{w}$, where $\bar{u}$ is out the nose of the aircraft, $\bar{v}$ is out the right wing, and $\bar{w}$ is nominally down. The angle E_{LG} is the angle between the $\bar{u}$ axis and the gun axis. The angle α is the aerodynamic angle of attack; that is, the angle between the aircraft velocity vector and the $\bar{u}$ axis.

Separating Eq (15) into scalar equations, expressed in terms of the components of the body-fixed axis system, and assuming that the component of $\bar{V}_m$ in the $\bar{v}$ direction is zero, and that the component of $\bar{V}_a$ in the $\bar{v}$ direction is zero,

18

yields (Ref 7: 45)

$$R_{ru} = -T_f[-K_b V_m \cos(E_{LG}) + V_{ru} + \tfrac{1}{2}T_f(A_{bu} + A_{ru})$$

$$+ T_f K_b C_b V_a \cos(\alpha)] \tag{16}$$

$$R_{rv} = -T_f[V_{rv} + \tfrac{1}{2}T_f(A_{bv} + A_{rv})] \tag{17}$$

$$R_{rw} = -T_f[-K_b V_m \sin(E_{LG}) + V_{rw} + \tfrac{1}{2}T_f(A_{bw} + A_{rw})$$

$$+ T_f K_b C_b V_a \sin(\alpha)] \tag{18}$$

where R_{ru}, R_{rv}, and R_{rw} are the components of the range vector required to obtain a hit, expressed in aircraft body-fixed coordinates.

The error signals to be displayed to the pilot can be defined as the angular difference, in radians, between the range components required for a hit and the present measured range components. Thus (Ref 7: 45)

$$e_{LV} = (R_{rw} - R_{tw})/R \tag{19}$$

$$e_{LW} = -(R_{rv} - R_{tv})/R \tag{20}$$

where e_{LV} and e_{LW} are the gunnery errors in elevation and traverse, respectively, R_{tv} and R_{tw} are components of the present target range, and R is the magnitude of the present range vector. Positive elevation error, e_{LV}, is decreased by positive pitch rate, and positive traverse error, e_{LW}, is decreased by positive yaw rate. Positive pitch rate is

defined as positive rotation about the body-fixed $\bar{v}$ axis, as given by the right hand rule. Positive yaw rate is defined as positive rotation about the body-fixed $\bar{w}$ axis, as given by the right hand rule.

A measure of bullet time-of-flight is required for computing the range vector components required for a hit. A method of calculating bullet time-of-flight is developed in the next section.

Time-of-Flight Calculation

The scalar relationship between future target range and bullet time-of-flight is illustrated in Figure 6.
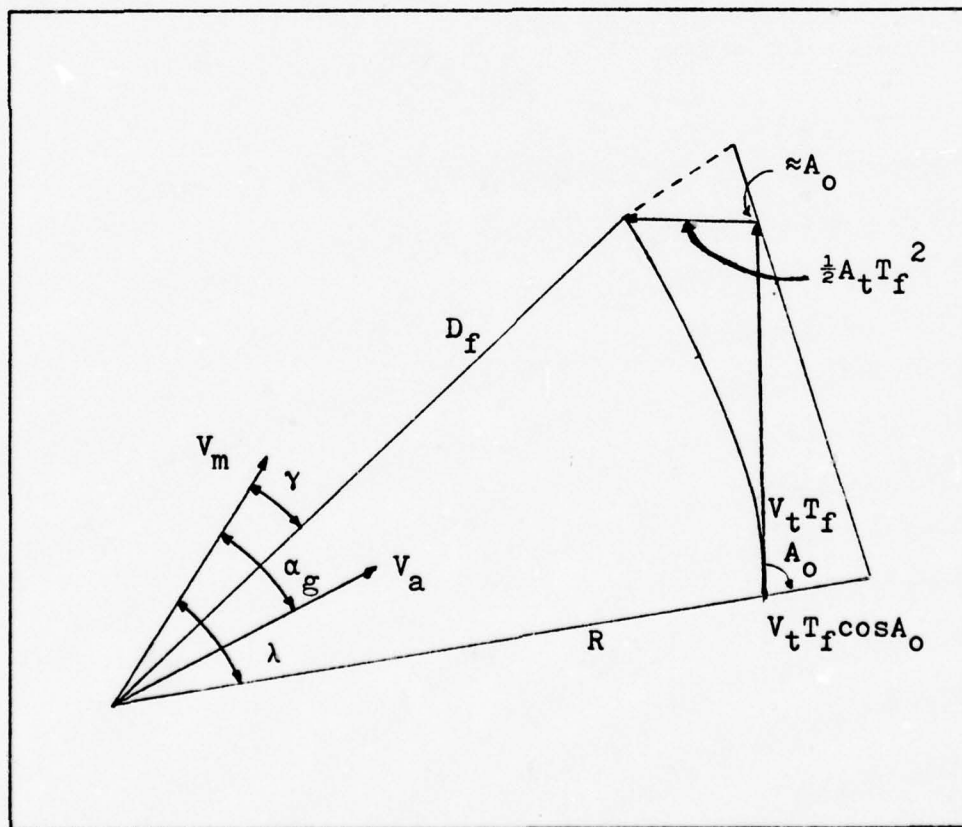
Figure 6. Time-of-Flight Calculation (from Ref 1, Chap.III,p.54)

20

From Figure 6,

$$\cos(\lambda - \gamma) \approx [R + V_t T_f \cos(A_o)]/[D_f + \tfrac{1}{2}A_t T_f^2 \sin(A_o)] \quad (21)$$

where

$$\gamma = [V_a/(V_a + V_m)]\alpha_g \quad (22)$$

and λ is the sight lead angle, A_o is the angle-off of the target heading, and α_g is the gun angle of attack. Also from Figure 6,

$$V_t \cos(A_o) = V_a \cos(\lambda - \alpha_g) + \dot{R} \quad (23)$$

where $\dot{R}$ is the range rate. Substituting Eq (23) into Eq (21) yields

$$\cos(\lambda - \gamma) \approx \{R + [V_a \cos(\lambda - \alpha_g) + R]T_f\}/[D_f + \tfrac{1}{2}A_t T_f^2 \sin(A_o)]$$

$$(24)$$

Solving Eq (24) for D_f yields

$$D_f = [R + V_a T_f \cos(\lambda - \alpha_g) + \dot{R}T_f]/\cos(\lambda - \gamma) - \tfrac{1}{2}A_t T_f^2 \sin(A_o)$$

$$(25)$$

Recalling Eq (11), which is repeated here for convenience,

$$T_f = D_f/(V_a + V_m - C_b D_f) \quad (11)$$

and substituting Eq (25) into Eq (11), yields the following quadratic equation for T_f:

21

$$C_b[V_a \cos(\lambda - \alpha_g) + \dot{R} - \frac{1}{2}A_t T_{fo} \sin(A_o)\cos(\lambda - \gamma)]T_f^2$$

$$+ \{C_b R + \dot{R} + V_a[\cos(\lambda - \alpha_g) - \cos(\lambda - \gamma)]$$

$$- [\frac{1}{2}A_t T_{fo} \sin(A_o) + V_m]\cos(\lambda - \gamma)\}T_f + R = 0 \qquad (26)$$

where T_{fo} is some nominal value of T_f. Since the effects of target acceleration, angle-off, lead angle, and angle-of-attack are second order, nominal values are used in the calculation. Thus, the time-of-flight computation can be mechanized as

$$C_b(V_a + \dot{R} - C_1)T_f^2 + (C_b R + \dot{R} - C_2)T_f + R = 0 \qquad (27)$$

where C_1 and C_2 are constants (Ref 1: Chap. III, p. 56). Eq (27) is easily solved using the quadratic formula and the smaller value is chosen as the bullet time-of-flight.

This chapter presented a general view of the Fire Fly integrated flight control/fire control system. A simplified diagram of the closed loop tracking task for the manual mode of operation was developed. The weapon delivery and gunnery equations were developed as was a method for calculating bullet time-of-flight. The next chapter presents the six degree of freedom equations of motion which describe the F-106 aircraft. The equations include second order stability derivatives and the effects of external fuel tanks. Also presented is the basic F-106 flight control system.

III. The F-106 Aircraft

The F-106 is a single engine all-weather interceptor built by General Dynamics/Convair. Two models of the F-106 exist, the single seat F-106A and the two seat F-106B. Although designed for training purposes, the F-106B can also be used for combat. The aircraft modeled in this simulation analysis is the F-106B configured with two wing-mounted external fuel tanks. This chapter develops the general equations of motion which are used to describe the aircraft and discusses the F-106 flight control system. The nonlinear aero-coefficients were obtained from Reference 8. The numerical values of all stability derivatives are presented in tabular form in Appendix B. These tabular values, which were obtained by curve fitting flight test data, were provided by the Air Force Flight Dynamics Laboratory. The reader is also referred to Appendix A which presents and discusses the digital computer model used in the simulation.

Equations of Motion

In this section, the equations which describe aircraft motion are presented. First, coordinate systems and sign conventions are discussed. Second, the assumptions upon which the equations of motion are based, are listed. Third, the equations which relate the orientation of the aircraft with respect to an Earth-fixed coordinate system are presented. Finally, the equations of translational motion and the

23
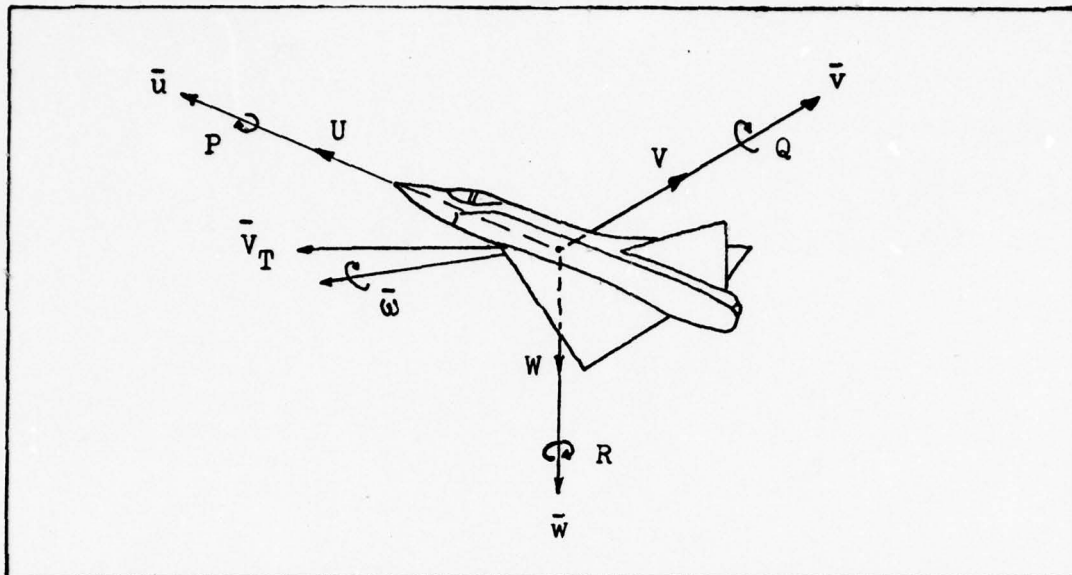
Figure 7. Motion of the Aircraft with Respect to Inertial
Space Resolved into Aircraft Body-Fixed Axes.

equations of angular motion are presented.

Coordinate Systems. Figure 7 depicts the motion of an
aircraft with respect to inertial space. Referring to
Figure 7, $\bar{V}_T$ is the total linear velocity vector. U, V, and
W are the components of the total velocity vector $\bar{V}_T$, expressed
in terms of a body-fixed coordinate system. The body-fixed
axis system $\bar{u}\bar{v}\bar{w}$ is the same axis system that was illustrated
in Figure 5 of Chapter Two. $\bar{\omega}$ is the total angular velocity
of the aircraft with respect to inertial space. P, Q, and R
are the components of $\bar{\omega}$ expressed in terms of the body-fixed
coordinate system.

Figure 8 shows the aerodynamic forces and moments which
act on an aircraft in flight, again expressed with respect to
the body-fixed coordinate system. F_x, F_y, and F_z are the

24
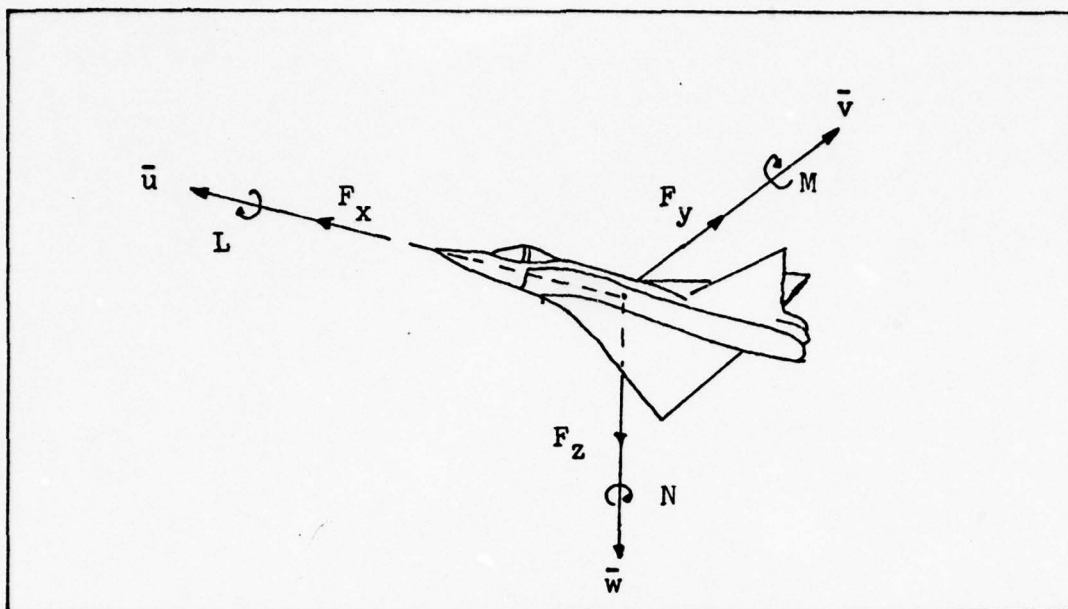
Figure 8. Aerodynamic Forces and Moments Acting on an
Aircraft in Flight.

aerodynamic force components, and L, M, and N are the aero-
dynamic moment components.

Assumptions. The development of the aircraft equations
of motion is based on the following assumptions:

1. The aircraft is a rigid body.

2. The mass and mass distribution of the aircraft are
constant over the time interval of interest.

3. The Earth is assumed to be non-rotating with respect
to inertial space since the rotation rate of the Earth is
sufficiently slow so as to be negligible in the time period
of interest. The Earth is also assumed to be flat since the
effects of the Earth's curvature are negligible for the problem
being considered.

4. The $\bar{u}\bar{w}$ plane is a plane of symmetry.
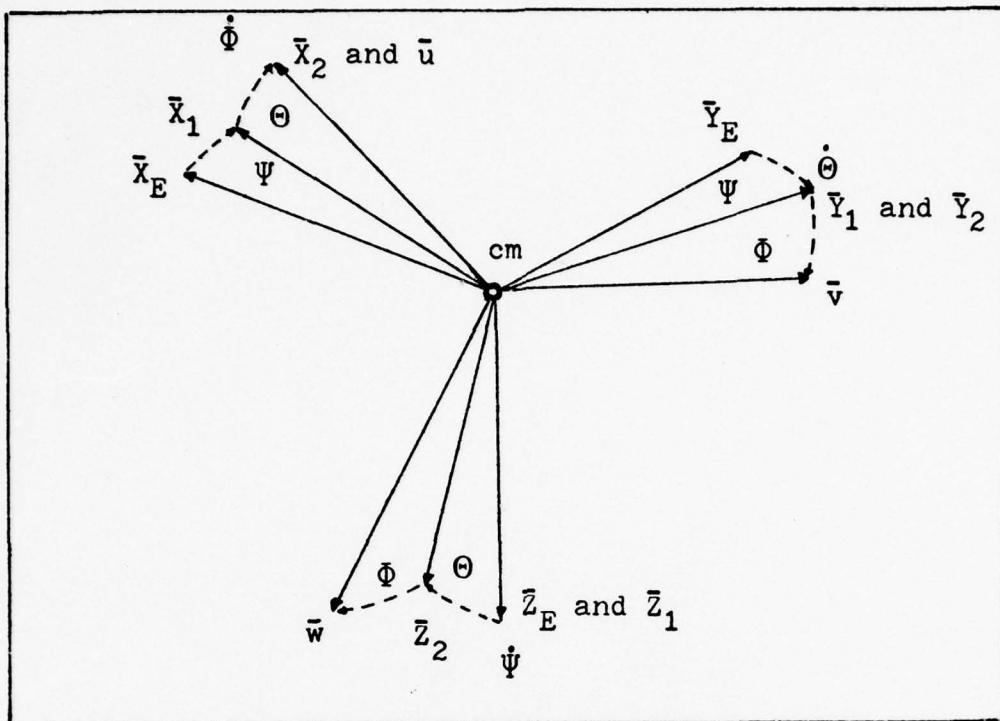
Figure 9. Orientation of the Body-Fixed Coordinate
System with Respect to an Earth-Fixed
Coordinate System (from Ref 9, Chap. II, p. 15)

Euler Angles. The orientation of the aircraft body-
fixed coordinate system with respect to an Earth-fixed, and
thus inertial by assumption 3, coordinate system is specified
by the sequential rotation through Ψ (the heading angle), Θ
(the pitch angle), and Φ (the roll angle). Figure 9 depicts
the rotations with the positive directions as shown. In
Figure 9, the Earth-fixed coordinate system $\bar{X}_E \bar{Y}_E \bar{Z}_E$ is
assumed to have its origin at the center of mass of the
aircraft. First, the $\bar{X}_E \bar{Y}_E \bar{Z}_E$ system is rotated about the $\bar{Z}_E$
axis, in the positive direction as determined by the right
hand rule, through the angle Ψ, and thus becomes $\bar{X}_1 \bar{Y}_1 \bar{Z}_1$.

26

Next, the $\bar{X}_1\bar{Y}_1\bar{Z}_1$ system is rotated about the $\bar{Y}_1$ axis through the angle Θ, yielding the coordinate system $\bar{X}_2\bar{Y}_2\bar{Z}_2$. Finally, the $\bar{X}_2\bar{Y}_2\bar{Z}_2$ system is rotated about the $\bar{X}_2$ axis through the angle Φ. The resulting coordinate system, $\bar{u}\bar{v}\bar{w}$, is the body-fixed coordinate system (Ref 9: Chap. II, p. 16). The components $\dot{\Psi}$, $\dot{\Theta}$, and $\dot{\Phi}$ shown in Figure 9 can be projected along the aircraft body axes $\bar{u}$, $\bar{v}$, and $\bar{w}$ to obtain

$$P = \dot{\Phi} - \dot{\Psi} \sin(\Theta) \tag{28}$$

$$Q = \dot{\Theta} \cos(\Phi) + \dot{\Psi} \cos(\Theta)\sin(\Phi) \tag{29}$$

$$R = -\dot{\Theta} \sin(\Phi) + \dot{\Psi} \cos(\Theta)\cos(\Phi) \tag{30}$$

Eqs (28), (29), and (30) can be solved for $\dot{\Psi}$, $\dot{\Theta}$, and $\dot{\Phi}$ to obtain (Ref 10: 13)

$$\dot{\Psi} = Q \sin(\Phi)/\cos(\Theta) + R \cos(\Phi)/\cos(\Theta) \tag{31}$$

$$\dot{\Theta} = Q \cos(\Phi) - R \sin(\Phi) \tag{32}$$

$$\dot{\Phi} = P + Q \sin(\Phi)\tan(\Theta) + R \cos(\Phi)\tan(\Theta) \tag{33}$$

Equations of Translational Motion. The equations of translational motion can be developed utilizing Newton's Second Law which states that the time rate of change of linear momentum is equal to the sum of the externally applied forces. The scalar equations of translational motion expressed in terms of the body-fixed coordinate system are (Ref 10: 8)

27

$$X = m(\dot{U} + QW - RV) \tag{34}$$

$$Y = m(\dot{V} + RU - PW) \tag{35}$$

$$Z = m(\dot{W} + PV - QU) \tag{36}$$

where m is the mass of the aircraft, $\dot{U}$, $\dot{V}$, and $\dot{W}$ represent the time rate of change of the linear velocity components, and X, Y, and Z represent the sum of all externally applied forces acting along the body-fixed axes $\bar{u}$, $\bar{v}$, and $\bar{w}$, respectively.

The summed force terms X, Y, and Z are composed of the effects of gravity, the aerodynamic forces, and the thrust forces. Thus,

$$X = g_x + F_x + F_{x_T} \tag{37}$$

$$Y = g_y + F_y + F_{y_T} \tag{38}$$

$$Z = g_z + F_z + F_{z_T} \tag{39}$$

where g_x, g_y, and g_z are the components of the gravity vector, F_x, F_y, and F_z are the aerodynamic force components, and F_{x_T}, F_{y_T}, and F_{z_T} are the thrust components. The gravity components are (Ref 10; 13)

$$g_x = -mg \sin(\Theta) \tag{40}$$

$$g_y = mg \cos(\Theta)\sin(\Phi) \tag{41}$$

$$g_z = mg \cos(\Theta)\cos(\Phi) \tag{42}$$

where $g = 32.2$ ft/sec^2.

28

The thrust side force, F_{y_T}, is assumed to be zero and the thrust components F_{x_T} and F_{z_T} can be expressed as

$$F_{x_T} = T \cos(\epsilon_T) \qquad (43)$$

$$F_{z_T} = T \sin(\epsilon_T) \qquad (44)$$

where T is the magnitude of the thrust and ϵ_T is the angle between the $\bar{u}$ body axis and the direction of the thrust vector. For the F-106, $\epsilon_T = 0$, thus

$$F_{x_T} = T \qquad (45)$$

$$F_{z_T} = 0 \qquad (46)$$

The longitudinal aerodynamic force terms F_x and F_y can be expressed in terms of the coefficients of lift and drag. Thus (Ref 11: 243)

$$F_x = \bar{q}S[\dot{C}_L \sin(\alpha) - C_D \cos(\alpha)] \qquad (47)$$

$$F_z = -\bar{q}S[C_L \cos(\alpha) + C_D \sin(\alpha)] \qquad (48)$$

where C_L and C_D are the dimensionless coefficients of lift and drag, respectively. The aerodynamic angle-of-attack α is given by

$$\alpha = \arctan(W/U) \qquad (49)$$

S is the wing reference area and $\bar{q}$ is the dynamic pressure. The coefficient of lift for the F-106 can be expressed as (Ref 8: 34)

29

$$C_L = C_{L_o} + C_{L_\alpha}\alpha + C_{L_{o_T}} + C_{L_{\alpha_T}}\alpha + C_{L_{\delta_E}}\delta_E \qquad (50)$$

where C_{L_o} is the lift coefficient for $\alpha = 0$

C_{L_α} is the lift curve slope

$C_{L_{o_T}}$ is the tank lift coefficient at $\alpha = 0$

$C_{L_{\alpha_T}}$ is the tank lift curve slope

$C_{L_{\delta_E}}$ is the change in lift coefficient due to elevator deflection

δ_E is the elevator deflection, in radians

α is the angle-of-attack, in radians.

The drag coefficient, C_D, is determined as a function of Mach number, lift coefficient, and elevator deflection. One method of determining the total drag coefficient, and the method used in constructing the digital model of the F-106 (see Appendix A), is a linear interpolation between two Mach numbers. Given two curves, C_{D_1} and C_{D_2}, which represent values of the drag coefficient at given Mach numbers, each plotted as a function of lift coefficient and elevator deflection, the total drag coefficient, C_D, can be calculated as

$$C_D = \Delta M_H K_1 C_{D_2} + \Delta M_L K_1 C_{D_1} \qquad (51)$$

30

where ΔM_H is the difference between a high reference Mach number and the actual Mach number, for example, $\Delta M_H = (.9 - \text{Mach})$, and ΔM_L is the difference between the actual Mach number and a low reference Mach number, for example, $\Delta M_L = (\text{Mach} - .8)$. K_1 is a constant whose value depends on the reference Mach numbers, and C_{D_2} and C_{D_1} are found by interpolation for a given lift coefficient and elevator deflection.

The aerodynamic side force, F_y, can be expressed as

$$F_y = F_{y_{Lin}} + F_{y_{NL}} \tag{52}$$

$F_{y_{Lin}}$ is given by (Ref 8: 34)

$$F_{y_{Lin}} = \bar{q} S [C_{y_\beta} \beta + (C_{y_P} P + C_{y_R} R) b / 2 V_T + C_{y_{\delta_R}} \delta_R + C_{y_{\delta_A}} \delta_A] \tag{53}$$

where P is the roll angular velocity, in radians/second

R is the yaw angular velocity, in radians/second

b is the reference wingspan

V_T is the magnitude of the total velocity

δ_R is the rudder deflection, in radians

δ_A is the aileron deflection, in radians

C_{y_β} is the change in side force coefficient due to β

C_{y_P} is the change in side force coefficient due to roll rate

C_{y_R} is the change in side force coefficient due to yaw rate

31

$C_{y_{\delta_R}}$ is the change in side force coefficient due to a change in rudder deflection

$C_{y_{\delta_A}}$ is the change in side force coefficient due to a change in aileron deflection.

The sideslip angle, β, is given by

$$\beta = \arcsin(V/V_T) \tag{54}$$

$F_{y_{NL}}$, the nonlinear component of the side force, can be expressed as (Ref 8; 34)

$$F_{y_{NL}} = \bar{q}S[(C_{y_{\beta_\alpha 2}}\alpha + C_{y_{\beta_\alpha}})\alpha + C_{y_{\beta|\beta|}}|\beta|]\beta$$

$$+ \bar{q}S[C_{y_{\beta_T}}\beta + C_{y_{\alpha_T}}(BL)_T \ P/2V_T] \tag{55}$$

where $|\beta|$ is the absolute value of the sideslip angle

$(BL)_T$ is the tank buttock line; the distance measured in the $\bar{u}\bar{w}$ plane, between the aircraft water line and the centerline of the external fuel tank

$C_{y_{\beta_\alpha}}$ is the change in C_{y_β} due to a change in α

$C_{y_{\beta_\alpha 2}}$ is a second order effect of α on C_{y_β}

$C_{y_{\beta|\beta|}}$ is the change in C_{y_β} due to a change in $|\beta|$

$C_{y_{\beta_T}}$ is the effect of the external fuel tanks on C_{y_β}

$C_{y_{\alpha_T}}$ is the effect of the external fuel tanks on C_{y_α}.

32

The summed force terms, X, Y, and Z can therefore be expressed as

$$X = -mg \sin(\Theta) + \bar{q}S[C_L \sin(\alpha) - C_D \cos(\alpha)] + T \qquad (56)$$

$$Y = mg \cos(\Theta)\sin(\Phi) + \bar{q}S[C_{y_\beta} \beta + (C_{y_P} P + C_{y_R} R)b/2V_T$$

$$+ C_{y_{\delta_R}} \delta_R + C_{y_{\delta_A}} \delta_A] + \bar{q}S[(C_{y_{\beta_{\alpha^2}}} \alpha + C_{y_{\beta_\alpha}})\alpha$$

$$+ C_{y_{\beta|\beta|}} |\beta|]\beta + \bar{q}S[C_{y_{\beta_T}} \beta + C_{y_{\alpha_T}} (BL)_T P/2V_T] \qquad (57)$$

$$Z = mg \cos(\Theta)\cos(\Phi) - \bar{q}S[C_L \cos(\alpha) + C_D \sin(\alpha)] \qquad (58)$$

Equations of Angular Motion. Like the equations of translational motion, the equations of angular motion are developed by applying Newton's Second Law to angular momentum. Newton's Law states that the time rate of change of angular momentum is equal to the sum of the externally applied moments. Thus, the scalar equations of angular motion, expressed in terms of the body-fixed coordinate system, are (Ref 10; 11)

$$L = \dot{P}I_x + QR(I_z - I_y) - (PQ + \dot{R})I_{xz} \qquad (59)$$

$$M = \dot{Q}I_y + PR(I_x - I_z) + (P^2 - R^2)I_{xz} \qquad (60)$$

$$N = \dot{R}I_z + PQ(I_y - I_x) + (QR - \dot{P})I_{xz} \qquad (61)$$

33

where I_x, I_y, and I_z are the moments of inertia about the $\bar{u}$,
$\bar{v}$, and $\bar{w}$ axes

I_{xz} is the product of inertia in the $\bar{u}\bar{w}$ plane

$\dot{P}$, $\dot{Q}$, and $\dot{R}$ are the time rates of change of the angular
velocity components

L is the total rolling moment

M is the total pitching moment

N is the total yawing moment.

The total rolling moment, L, can be expressed as the sum
of a linear component, L_{Lin}, and a nonlinear component, L_{NL},
where the latter contains the effects of the external fuel
tanks. L_{Lin} can be written as (Ref 8; 34)

$$L_{Lin} = \bar{q}Sb[C_{\ell_\beta}\beta + (C_{\ell_P}P + C_{\ell_R}R)b/2V_T + C_{\ell_{\delta_R}}\delta_R + C_{\ell_{\delta_A}}\delta_A]$$

$$+ F_z(Y_{ref} - Y_{cg}) - F_y(Z_{ref} - Z_{cg}) \tag{62}$$

where b is the reference wingspan

F_z is the aerodynamic force in the $\bar{w}$ direction

F_y is the aerodynamic side force

$Y_{ref} - Y_{cg}$ is the cg moment arm in the $\bar{v}$ direction

$Z_{ref} - Z_{cg}$ is the cg moment arm in the $\bar{w}$ direction

C_{ℓ_β} is the change in C_ℓ for a change in sideslip

C_{ℓ_P} is the change in C_ℓ for a change in roll rate

C_{ℓ_R} is the change in C_ℓ for a change in yaw rate

34

$C_{\ell_{\delta_R}}$ is the change in C_ℓ for a change in rudder deflection

$C_{\ell_{\delta_A}}$ is the change in C_ℓ for a change in aileron deflection

The nonlinear rolling moment, L_{NL}, is given by (Ref 8: 34-35)

$$L_{NL} = \bar{q}Sb\{\beta[(C_{\ell_{\beta_\alpha 2}}\alpha + C_{\ell_{\beta_\alpha}})\alpha + C_{\ell_{\beta |\beta|}}|\beta| \ ] + [(C_{\ell_{P_\alpha 2}}\alpha$$

$$+ C_{\ell_{P_\alpha}})P + C_{\ell_{R_\alpha}}R]\alpha(b/2V_T)\} + \bar{q}Sb\{C_{\ell_{\beta_T}}\beta - [C_{\ell_{o_T}}(BL)_T$$

$$+ C_{y_{\alpha_T}}(2.33 \text{ ft})](BL)_T \ P/2V_T\} \tag{63}$$

where $C_{\ell_{\beta_\alpha}}$ is the change in C_{ℓ_β} for a change in α

$C_{\ell_{\beta_\alpha 2}}$ is a second order effect of α on C_{ℓ_β}

$C_{\ell_{\beta |\beta|}}$ is the change in C_{ℓ_β} due to a change in $|\beta|$

$C_{\ell_{P_\alpha}}$ is the change in C_{ℓ_P} due to a change in α

$C_{\ell_{P_\alpha 2}}$ is a second order effect of α on C_{ℓ_P}

$C_{\ell_{R_\alpha}}$ is the change in C_{ℓ_R} due to a change in α

$C_{\ell_{\beta_T}}$ is the effect of the tanks on C_{ℓ_β}

$C_{\ell_{o_T}}$ is the effect of the tanks on C_{ℓ_o}

$C_{y_{\alpha_T}}$ is the effect of the tanks of C_{y_α}.

The total pitching moment, M, is the sum of the pitching moment due to thrust, M_T, a linear pitching moment, M_{Lin}, and a pitching moment due to the external fuel tanks, M_{Tank}. The pitching moment due to thrust is (Ref 12: 27)

$$M_T = z_o\, F_{x_T} - x_o\, F_{z_T} \tag{64}$$

but since $F_{z_T} = 0$ from Eq (46)

$$M_T = z_o\, F_{x_T} = z_o\, T \tag{65}$$

where z_o is the distance, measured in the $\bar{w}$ direction, between the aircraft center of gravity and the origin of the thrust vector.

The linear pitching moment, M_{Lin}, is (Ref 8: 35)

$$M_{Lin} = \bar{q}Sc[C_{m_o} + C_{m_q}(Q + \dot{\alpha})c/V_T + C_{m_{\delta_E}}\delta_E]$$

$$- F_z[(NP)c - X_{cg}] + F_x(Z_{ref} - Z_{cg}) \tag{66}$$

where c is the mean aerodynamic chord

$\dot{\alpha}$ is the time rate of change of angle-of-attack

δ_E is the elevator deflection, in radians

(NP) is the aircraft neutral point

X_{cg} is the distance, measured in the $\bar{u}$ direction, from
the wing leading edge at the wing root to the aircraft
center of gravity

36

C_{m_o} is the pitching moment coefficient for $\alpha \neq 0$

C_{m_q} is the pitching moment coefficient due to pitch rate

$C_{m_{\delta_E}}$ is the pitching moment coefficient due to elevator deflection.

The tank pitching moment is given by (Ref 8; 35)

$$M_{Tank} = \bar{q}Sc(C_{m_{o_T}} + C_{m_{\alpha_T}}\alpha) \qquad (67)$$

where $C_{m_{o_T}}$ and $C_{m_{\alpha_T}}$ are the pitching moment coefficients due to the external tanks.

The total yawing moment, N, is expressed as the sum of a linear yawing moment, N_{Lin}, and a nonlinear yawing moment, N_{NL}, where N_{NL} includes the effects of the external tanks. The linear yawing moment is given by (Ref 8; 35)

$$N_{Lin} = \bar{q}Sb[C_{n_\beta}\beta + (C_{n_P}P + C_{n_R}R)b/2V_T + C_{n_{\delta_R}}\delta_R + C_{n_{\delta_A}}\delta_A]$$

$$+ F_y[(NP)c - X_{cg}] - F_x(Y_{ref} - Y_{cg}) \qquad (68)$$

where C_{n_β} is the change in yawing moment coefficient due to β

C_{n_P} is the change in C_n due to roll rate

C_{n_R} is the change in C_n due to yaw rate

$C_{n_{\delta_R}}$ is the change in C_n due to rudder deflection

$C_{n_{\delta_A}}$ is the change in C_n due to aileron deflection.

The nonlinear yawing moment is expressed as (Ref 8: 35)

$$N_{NL} = \bar{q}Sb[(C_{n_{\beta_{\alpha}2}}\alpha + C_{n_{\beta_{\alpha}}})\alpha + (C_{n_{\beta|\beta|}} \ |\beta| + \Delta C_{n_{\beta}})\beta$$

$$+ (C_{n_{\delta_A\alpha}}\alpha + C_{n_{\delta_A\delta_E}}\delta_E)\delta_A] + \bar{q}Sb[C_{n_{\beta_T}}\beta$$

$$- 0.6(BL)_T \ P/2V_T] \tag{69}$$

where $C_{n_{\beta_{\alpha}2}}$ is a second order effect of α on $C_{n_{\beta}}$

$C_{n_{\beta_{\alpha}}}$ is the change in $C_{n_{\beta}}$ due to α

$C_{n_{\beta|\beta|}}$ is the change in $C_{n_{\beta}}$ due to $|\beta|$

$\Delta C_{n_{\beta}}$ is the incremental change in C_n due to β

$C_{n_{\delta_A\alpha}}$ is the change in $C_{n_{\delta_A}}$ due to α

$C_{n_{\delta_A\delta_E}}$ is the change in $C_{n_{\delta_A}}$ due to δ_E

$C_{n_{\beta_T}}$ is the effect of the tanks on $C_{n_{\beta}}$.

The total moments, L, M, and N can then be expressed as

$$L = \bar{q}Sb[C_{\ell_\beta}\beta + (C_{\ell_P}P + C_{\ell_R}R)b/2V_T + C_{\ell_{\delta_R}}\delta_R + C_{\ell_{\delta_A}}\delta_A]$$

$$+ F_z(Y_{ref} - Y_{cg}) - F_y(Z_{ref} - Z_{cg}) + \bar{q}Sb\{\beta[(C_{\ell_{\beta_\alpha 2}}\alpha + C_{\ell_{\beta_\alpha}})\alpha$$

$$+ C_{\ell_{\beta|\beta|}}|\beta|] + [(C_{\ell_{P_\alpha 2}}\alpha + C_{\ell_{P_\alpha}})P + C_{\ell_{R_\alpha}}R]\alpha(b/2V_T)\}$$

$$+ \bar{q}Sb\{C_{\ell_{\beta_T}}\beta - [C_{\ell_{o_T}}(BL)_T + C_{y_{\alpha_T}}(2.33 \text{ ft})](BL)_T \, P/2V_T\}$$

(70)

$$M = \bar{q}Sc[C_{m_o} + C_{m_q}(Q + \dot{\alpha})c/V_T + C_{m_{\delta_E}}\delta_E] - F_z[(NP)c - X_{cg}]$$

$$+ F_x(Z_{ref} - Z_{cg}) + z_o T + \bar{q}Sc(C_{m_{o_T}} + C_{m_{\alpha_T}}\alpha)$$

(71)

$$N = \bar{q}Sb[C_{n_\beta}\beta + (C_{n_P}P + C_{n_R}R)b/2V_T + C_{n_{\delta_R}}\delta_R + C_{n_{\delta_A}}\delta_A]$$

$$+ F_y[(NP)c - X_{cg}] - F_z(Y_{ref} - Y_{cg}) + \bar{q}Sb[(C_{n_{\beta_\alpha 2}}\alpha + C_{n_{\beta_\alpha}})\alpha$$

$$+ (C_{n_{\beta|\beta|}}|\beta| + \Delta C_{n_\beta})\beta + (C_{n_{\delta_A}}\alpha + C_{n_{\delta_A \delta_E}}\delta_E)\delta_A]$$

$$+ \bar{q}Sb[C_{n_{\beta_T}}\beta - 0.6(BL)_T \, P/2V_T]$$

(72)

39

In this section the six degree of freedom nonlinear equations of aircraft motion were developed. These equations account for the effects of the aerodynamic forces and moments acting on the aircraft, the force of gravity, the effects of thrust, and the effects of external fuel tanks. The equations which specify the orientation of the aircraft with respect to an Earth-fixed coordinate system were also presented. The development of the equations of motion was based on the assumptions that the aircraft is a rigid body and that the aircraft mass and mass distribution remain constant over the time interval of interest. Further, it was assumed that the Earth-fixed coordinate system is nonrotating with respect to inertial space, and finally, that the body-fixed $\overline{uw}$ plane is a plane of symmetry. The equations describing the orientation of the aircraft with respect to the Earth-fixed system are given by Eqs (31), (32), and (33). The equations of translational motion are given by Eqs (34), (35), and (36), where the summed force terms X, Y, and Z are given by Eqs (56), (57), and (58), respectively. The equations of angular motion are given by Eqs (59), (60), and (61), where the total moments L, M, and N are given by Eqs (70), (71), and (72), respectively.

The above equations were used to describe the motion of the F-106 aircraft in the digital computer simulation. In order to completely describe the aircraft, one must specify not only the equations of motion, but also the aircraft flight control system.

F-106 Flight Control System

The F-106 utilizes elevons for both pitch and roll control, and a conventional rudder for directional control. The elevons deflect symmetrically for pitch attitude changes and differentially to initiate roll angle. The longitudinal flight control system utilizes a pitch damper as shown in Figure 10. Pitch rate q is fed back through a scheduled gain K_q and a washout circuit with a scheduled time constant τ_q. The scheduled gain and time constant are functions of the air density ratio. The specific values are listed in Appendix B. The output of the washout circuit is fed through an authority limiter with limits of ± 1 degree and then to a series actuator. The resulting output is compared to the
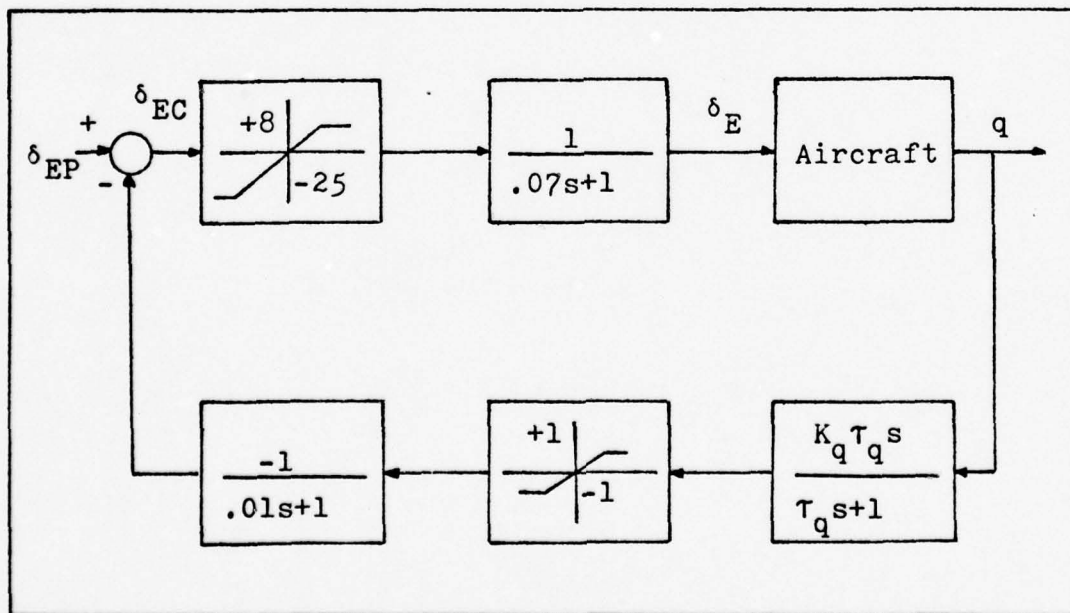
Figure 10. F-106 Longitudinal Flight Control System (from Ref 13: 51).

41

pilot's pitch command, δ_{EP}. The differenced quantity, δ_{EC}, is fed through a pitch limiter which limits the commanded input to between +8 degrees and -25 degrees. The output of the limiter is fed to the power actuator and the resulting output, δ_E, is the elevon deflection for pitch, in degrees.

The lateral-directional control system includes a yaw damper and differential elevon-to-rudder crossfeed for turn coordination. A block diagram of the lateral-directional control system is shown in Figure 11. The yaw damper employs feedback of roll rate P and yaw rate R. The roll rate is fed through a scheduled gain K_P and then through a simple washout circuit. The scheduled gain, K_P, is a function of dynamic pressure. Specific values of K_P are listed in Appendix B. The yaw rate R is fed through a gain of -1 and then a simple washout circuit. The pilot's differential elevon command, δ_{AP}, is fed through a power actuator and then to the elevon control surfaces as δ_A. The commanded roll, δ_{AP}, is also fed through a gain K_{δ_A}, and added to the pilot's rudder command, δ_{RP}. The gain K_{δ_A} is scheduled as a function of dynamic pressure. The specific values of K_{δ_A} are also listed in Appendix B.

This chapter presented the equations of motion which describe the F-106B aircraft configured with external fuel tanks. The basic flight control systems were also presented. The next chapter develops the analytical pilot model which was used for the closed loop simulation.

42

Figure 11. F-106 Lateral-Directional Control System (from Ref 13:51).

43
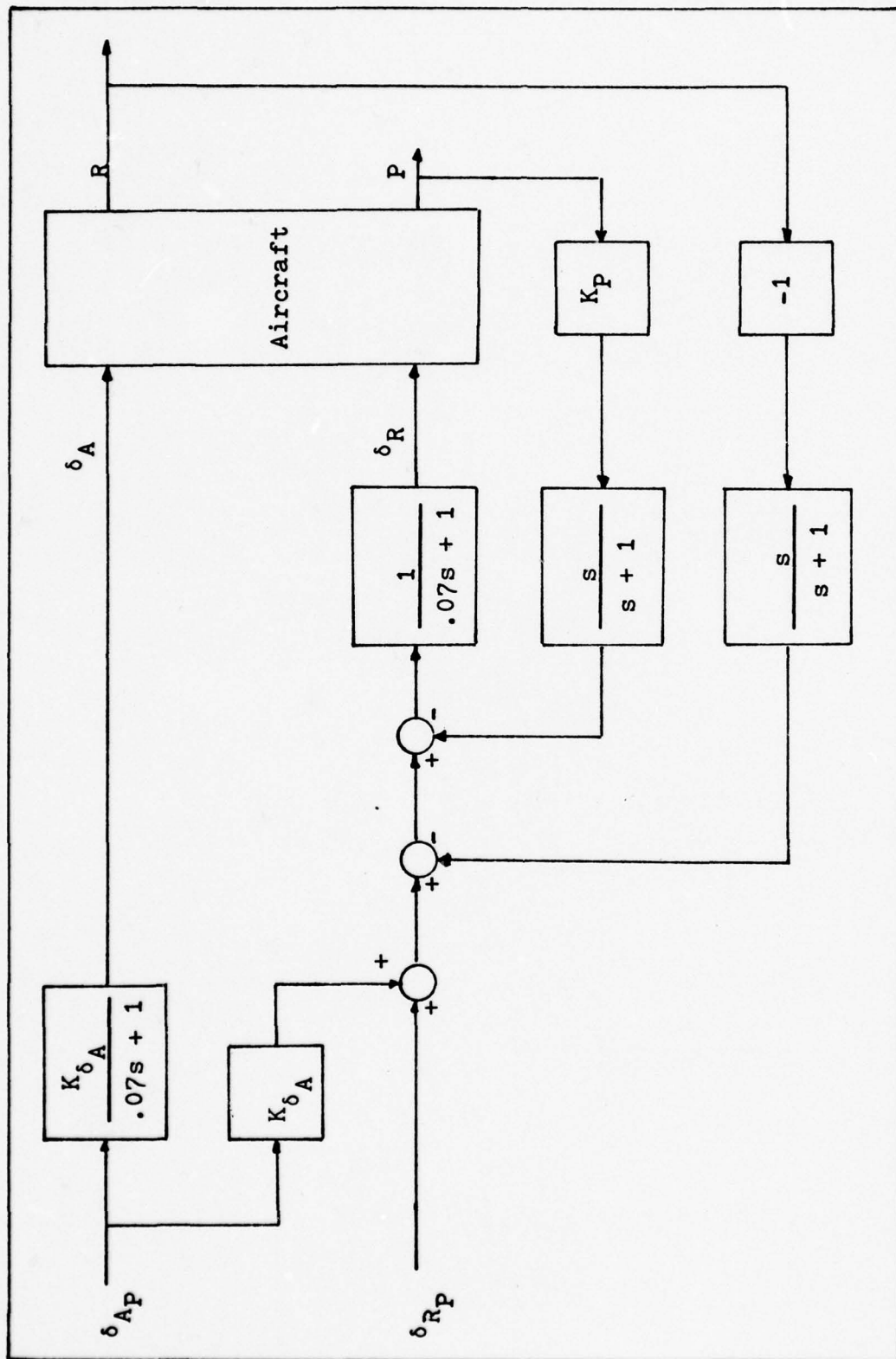
IV. The Pilot Model

General Considerations

For closed loop digital simulation of the air-to-air gunnery tracking task, a suitable analytical model of the pilot must be developed. This analytical model should relate the air-to-air gunnery errors to aircraft steering commands in a way which approximates the response of a human pilot. To realistically develop such a model, one needs to know how the human pilot performs in relation to the particular aircraft/weapon delivery system and the specific aerial gunnery task being considered.

Perhaps the most suitable method for obtaining a measure of the human pilot's response is man-in-the-loop simulation. From man-in-the-loop studies, one can obtain time histories of the tracking error response and a measure of the pilot's frequency response characteristics. By controlling the tracking task so that it can be duplicated in an all digital simulation, one seeks to develop an analytical model which exhibits tracking and frequency response characteristics which are similar to those observed for the human pilot. For the system simulated in this report, however, appropriate man-in-the-loop studies have not yet been completed. Therefore, an appropriate analytical pilot model must be developed from other sources.

In the development of the Terminal Aerial Weapon Delivery Simulation (TAWDS) programs, McDonnell Aircraft

Company (McAir) proposed and validated a multi-axis analytical pilot model for the F-4 aircraft for use in aerial gunnery tasks. A complete discussion of the TAWDS pilot model development can be found in Reference 14. The TAWDS pilot model was used successfully in the simulation of F-4 aircraft configurations with widely varying flying qualities. Therefore, it was felt that the basic structure of the TAWDS pilot model was appropriate for preliminary evaluation of the F-106/Fire Fly director gunsight system.

The Generic Pilot Model

The TAWDS pilot model for air-to-air gunnery was developed for use in the terminal phase of air-to-air tracking, where the tracking task was assumed to be deterministic in that the target was not maneuvering in a random manner. The result of this assumption is that the pilot directly observes the effect of his control inputs on the tracking errors (Ref 6: 66). McAir found that the characteristics of the tracking error time histories for man-in-the-loop simulations were similar, regardless of the particular pilot, the aircraft flying qualities, or the characteristics of the gunsight.

The elevation tracking error contains two predominant frequency components, both of which exhibit a limit cycle type of response. The high frequency component is due to the pilot's interaction with the aircraft short period dynamics, and the low frequency component results from the pilot's interaction with the closed loop poles which result

from the relative geometry between the attacker and the target.
The traverse tracking error is a single frequency limit cycle
response with a period of four to eight seconds (Ref 6: 68-69).
The TAWDS pilot model was structured so as to exhibit responses
in the elevation and traverse tracking error time histories
which were similar to those observed for the human pilot.

A block diagram of the TAWDS pilot model is shown in
Figure 12. The model represents the pilot as a proportional
plus derivative observer of both the elevation and traverse
tracking errors, with deadzones on the error rates. The
simple lag networks which filter the true errors represent
the pilot's response delay and subsequent smoothing of errors
which contain noise or which have frequencies above the
pilot's observation bandwidth (Ref 6: 71).

In the longitudinal portion of the pilot model, the
smoothed error signal e_{LVS}, is fed through a deadzone $DZ_{\dot{e}_{LV}}$.
The outputs of the deadzone and the proportional gain block
K_R are summed to produce a projected error e'_{LV}. This
projected error represents the high frequency component of
the tracking error. The smoothed error signal e_{LVS}, is also
fed through a second order low pass filter and a gain K_L.
The resulting error signal is the low frequency component of
the tracking error. This low frequency component is then
added to the projected error e'_{LV}. The resulting signal is
multiplied by the pilot's transmission gain, K_{PE}, to determine
the pilot's rate input to the control stick, $\dot{\delta}_P$ (Ref 6: 70-72).

46
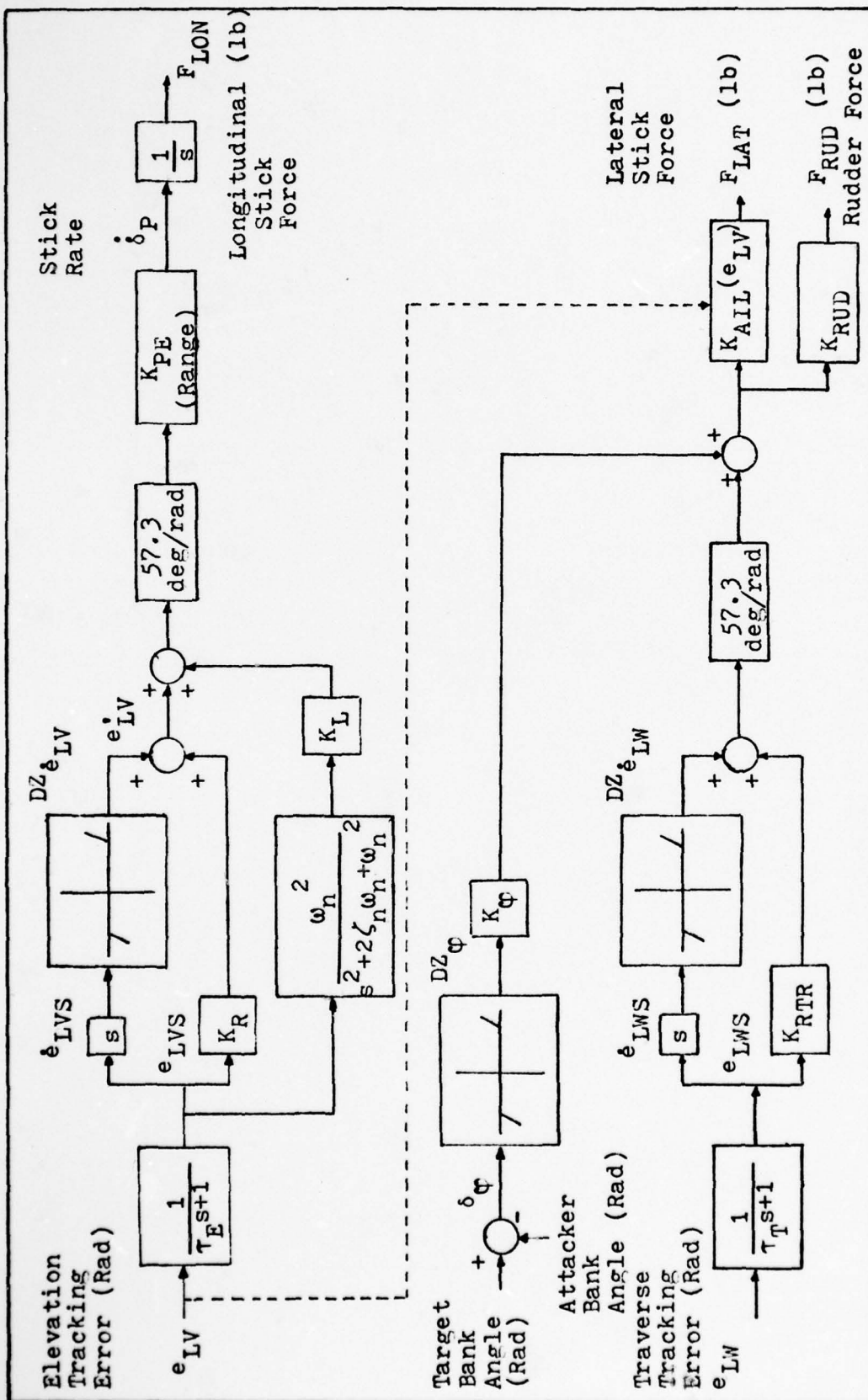
Figure 12. Generic Multi-Axis Pilot Model for Air-to-Air Gunnery (from Ref 14, 27).

47

In the lateral portion of the pilot model, the smoothed error e_{LWS} is fed through a proportional gain block, K_{RTR}. The smoothed error signal is also differentiated and fed through a deadzone $DZ_{\dot{e}_{LW}}$. The output of the deadzone is combined with the signal from the K_{RTR} block to form the projected lateral error $\dot{e}_{LW}$. This signal is added to the signal from the output of the gain block K_{φ}. The portion of the model which feeds differential bank angle through the deadzone DZ_{φ} and the gain K_{φ} represents the pilot's ability to adjust his bank angle based on his perception of the bank angle difference between his aircraft and the target. After combining the projected error and the error due to differential bank angle, the resulting signal is fed through the pilot lateral transmission gain, K_{AIL}. K_{AIL} is shown as a function of elevation tracking error, e_{LV}, since the pilot tends to act as a radial controller in attempting to null both elevation and traverse errors simultaneously. The projected error is also fed through a rudder pedal gain K_{RUD}, since the pilot will probably try to coordinate his lateral stick and rudder commands (Ref 6: 74-76).

The TAWDS studies determined a range of parameter values for the multi-axis pilot model. Table I contains a listing of the range of recommended values for an F-4 aircraft configured with a director gunsight. Because the parameters listed in Table I affect the stability of the closed loop tracking task, the specified values are strictly applicable

only for the F-4 aircraft. However, the recommended range
of values was used as a guide in choosing first trial
parameter values for the F-106 pilot model. The following
paragraphs discuss the function of each parameter in the
pilot model. This discussion is adapted from Reference 14,
pages 29 through 34.

Table I. Pilot Model Parameter Values for an F-4 Aircraft
with Director Gunsight (from Ref 6: 73, 76)

Longitudinal Parameters	K_{PE}		K_R	K_L
Range of Values	$0.75\ K_{CO}$-$1.25\ K_{CO}$		.75-1.25	1.0-3.0
Longitudinal Parameters	τ_E		$(\omega_n,\ \zeta_n)$	$DZ_{\dot{e}_{LV}}$
Range of Values	0.0-0.05		1.0, 0.6	5.0 mr/sec

Lateral Parameters	K_φ	K_{RTR}	K_{AIL}	K_{RUD}
Range of Values	0.0-0.1	1.0	$\leq .36$	0.0
Lateral Parameters	τ_T	$DZ_{\dot{e}_{LW}}$	DZ_φ	
Range of Values	0.0-0.05	5.0 mr/sec	5.0 deg	

Each parameter in the pilot model contributes to the overall objective of matching as closely as possible the tracking characteristics of the human pilot. The prefilter time constants, τ_E and τ_T, represent the pilot's ability to smooth observed errors. The frequency and damping parameters of the pilot's low pass filtering process, ω_n and ζ_n, represent the pilot's interaction with the relative geometry of the elevation tracking task. The gain K_L determines the amplitude of the low frequency component in the elevation tracking error. The deadzone on the elevation error rate, $DZ_{\dot{e}_{LV}}$, produces the desired limit cycle response in the high frequency component of elevation tracking error. The gain K_R affects the amplitude of the high frequency component. The longitudinal pilot gain, K_{PE}, also affects the amplitude of the high frequency component. Referring to Table I, it can be seen that the range of recommended values for K_{PE} is a function of K_{CO}. K_{CO} is the value of gain at which the closed loop system poles due to the aircraft short period mode pass from the left half s-plane to the right half s-plane. Thus the value of K_{PE} chosen must be large enough to excite the high frequency mode of the elevation tracking error, but not so high as to cause the tracking to become unstable. The value of K_{PE} is also a function of the target range, but constant gain settings were used in the TAWDS program development. In the F-106 simulation studies described in this report, constant values were chosen for K_{PE} since all simulation runs were begun at the

50

same range, and the overall change in range magnitude was not significant enough to warrant gain scheduling.

The deadzone $DZ_{\dot{e}_{LW}}$ describes the pilot's ability to perceive traverse error rates. The gain parameters K_{RTR} and K_{AIL} affect the amplitude and frequency of the traverse error. The values of K_{RTR} and K_{AIL} are set so as to stabilize the lateral tracking task and produce the desired four to eight second period response. K_{AIL} is shown as a function of true elevation tracking error to represent the pilot's intentional coupling as he tries to null elevation and traverse errors simultaneously. As with K_{PE}, constant values of K_{AIL} were used in both the TAWDS and F-106 simulation studies.

The gain parameter K_{RUD} models the pilot's rudder pedal commands. Man-in-the-loop simulations by McAir showed that the pilot's rudder force commands were usually negligible during terminal air-to-air tracking. The deadzone DZ_{φ} and the gain parameter K_{φ} relate pilot stick forces due to the sensed differential bank angle between the target and attacker. Differential bank angle feedback is probably not a primary input during terminal gunnery tracking, but the pilot may use differential bank angle cues to prevent excessive wing rock (Ref 14: 32).

McAir was successful in utilizing the multi-axis analytical pilot model discussed above to obtain tracking responses similar to those of human pilots performing the same task. The TAWDS studies tested the pilot model with F-4 aircraft models which were configured so as to produce

51

widely varying sets of flying qualities. Because the TAWDS pilot model was used successfully regardless of the aircraft flying qualities, the same basic structure was chosen for the F-106 digital simulations performed in the evaluation of the Fire Fly director gunsight. A discussion of the specific F-106 pilot model is presented in the next section.

F-106 Pilot Model

The structure of the F-106 pilot model is basically the same as the TAWDS pilot model, and parameter values were chosen to be nominally within the range of values recommended in Table I. The value of K_{PE}, the longitudinal pilot gain, was chosen by root locus analysis. This value was chosen to be high enough to stabilize the low frequency component of the elevation tracking error. The upper value of K_{PE} was limited so as not to cause the complex poles which are due to the pilot's interaction with the aircraft short period dynamics, to cross over into the right half s-plane (Ref 14: 55). If the deadzone $DZ_{\dot{e}_{LV}}$ is removed from the pilot model, the longitudinal pilot model transfer function from elevation tracking error to longitudinal force command is (Ref 14:29)

$$\frac{F_{LON}}{e_{LV}} = \frac{K_{PE}[s^3 + (2\zeta_n\omega_n + K_R)s^2 + (\omega_n^2 + K_R 2\zeta_n\omega_n)s + (K_L + K_R)\omega_n^2]}{s(s^2 + 2\zeta_n\omega_n s + \omega_n^2)(\tau_E s + 1)}$$

$$(73)$$

The parameters of the transfer function were set to
nominal values and a root locus for the closed loop longi-
tudinal system was determined as a function of K_{PE}. (The
EASY Analysis Program provides a straightforward tool for
producing root loci about a linearized operating point).
A partial root locus for the longitudinal system is shown
in Figure 13. The longitudinal system has two open loop
poles which start at s = 0 and move into the right half s-plane
and then back toward the pilot model complex zeros as the
gain K_{PE} is increased. For the nominal pilot model parameters
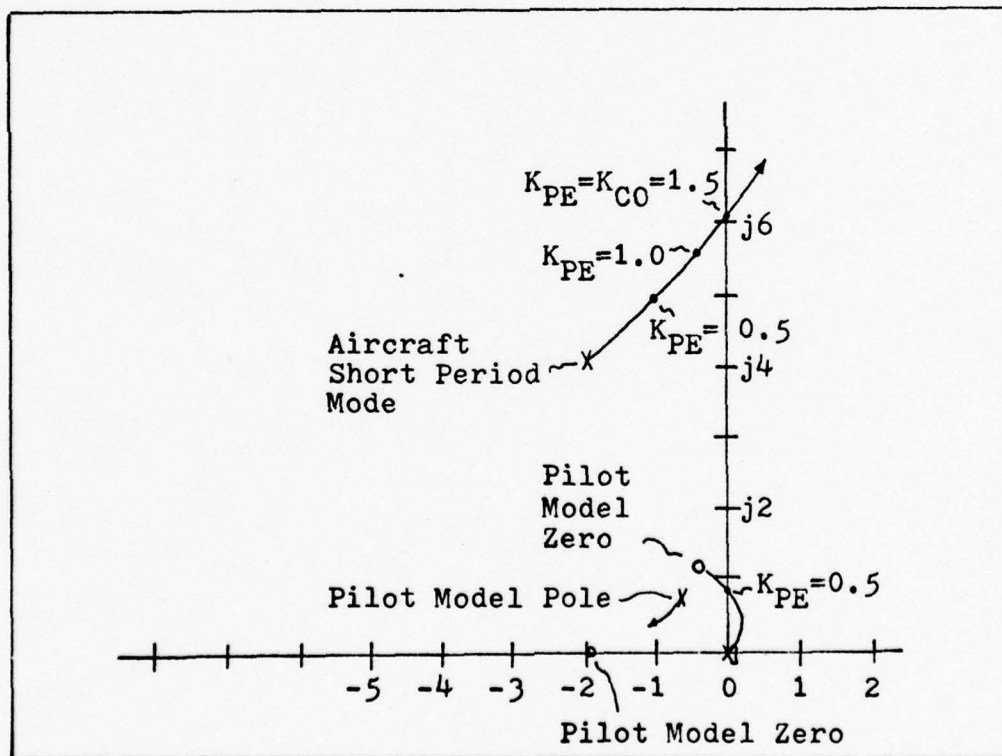
Figure 13. Partial Root Locus for Closed Loop Longitudinal
System.

53
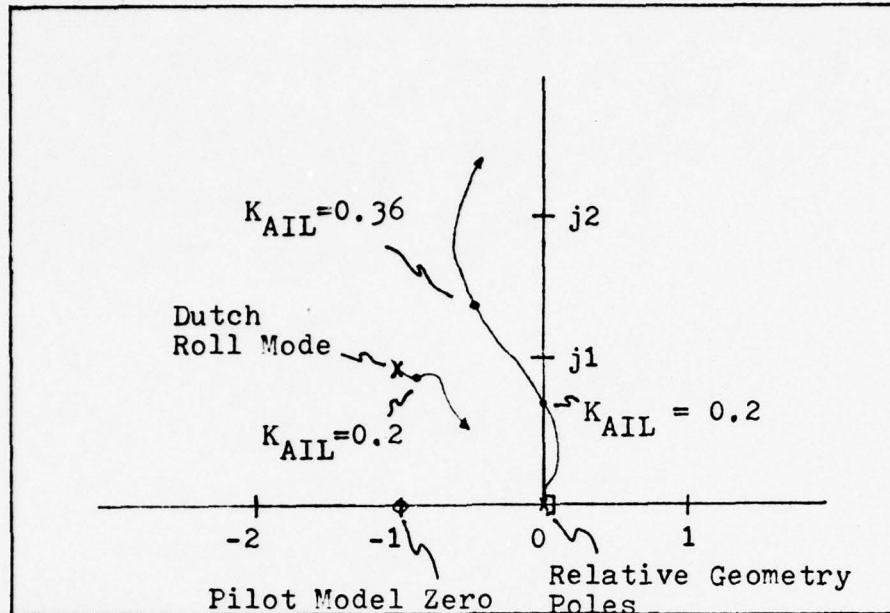
Figure 14. Partial Root Locus for Closed Loop
Lateral System.

the minimum value of K_{PE} for stability is $K_{PE} = 0.5$. As K_{PE} is increased, the complex poles due to the aircraft short period mode move toward the imaginary axis. The value of K_{PE} for which the root locus branch due to the aircraft short period crosses the imaginary axis is the crossover gain, K_{CO}. From Figure 13, this value is $K_{PE} = K_{CO} = 1.5$. The nominal gain value chosen for the simulation analysis was $K_{PE} = 1.0$.

In the lateral pilot model, the value of K_{AIL}, the lateral pilot transmission gain, must be set high enough to stabilize the complex poles resulting from the relative geometry of the encounter (Ref 14: 55). By removing the deadzone $DZ_{\dot{e}_{LW}}$ from the lateral pilot model and assuming K_{φ}

and K_{RUD} to be zero, the transfer function from traverse tracking error to lateral force command is

$$\frac{F_{LAT}}{e_{LW}} = \frac{K_{AIL}(s + K_{RTR})}{\tau_T s + 1} \tag{74}$$

With the parameters set to nominal values, a root locus for the closed loop lateral system was determined as a function of K_{AIL}. A partial root locus for the lateral system is shown in Figure 14. The open loop relative geometry poles at $s = 0$ move into the right half s-plane and then back toward the zero at $s = -K_{RTR}$ as the value of K_{AIL} is increased. The minimum value of K_{AIL} for system stability is $K_{AIL} = 0.2$. For the simulation analysis, a value of $K_{AIL} = 0.36$, which corresponds to the maximum recommended value in Table I, was used as the nominal value.

Figure 15 is a block diagram of the pilot model used in the F-106/Fire Fly director gunsight simulation. The parameter values shown in each block of the figure are the nominal values which were used for the simulation. Two adjustments were made to the pilot model structure. First, the contribution of the differential bank angle portion of the lateral pilot model was converted to degrees for proper dimensionality. Second, the output force commands, F_{LON}, F_{LAT}, and F_{RUD}, which were given in units of pounds in the TAWDS model, were assumed to be multiplied by a gain of one degree/pound before being fed to the aircraft flight
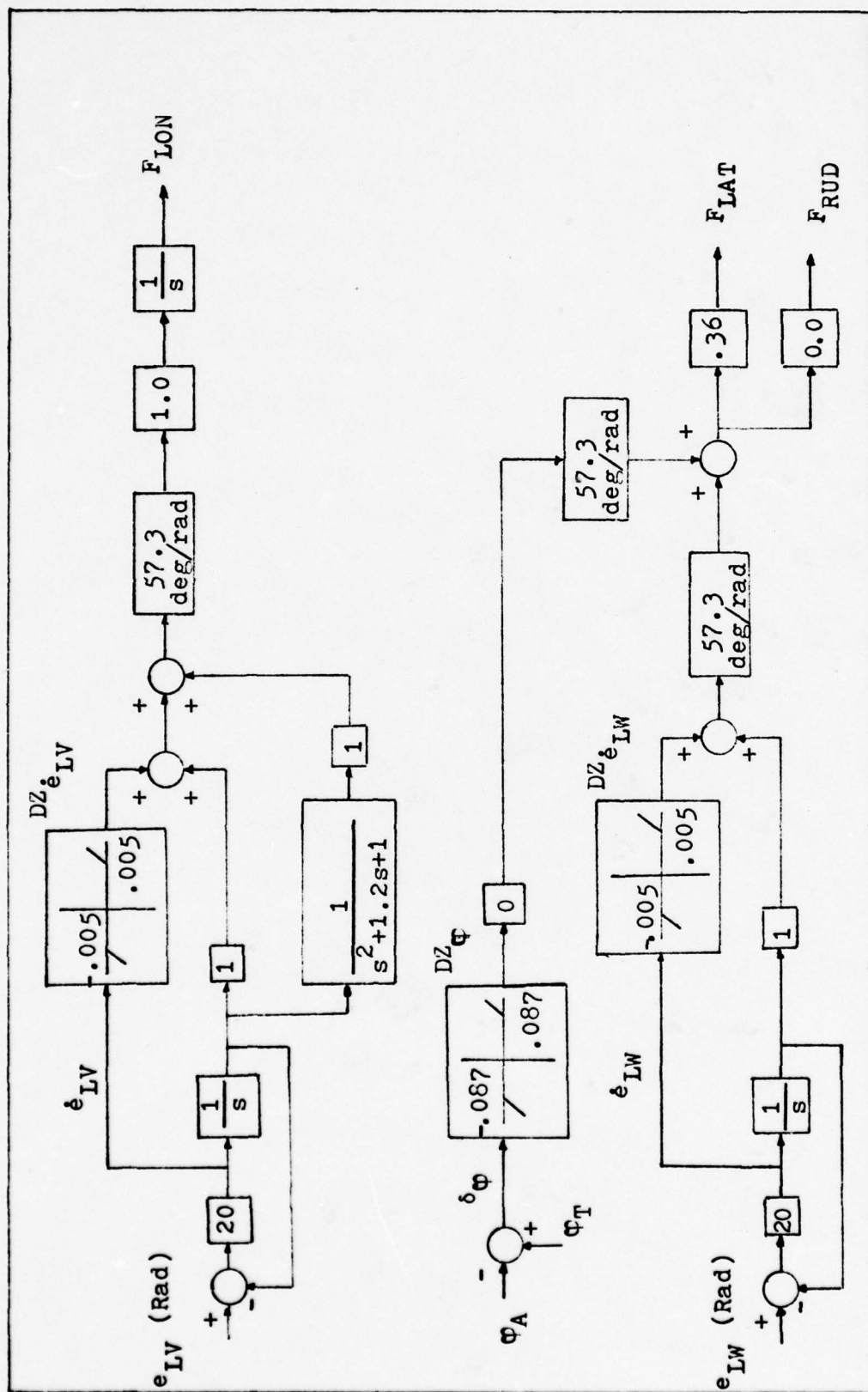
Figure 15. F-106 Multi-Axis Pilot Model for Air-to-Air Gunnery (Nominal Parameter Values).

56

control system.

The simulation results are discussed in the next chapter.
Tracking error time histories are determined against targets
in straight and level flight, and 30, 60, and 70 degree bank
turns. In addition, the effects of changing the pilot
model parameter values are demonstrated.

V. <u>Simulation</u> <u>Results</u>

<u>Introduction</u>

In Chapter Two, the basic equations of the Fire Fly
director gunsight system were developed. Chapter Three
presented the nonlinear equations of motion which describe
the F-106B aircraft. In Chapter Four, an analytical pilot
model for air-to-air gunnery was developed for the F-106.
Thus, the necessary elements for a closed loop digital
simulation have been presented. The simulation was conducted
using the EASY Dynamic Analysis Programs. The closed loop
system, including the equations necessary to describe the
motion of the target, was modeled using the EASY Model
Generation Program. A complete listing of the closed loop
model, and a discussion of the modeling procedure, can be
found in Appendix A. The EASY Analysis Program was used for
the time simulation of manually controlled air-to-air gunnery,
the results of which are presented below.

The objectives of the simulation effort were to
evaluate the terminal air-to-air gunnery tracking performance
of the F-106 configured with the Fire Fly manual director
gunsight, and to adapt the TAWDS multi-axis pilot model for
use in closed loop simulation analysis. In addition, the
usefulness of the EASY programs for modeling and simulation
of dynamic, nonlinear closed loop systems was demonstrated.

At the beginning of each simulation run, the attacking
aircraft was trimmed for constant altitude flight at 10,000

feet, at a speed of Mach .8, and with an initial bank angle
equal to that of the target. This initial trim condition
caused the stick forces at the beginning of each simulation
run to be zero. The initial position of the target with
respect to the attacker was set so that the elevation and
traverse tracking errors were near zero. The initial angle-
off of the target with respect to the attacker was less than
two degrees for each simulation run. The initial target
range was set at 2000 feet and the target speed remained
constant at Mach .8. The target maneuvers consisted of
constant altitude, constant bank angle, constant rate turns.
Range variations for each 10 second simulation were less
than 250 feet, and the maximum angle-off encountered was
10 degrees.

The discussion of the simulation results is divided
into two sections. In the first section, the results of
simulation runs against targets in straight and level flight,
and in constant rate turns of 30, 60, and 70 degrees of bank
are discussed. These simulation runs were conducted using
the nominal pilot model parameter values as determined in
Chapter Four. In the second section, pilot model parameter
values are varied to demonstrate the effects of these
variations on tracking performance.

Simulation results are presented as time history plots
of elevation and traverse tracking errors and the corresponding
longitudinal and lateral pilot stick forces. In accordance
with the conventions specified in Chapter Two, positive

elevation tracking error is decreased by positive pitch rate; that is, by positive rotation about the body-fixed $\bar{v}$ axis, as given by the right hand rule. Positive traverse tracking error is decreased by positive yaw rate; that is, by positive rotation about the body-fixed $\bar{w}$ axis, as given by the right hand rule. Positive longitudinal stick force is defined as aft stick, the direction of stick movement required to produce positive pitch rate. Positive lateral stick force is defined as movement of the stick to the pilot's right, and positive rudder pedal force is defined as right rudder pedal deflection.

Tracking Response with Nominal Pilot Model Parameter Values

In this section, the tracking performance of the F-106/ Fire Fly director gunsight is discussed. Target maneuvers consisted of straight and level flight, and constant altitude, constant rate turns at 30, 60, and 70 degrees of bank. The nominal pilot model parameter values, as determined in Chapter Four, were used for the simulation runs presented in this section. A listing of the nominal parameter values is presented in Table II. The nominal values were not chosen to obtain the best tracking performance, but were selected to be within the range of values recommended in the TAWDS programs.

The discussion in Chapter Two indicated that for the target maneuvers simulated in this thesis, the time required for the Kalman filter to process target state information has a negligible effect on tracking performance.

Table II. Nominal Pilot Model Parameters

Longitudinal Parameters	K_{PE}	K_L	K_R	τ_E	$DZ_{\dot{e}_{LV}}$	(ζ_n, ω_n)
Nominal Values	1.0	1.0	1.0	0.05	5.0 mr/sec	0.6,1.0

Lateral Parameters	K_{AIL}	K_{RTR}	K_{RUD}	K_φ	τ_T	$DZ_{\dot{e}_{LW}}$	DZ_φ
Nominal Values	0.36	1.0	0.0	0.0	0.05	5.0 mr/sec	5.0 deg

This fact is illustrated by comparing the tracking error time histories for a target in a 60 degree bank turn with the time histories for the same target maneuver, but with a simple lag transfer function with a time constant of one second inserted into the model to simulate the information processing delay. Figures 16 and 17 depict the tracking error time histories with no delay, and Figures 18 and 19 show the time histories with the one second delay. Since the error time histories are identical, the effects of the information processing delay for the assumed filter model are neglected for the remainder of the simulation runs.

A strict judgement as to whether the tracking error time histories presented in this section are actually similar to those which would be obtained by a human pilot flying the

Figure 16. Elevation Tracking Error and Stick Force vs. Time for 60 Deg Bank Target/ Nominal Pilot Model Gains/No Processing Delay.

62

Figure 17. Traverse Tracking Error and Stick Force vs. Time for 60 Deg Bank Target/ Nominal Pilot Model Gains/No Processing Delay.

Figure 18. Elevation Tracking Error and Stick Force vs. Time for 60 Deg Bank Target/ Nominal Pilot Model Gains/1.0 Sec Processing Delay.
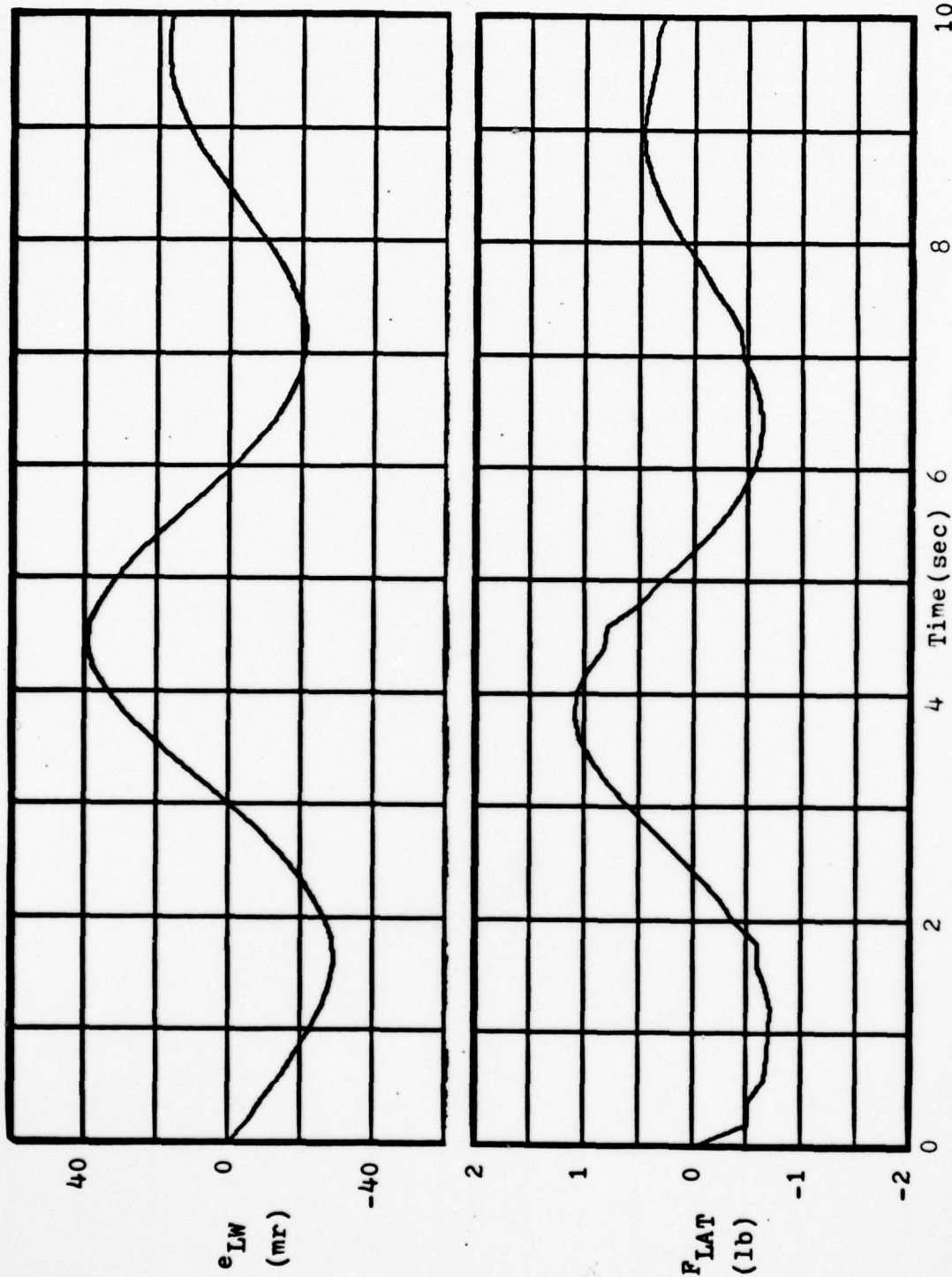
Figure 19. Traverse Tracking Error and Stick Force vs. Time for 60 Deg Bank Target/ Nominal Pilot Model Gains/1.0 Sec Processing Delay.

65

same aircraft/sight configuration against the same targets,
cannot be made until actual man-in-the-loop simulation data
is available for comparison. However, the tracking error
time histories in this section demonstrate the type of
tracking response predicted by McAir (Ref 6: 66-69). The
elevation error response contains two frequency components.
The high frequency component is most apparent in the first
four seconds of each simulation run, while the low frequency,
lightly damped component is clearly present throughout the
time histories. The traverse tracking error response
consists of a single frequency component which has a period
of five to nine seconds. The most significant difference
between the tracking error time histories obtained in this
section and those illustrated in Reference 6, is in the magni-
tude of the tracking errors, particularly the traverse track-
ing error. The error magnitudes are dependent, at least to
some degree, on the pilot model parameter values, as will be
demonstrated later in the chapter.

The longitudinal and lateral pilot stick force time
histories depict the relative stick forces applied by the
pilot model where the reference trim stick forces in both
the longitudinal and lateral axes are zero.

The tracking error time histories and corresponding
stick forces for a 60 degree bank target were shown in
Figures 16 and 17. Figures 20 and 21 present plots for the
same target, but with the simulation time extended to 20
seconds to illustrate the limit cycle type of tracking error
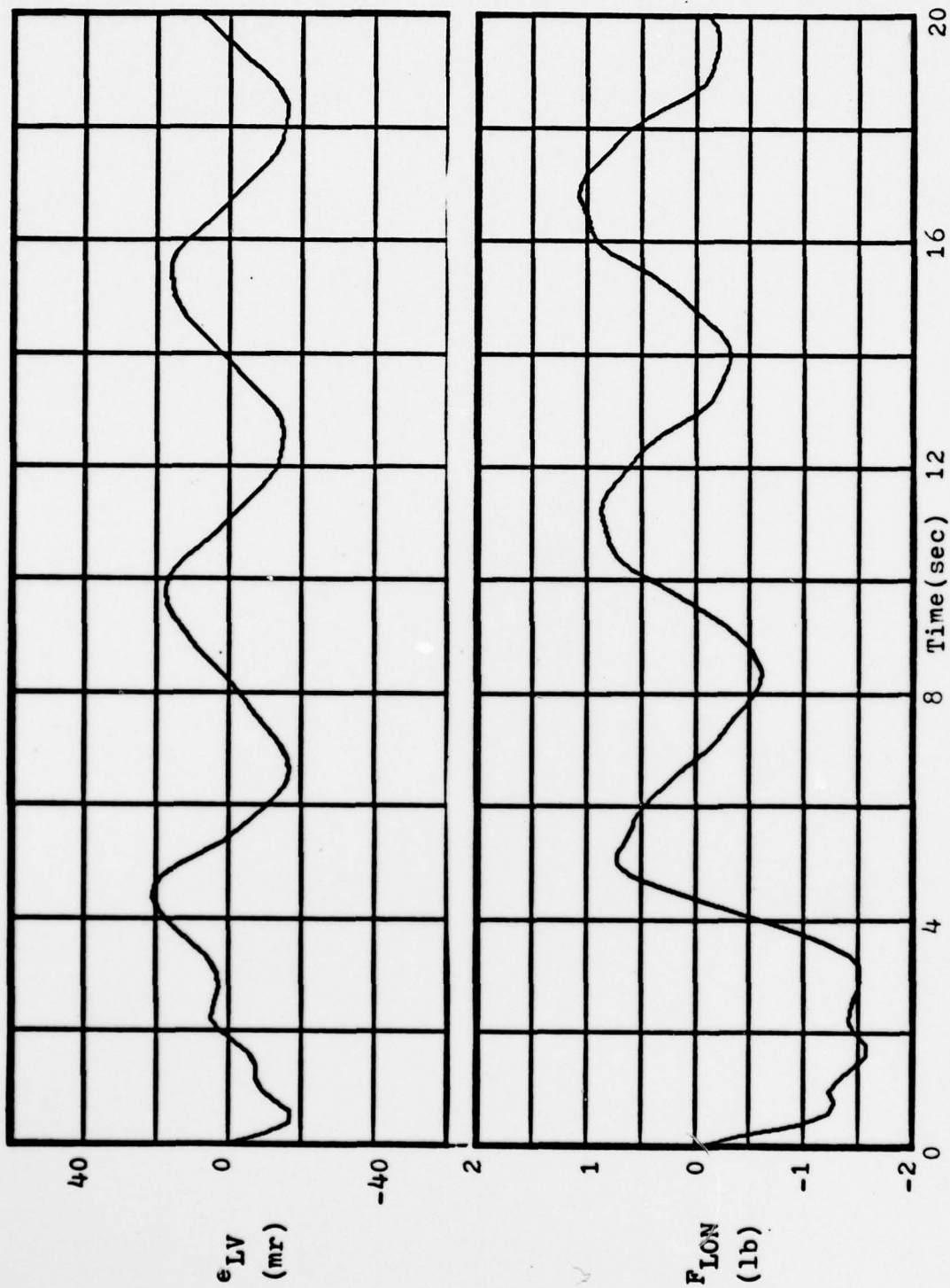
Figure 20. Elevation Tracking Error and Stick Force vs. Time for 60 Deg Bank Target/ Nominal Pilot Model Gains/20 Sec Simulation.
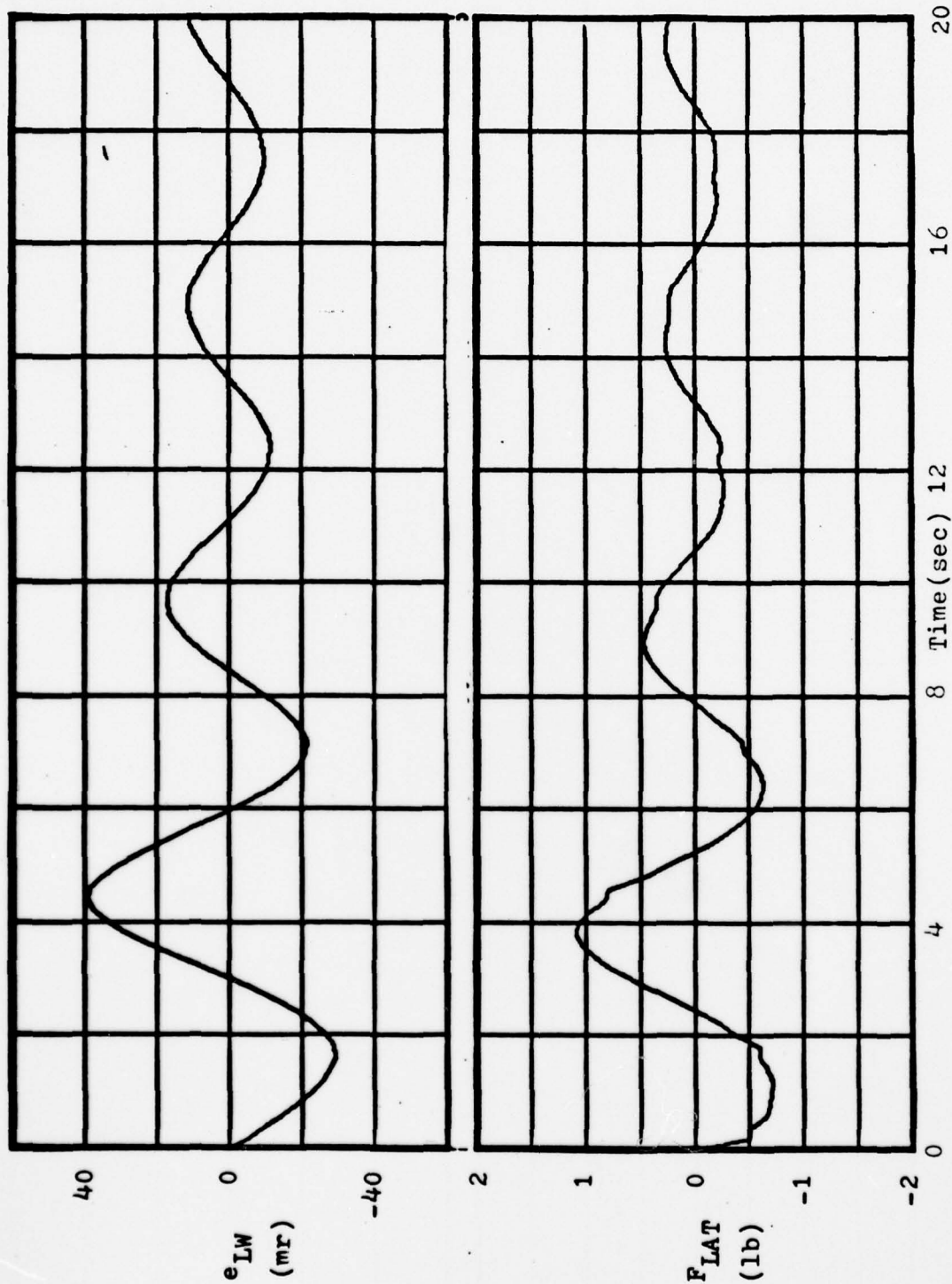
Figure 21. Traverse Tracking Error and Stick Force vs. Time for 60 Deg Bank Target/ Nominal Pilot Model Gains/20 Sec Simulation.

68

response over the longer tracking period. Figures 22 and 23 show the tracking error and stick force responses for a 70 degree bank target. It should be noted that the scale for plotting the longitudinal stick force time history for the 70 degree bank target in Figure 22 is doubled.

Tracking error and stick force time histories for a 30 degree bank target are shown in Figures 24 and 25. The traverse tracking error response depicted in Figure 25 diverges because with the value of K_{RTR} in the pilot model set to 1.0 as in Table II, the lateral closed loop system is unstable. The instability can be corrected by reducing the value of K_{RTR} to 0.5. This moves the closed loop zero in the lateral pilot model closer to the s-plane origin and thus pulls the unstable closed loop poles back into the left half s-plane.

For a target in straight and level flight, the F-106/ Fire Fly manual director gunsight system tracks to within one milliradian in both elevation and traverse during a 10 second simulation. The longitudinal and lateral stick forces are negligible. Thus, plots of error time histories and stick forces for a straight and level target are omitted.

The simulation time history plots presented in this section indicate that the tracking responses for targets in 60 and 70 degrees of bank are stable when the pilot model parameter values are set to the nominal values shown in Table II. Tracking response for a target in 30 degrees of bank is stable in elevation tracking and will be stable in
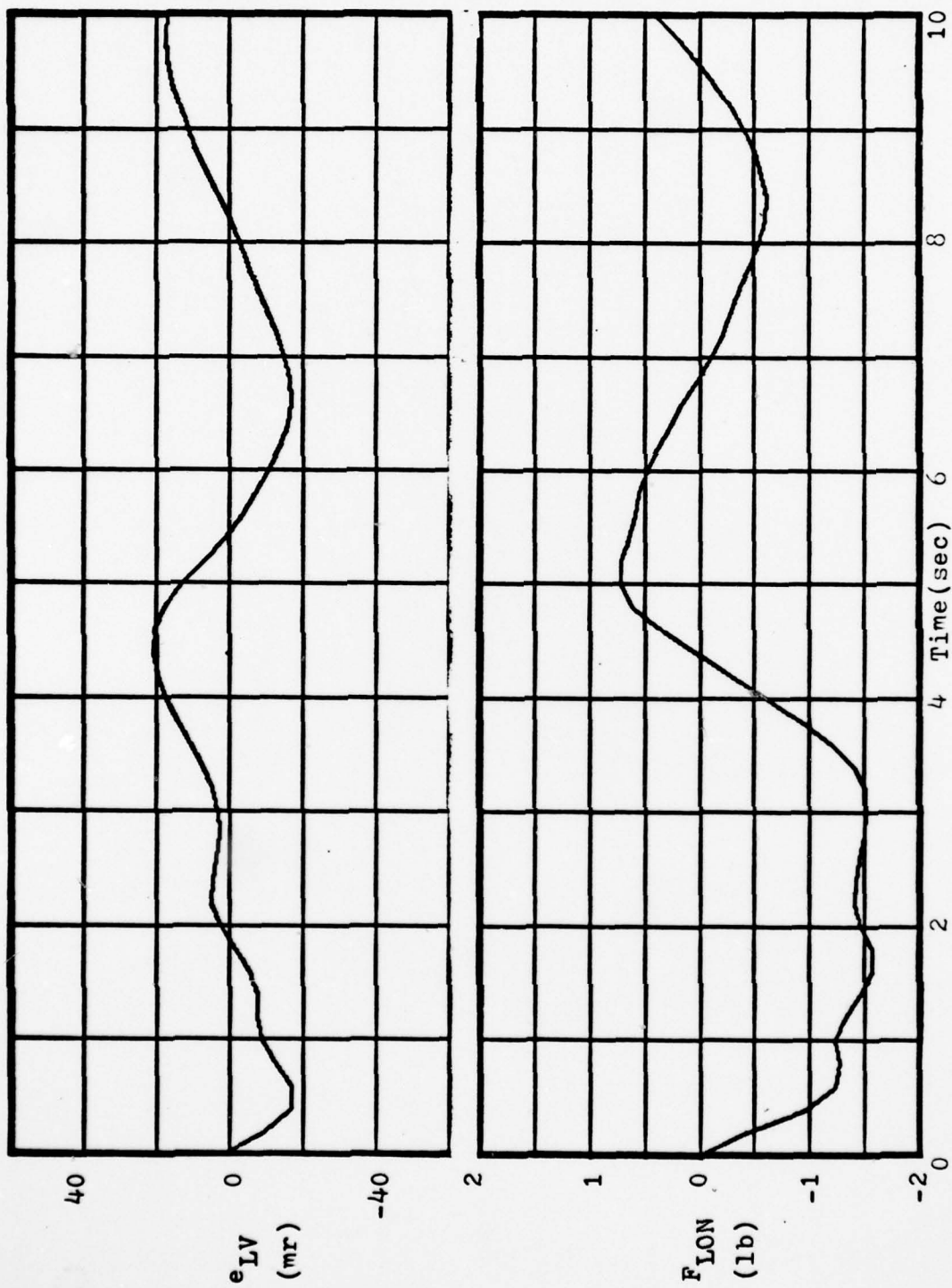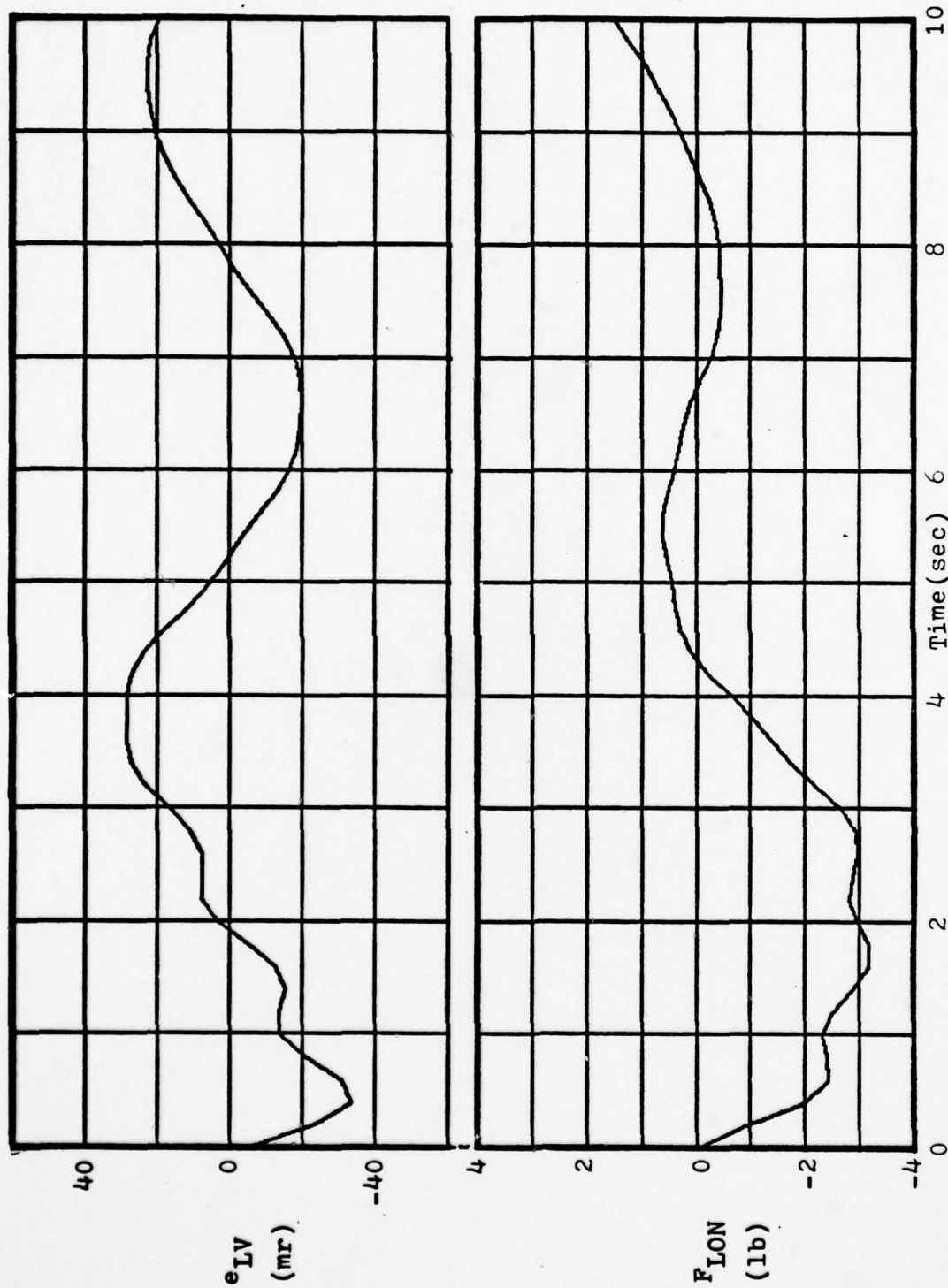
Figure 22. Elevation Tracking Error and Stick Force vs. Time for 70 Deg Bank Target/
Nominal Pilot Model Gains.
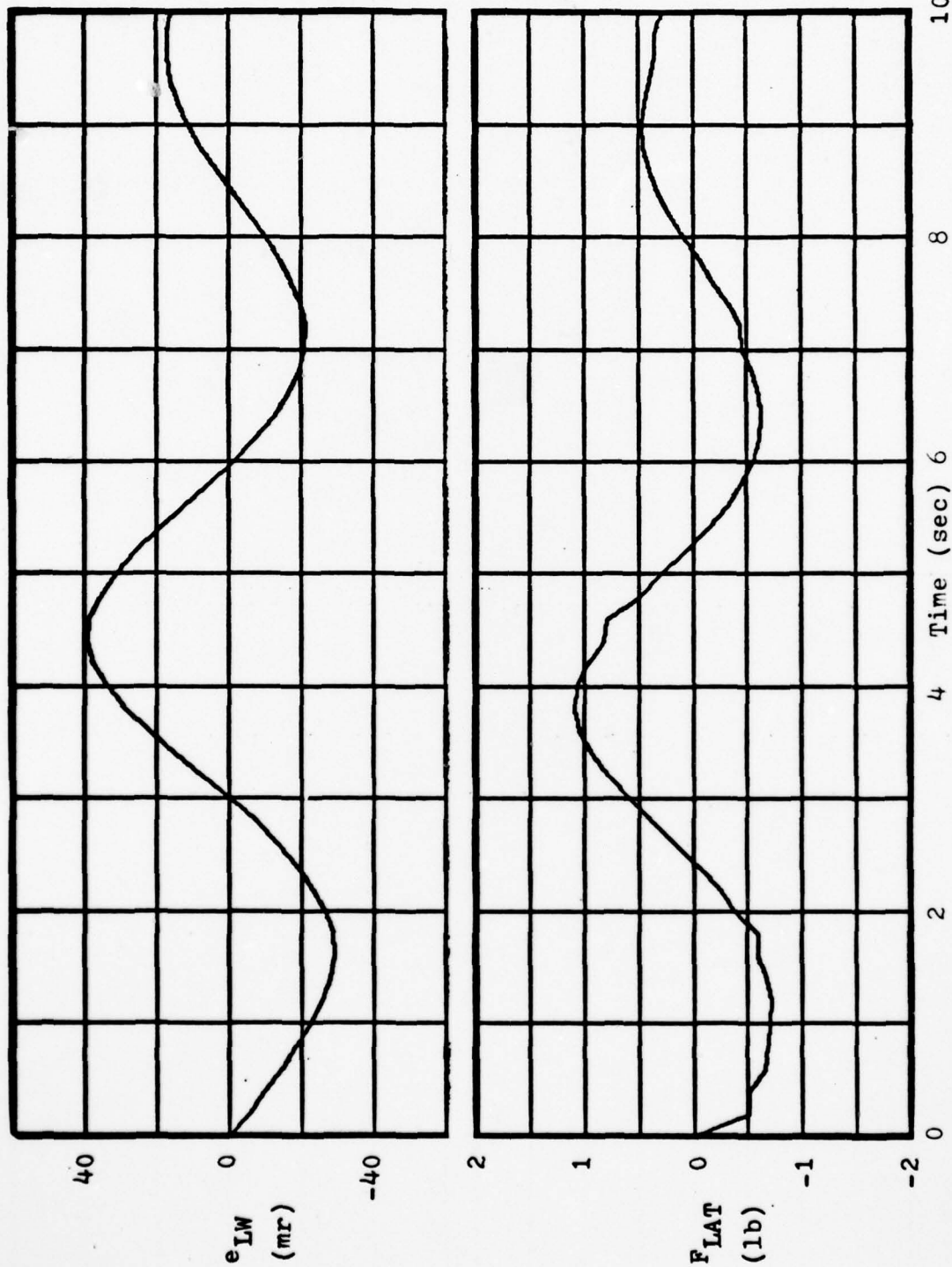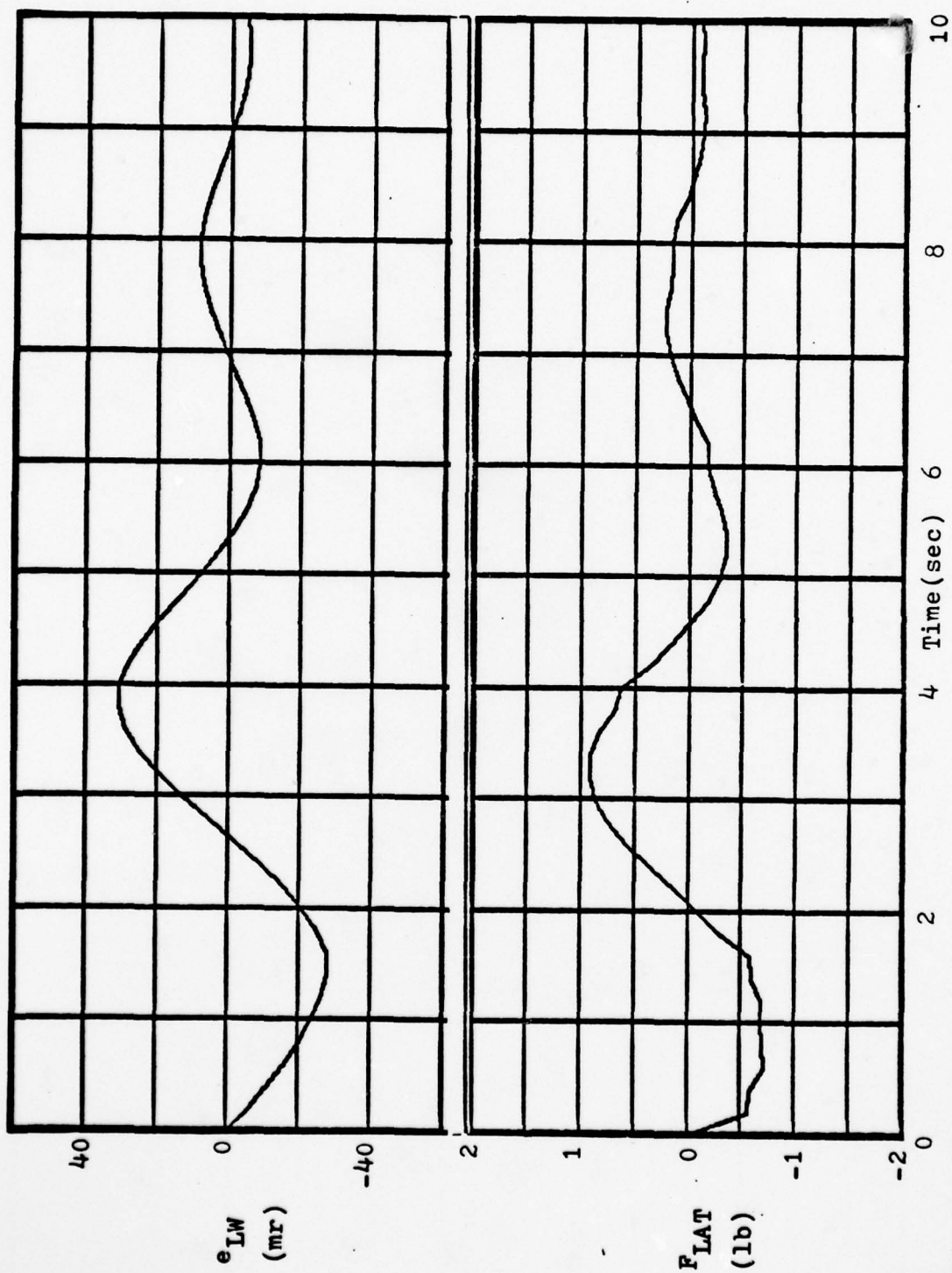
Figure 23. Traverse Tracking Error and Stick Force vs. Time for 70 Deg Bank Target/Nominal Pilot Model Gains.

71

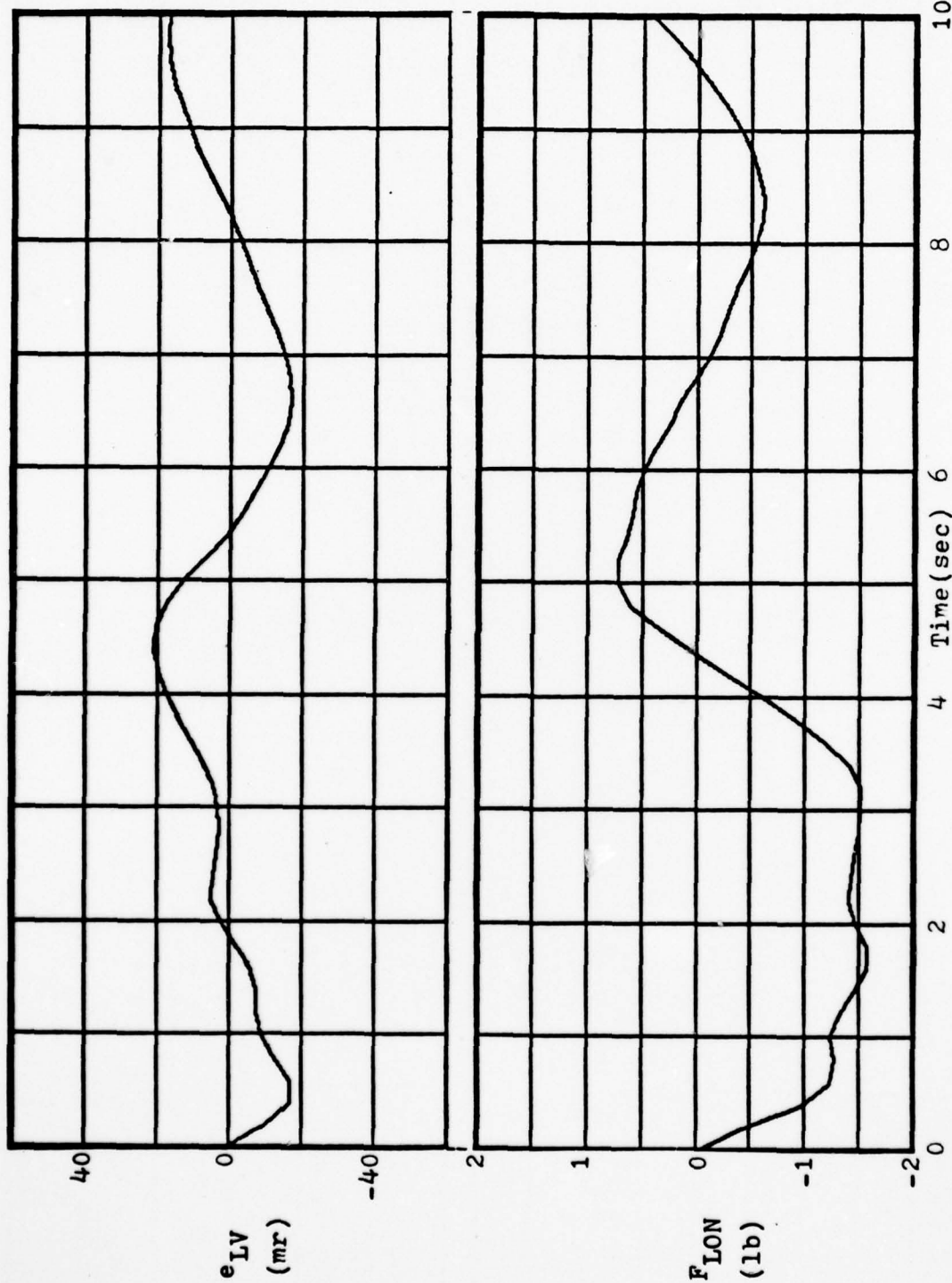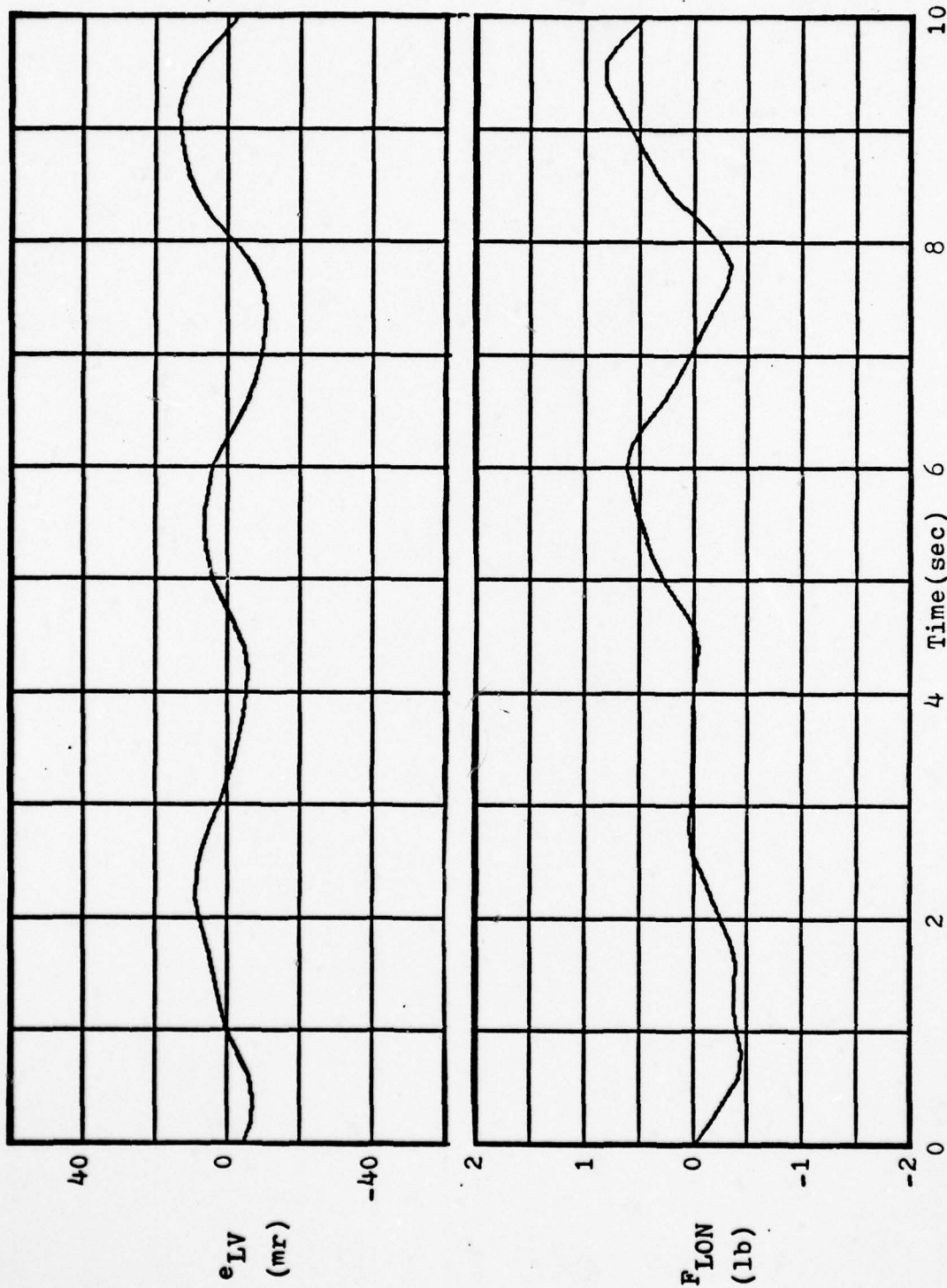**Figure 24.** Elevation Tracking Error and Stick Force vs. Time for 30 Deg Bank Target/ Nominal Pilot Model Gains.

72

Figure 25. Traverse Tracking Error and Stick Force vs. Time for a 30 Deg Bank Target/ Nominal Pilot Model Gains.

73

traverse tracking if the value of K_{RTR} is set to 0.5. These
tracking responses must be compared to the tracking responses
obtained in man-in-the-loop simulations with the same aircraft/
sight configuration to determine their true validity, but
the tracking responses obtained here do exhibit the same
structure as those obtained in the TAWDS program. In the
next section, the nominal pilot model parameter values are
varied in simulation runs against targets in 60 degree bank
turns.

Tracking Error Response with Varied Pilot Model Parameters

In this section several of the pilot model parameter
values are changed from the nominal values listed in Table II.
All simulation runs are conducted against targets in 60
degree bank turns. The longitudinal and lateral pilot
transmission gains, K_{PE} and K_{AIL}, are varied. Then, the
value of K_{RUD}, the rudder pedal force gain, is increased
from the nominal value of zero. Next, the effects of adding
differential bank angle feedback to the total pilot model are
determined. Finally, simulation runs are conducted with a
combination of different pilot model parameter values to
obtain the best tracking response. No claim is made that the
responses obtained by these final simulation runs are
indicative of the responses which can be expected with human
pilots flying the same aircraft/sight configuration. The
runs were made strictly to show the effects of parameter
value changes on the tracking response.
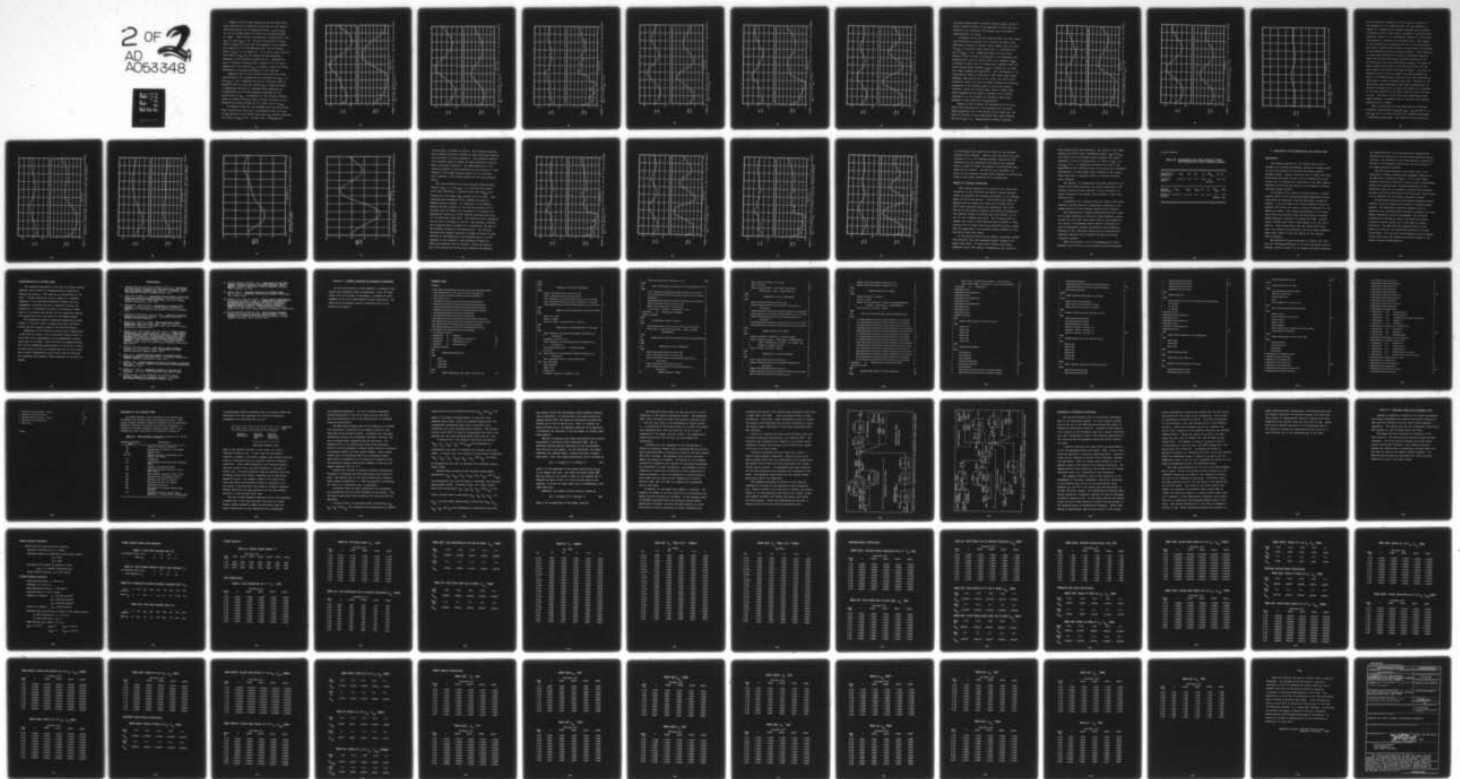
Figures 26 and 27 show tracking error and stick force
time histories for a simulation conducted with the longitu-
dinal and lateral pilot transmission gains, K_{PE} and K_{AIL},
set to the minimum values for which the tracking response
is stable. These values, as determined in Chapter Four, are
$K_{PE} = 0.5$ and $K_{AIL} = 0.2$. The plot of elevation tracking
error in Figure 26 shows that the response is very sluggish
when compared to the corresponding plot for the nominal
value of $K_{PE} = 1.0$ in Figure 16. It is noted, also, that the
lower value of K_{PE} does not excite the high frequency
component of the elevation tracking error. Comparing the
plot of traverse tracking error in Figure 27 to the corre-
sponding plot for nominal K_{AIL} in Figure 17 shows only minor
differences in magnitude and period of the response.

Figures 28 and 29 show tracking error and stick force
time histories for a simulation run conducted with $K_{PE} = 1.5$
and $K_{AIL} = 0.54$. Comparing the plot of elevation error in
Figure 28 with the plot for nominal K_{PE} in Figure 16 shows
a significant reduction in tracking error magnitude and
a predominance of the high frequency component for the
higher value of K_{PE}. A comparison of the traverse tracking
errors in Figures 29 and 17 shows a modest decrease in both
magnitude and period length for the higher value of K_{AIL}.

In Figures 30 and 31, the tracking error and stick force
time histories are shown for a run conducted with the value
of K_{PE} returned to its nominal value and K_{AIL} further increased
to a value of $K_{AIL} = 0.87$. In this case, a comparison of
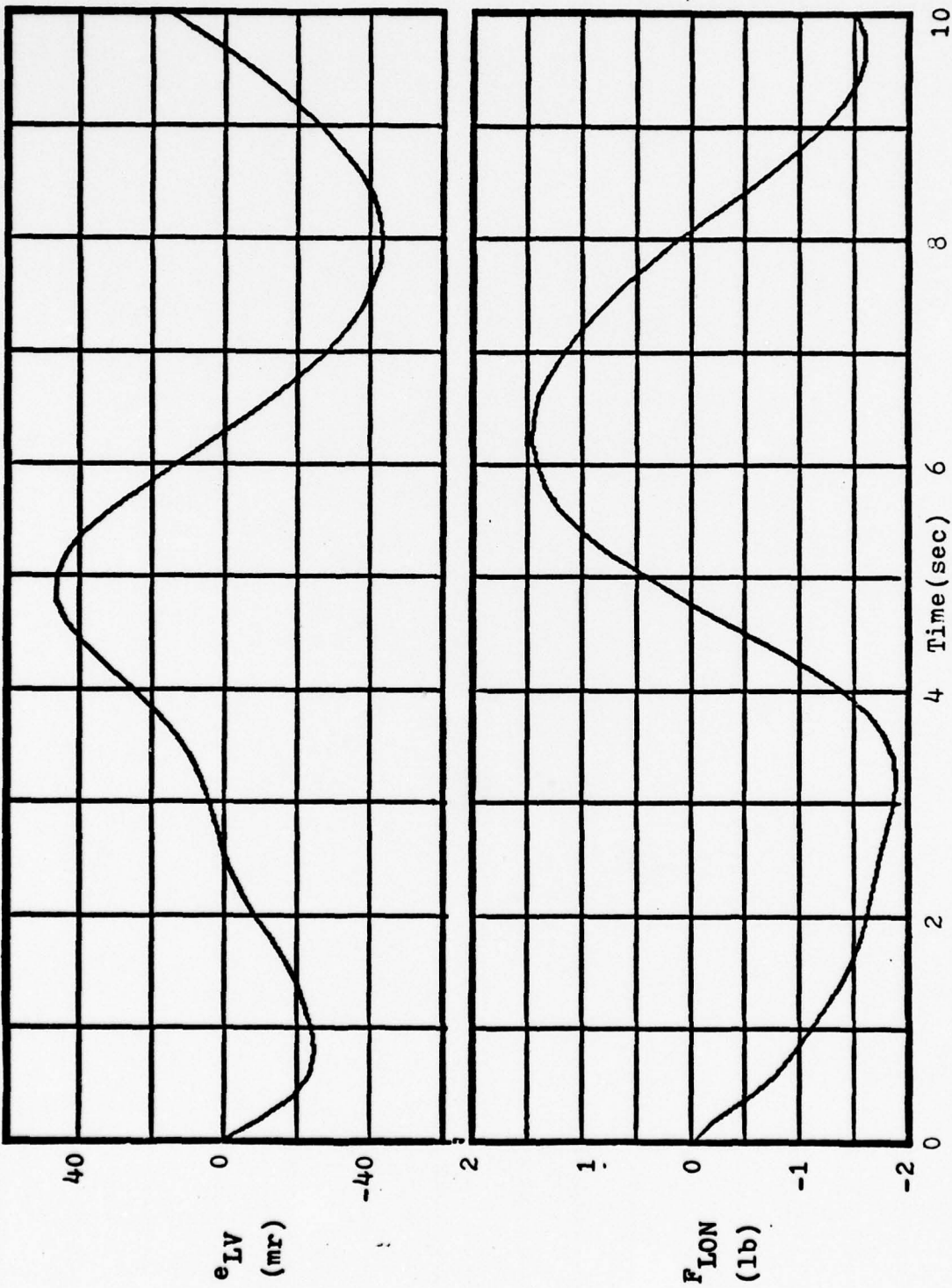
Figure 26. Elevation Tracking Error and Stick Force vs. Time for 60 Deg Bank Target/ K_{PE} = 0.5 and K_{AIL} = 0.2.
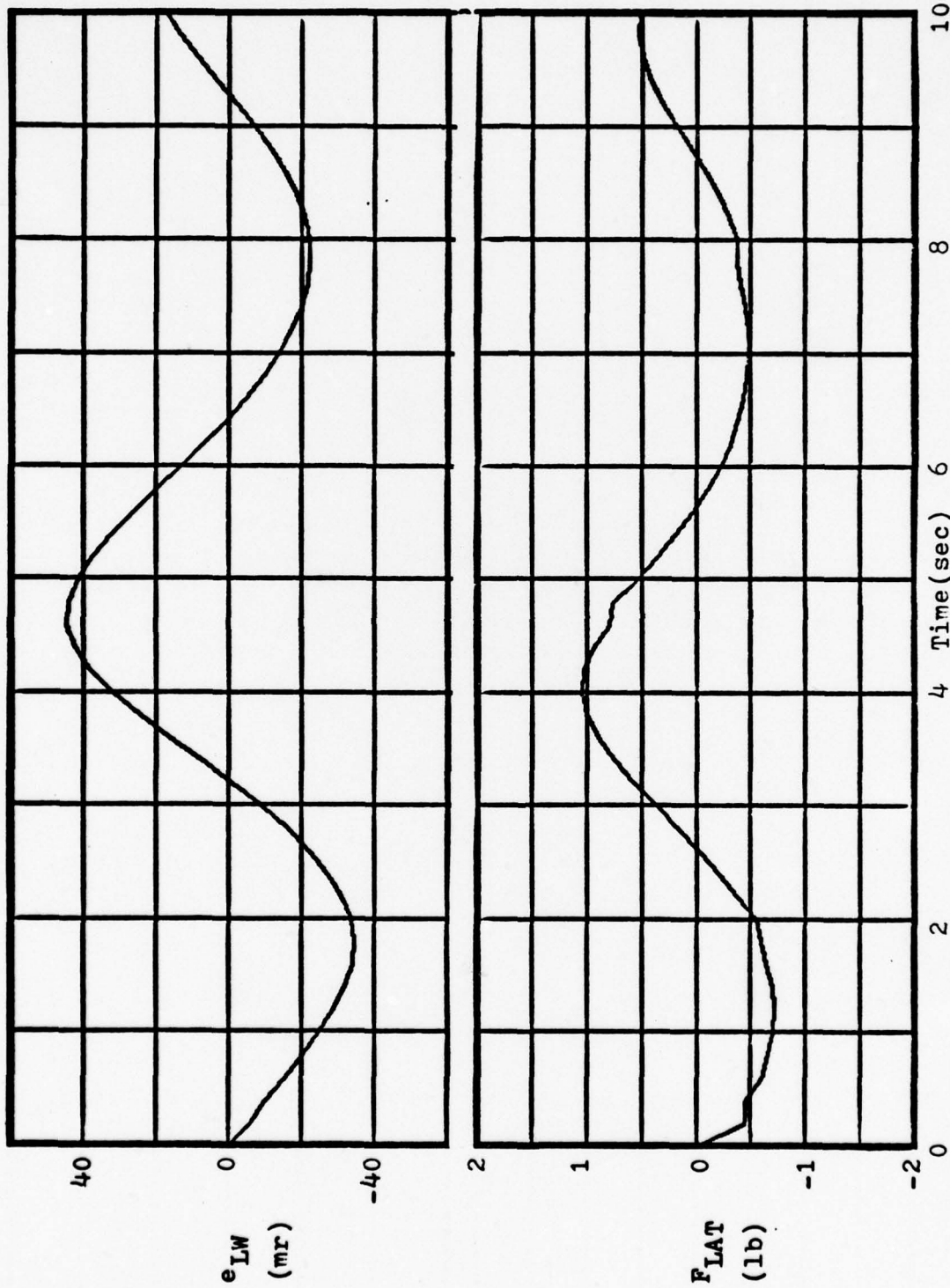
Figure 27. Traverse Tracking Error and Stick Force vs. Time for 60 Deg Bank Target/ $K_{PE} = 0.5$ and $K_{AIL} = 0.2$.

Figure 28. Elevation Tracking Error and Stick Force vs. Time for 60 Deg Bank Target/ $K_{PE} = 1.5$ and $K_{AIL} = 0.54$.

Figure 29. Traverse Tracking Error and Stick Force vs. Time for 60 Deg Bank Target/ K_{PE} = 1.5 and K_{AIL} = 0.54.

79

Figure 30. Elevation Tracking Error and Stick Force vs. Time for 60 Deg Bank Target/ K_{PE} = 1.0 and K_{AIL} = 0.87.

80

Figure 31. Traverse Tracking Error and Stick Force vs. Time for 60 Deg Bank Target/ $K_{PE} = 1.0$ and $K_{AIL} = 0.87$.

81

traverse tracking error responses between Figures 31 and 17 shows a marked decrease in the magnitude of the error and a decrease in the period of the response from 6 seconds to approximately 4.7 seconds.

In Figures 32 and 33, the tracking error and stick force time histories are plotted for a run with the pilot model parameters returned to nominal values, except that the value of K_{RUD}, the pilot's rudder pedal gain, is increased from zero to $K_{RUD} = 0.05$. Comparing Figures 32 and 33 with Figures 16 and 17 shows no difference in the tracking error responses and a plot of rudder pedal force commands (F_{RUD}) in Figure 34 shows that the rudder pedal commands follow the pilot lateral force commands (F_{LAT}) in Figure 33, but that the rudder commands are negligible. This corresponds to the claim made by McAir in Reference 6 that rudder pedal force commands, when used at all by the pilot, are used to help coordinate turns, but that the rudder commands are generally negligible in the terminal phase of air-to-air gunnery tracking. Since the sideslip angle without rudder pedal force commands did not exceed 0.5 degrees for a typical simulation run, the benefits of including rudder pedal commands in this model were insignificant.

Figures 35 and 36 depict the tracking error and stick force time histories for a run conducted with the pilot model parameters set at the nominal values except that the value of the gain on the differential bank angle feedback was set to $K_\varphi = 0.1$. Comparing the elevation tracking
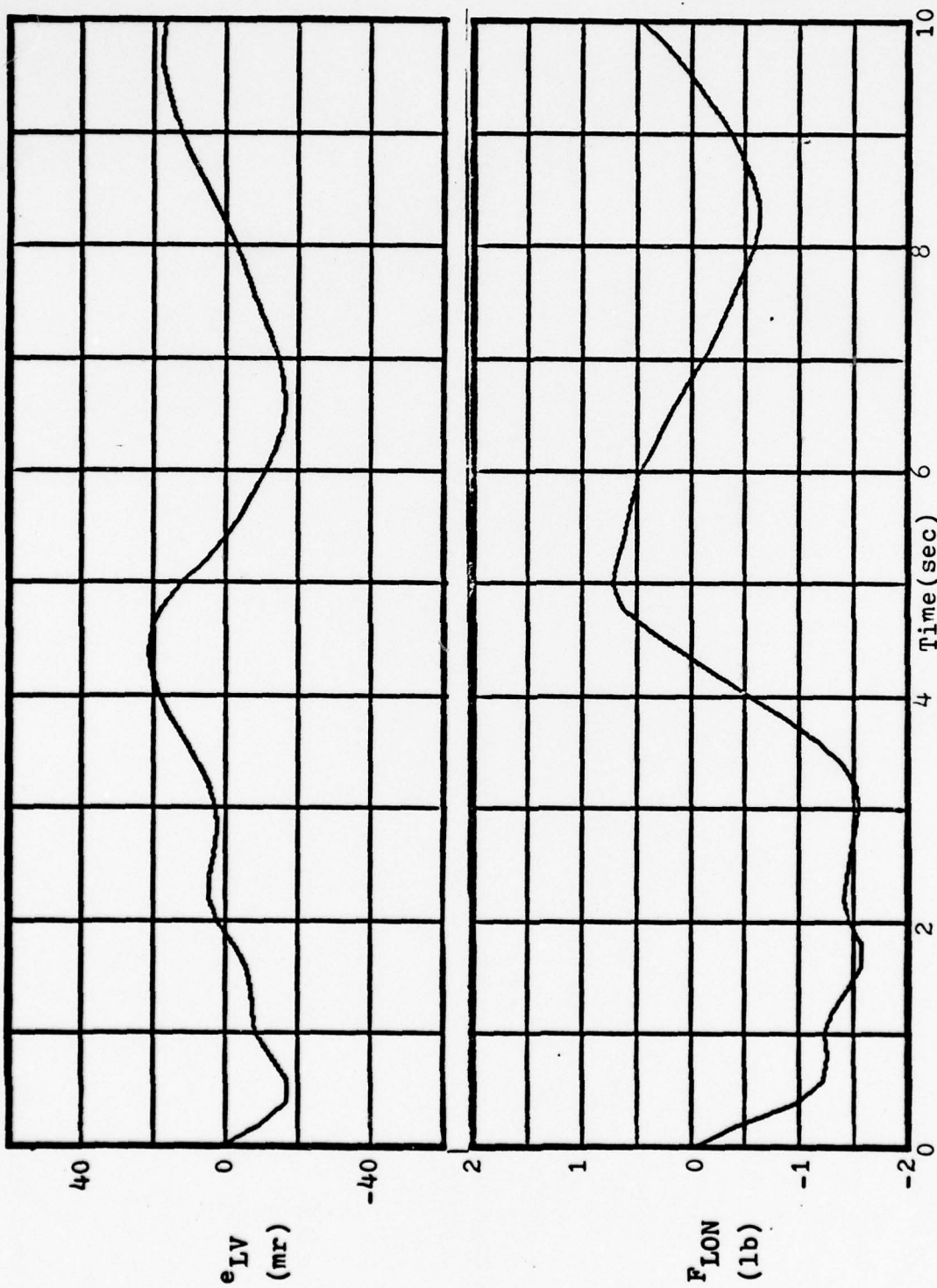
Figure 32. Elevation Tracking Error and Stick Force vs. Time for 60 Deg Bank Target/ Nominal Pilot Model Gains/ K_{RUD} = 0.05.

83
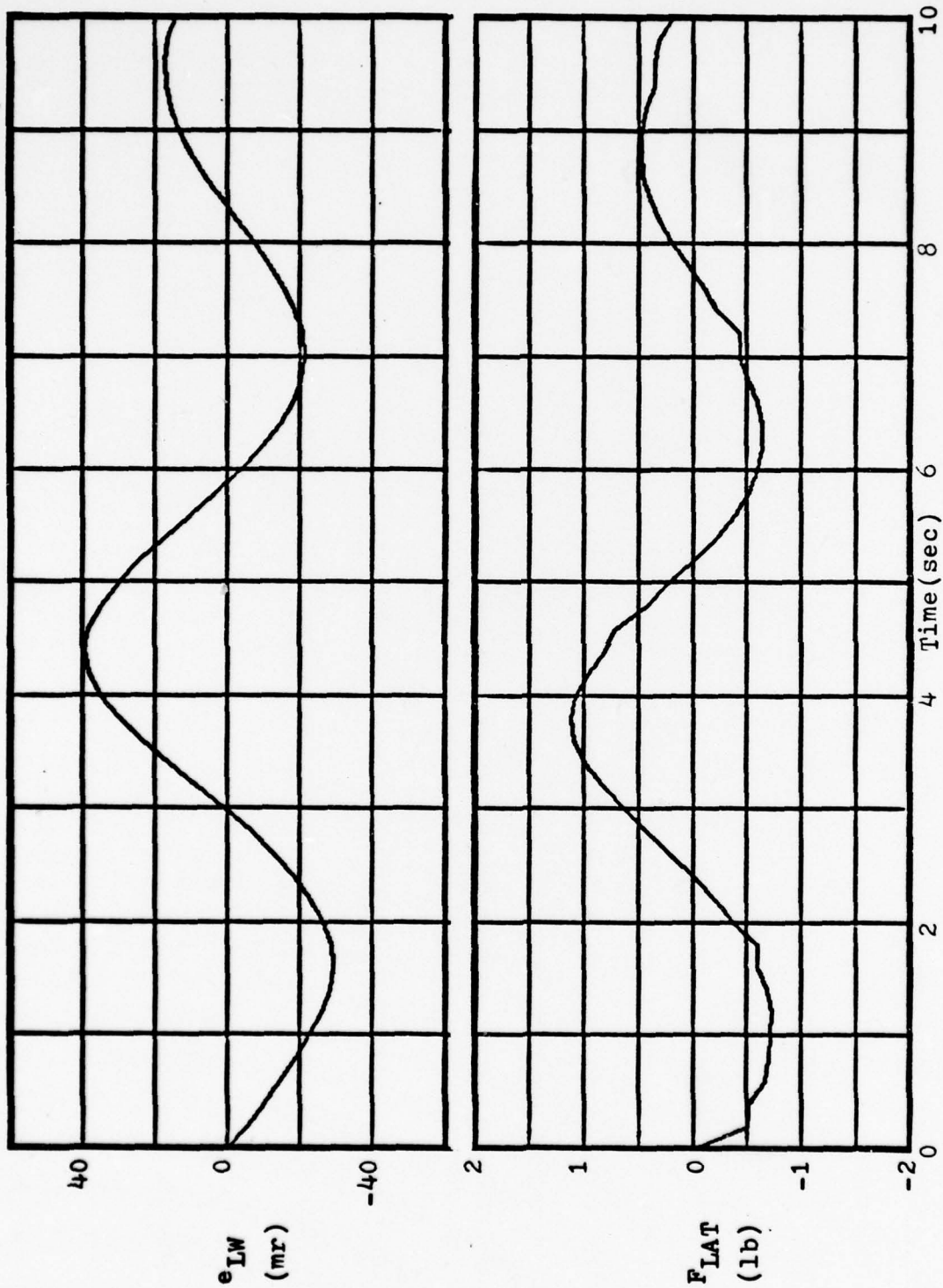
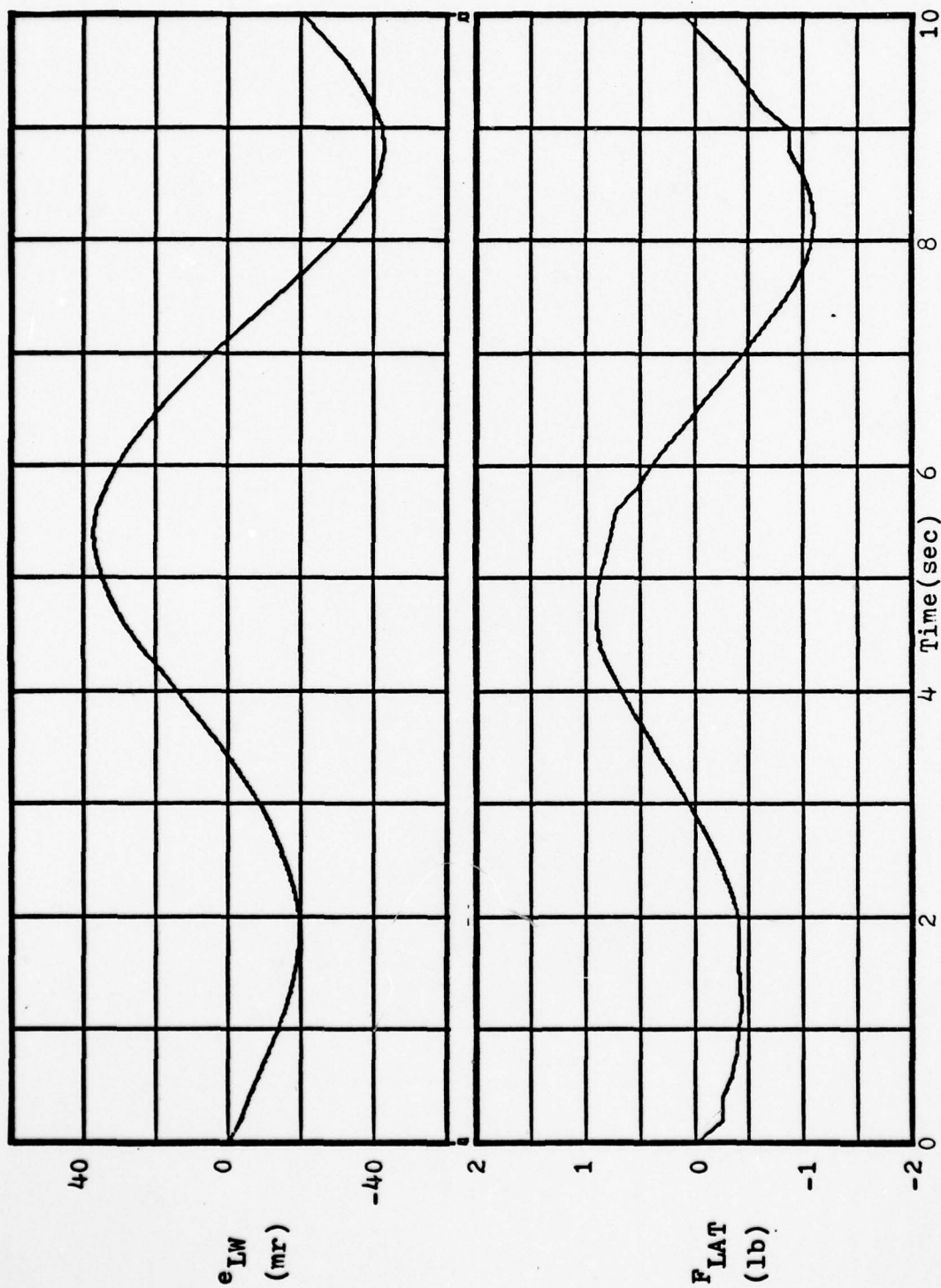**Figure 33.** Traverse Tracking Error and Stick Force vs. Time for 60 Deg Bank Target/ Nominal Pilot Model Gains/ K_{RUD} = 0.05.
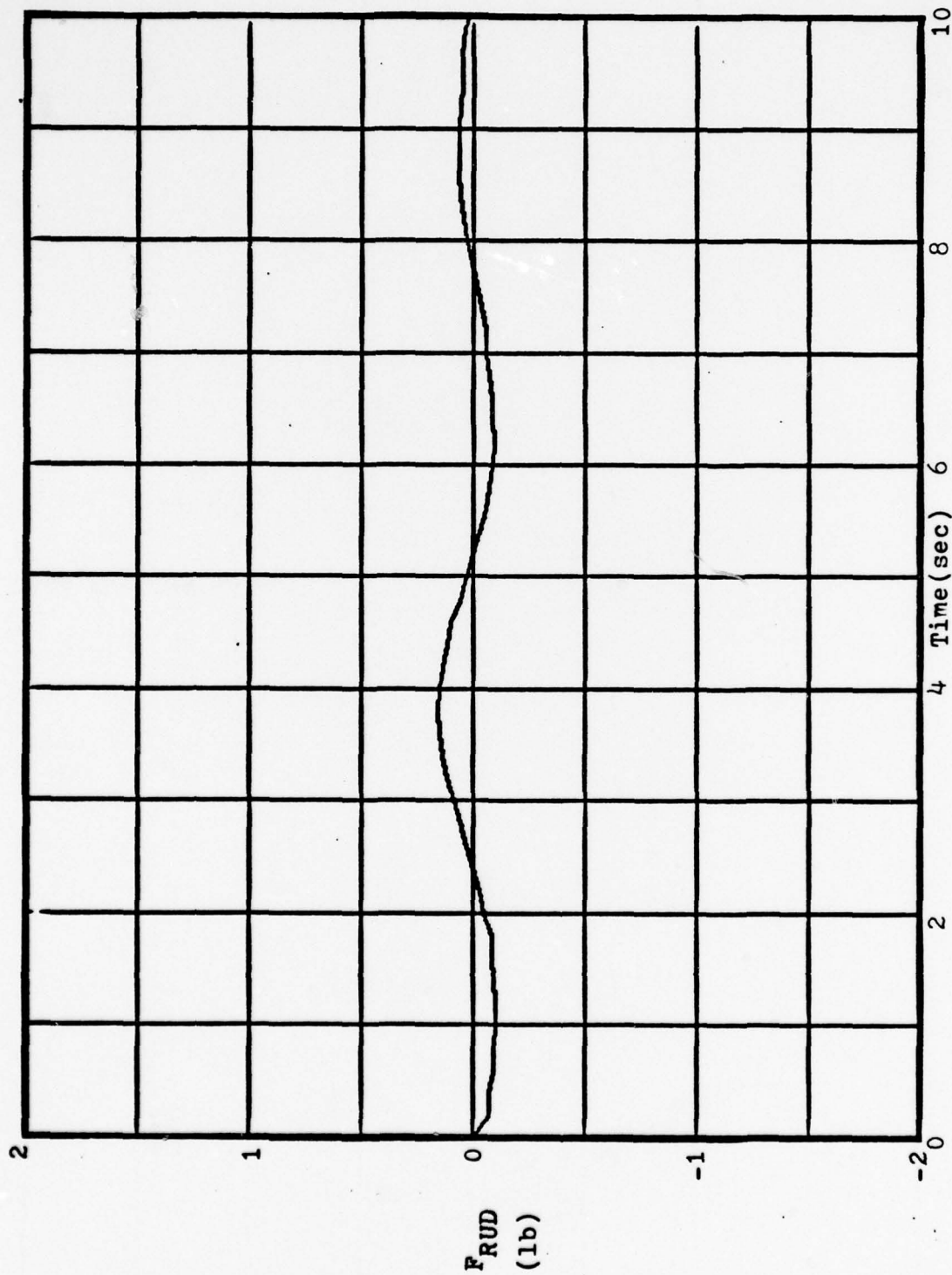
Figure 34. Rudder Pedal Force vs. Time for 60 Deg Bank Target/Nominal Pilot Model Gains/ K_{RUD} = 0.05.

85

error responses of Figures 35 ar.d 16 shows a decrease in the magnitude of the tracking errors for the response in Figure 35. Comparing the traverse tracking error responses of Figures 36 and 17 also shows a decrease in tracking error magnitude overall, but a significant increase in the initial time required to achieve zero traverse error. The changes in the tracking error responses are due to the differential bank angle feedback which reduces the bank angle oscillations of the attacker during the tracking maneuver. This reduction in bank angle oscillation is shown by comparing Figure 37, where the attacker bank angle is plotted versus time for the simulation run with differential feedback, to Figure 38 where attacker bank angle is plotted versus time for the same target, but without bank angle feedback. The plots in Figures 37 and 38 tend to support the theory advanced by McAir in the TAWDS program that the pilot uses differential bank angle to prevent excessive wing rock. However, if the pilot model uses differential bank angle feedback when the traverse tracking error is large, the result is an increase in the time required for the pilot model to drive the error to zero. Therefore, if the pilot uses differential bank angle feedback, he probably uses it only when the traverse tracking error is small.

Next, a simulation run was conducted which combined relatively high values of K_{PE} and K_{AIL}. K_{PE} was set to 1.5 and K_{AIL} to 1.0 to show the effect on tracking performance of relatively high gains. The results of this simulation

86
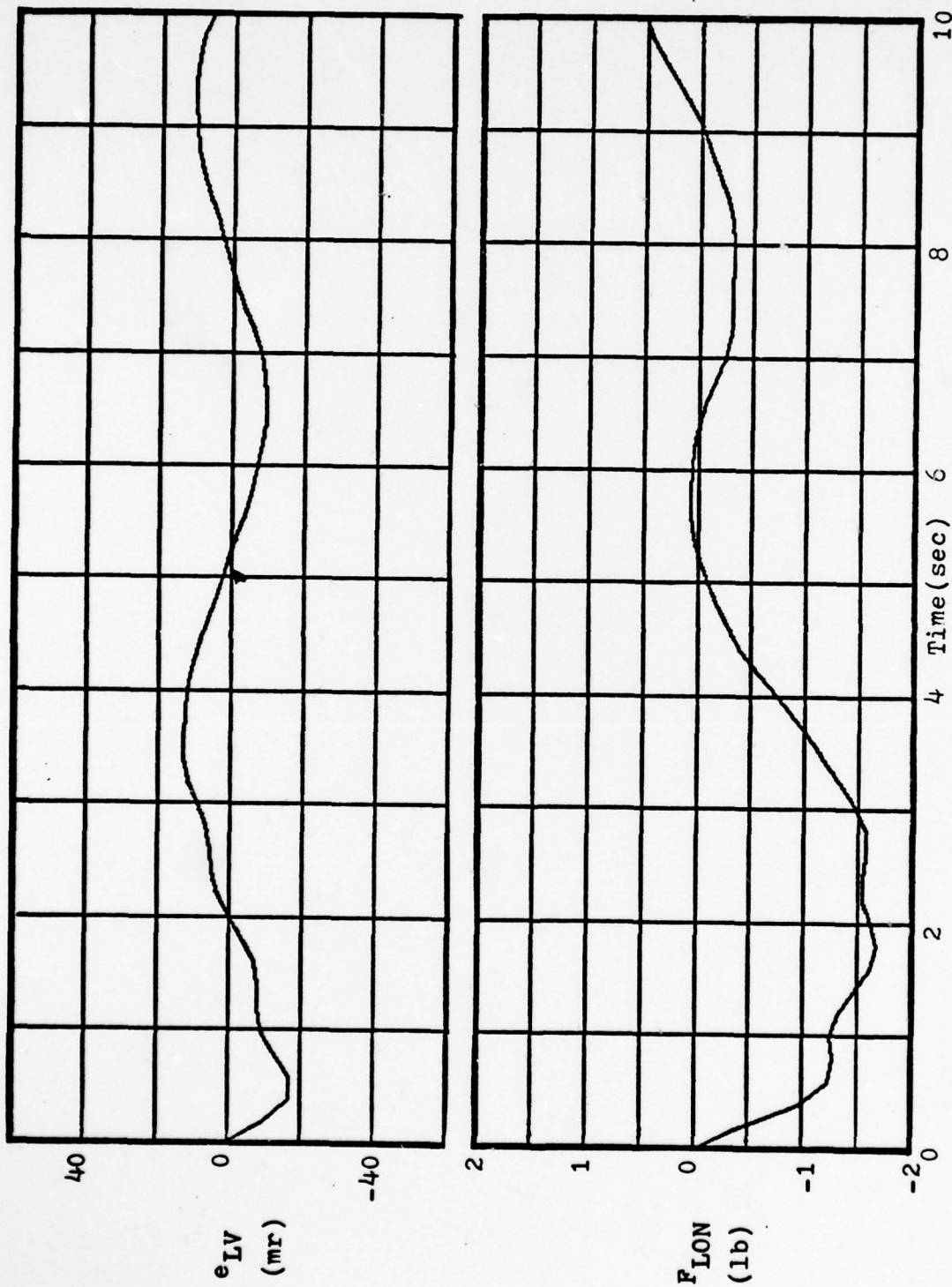
Figure 35. Elevation Tracking Error and Stick Force vs. Time for 60 Deg Bank Target/ Nominal Pilot Model Gains and Differential Bank Angle Feedback.

87
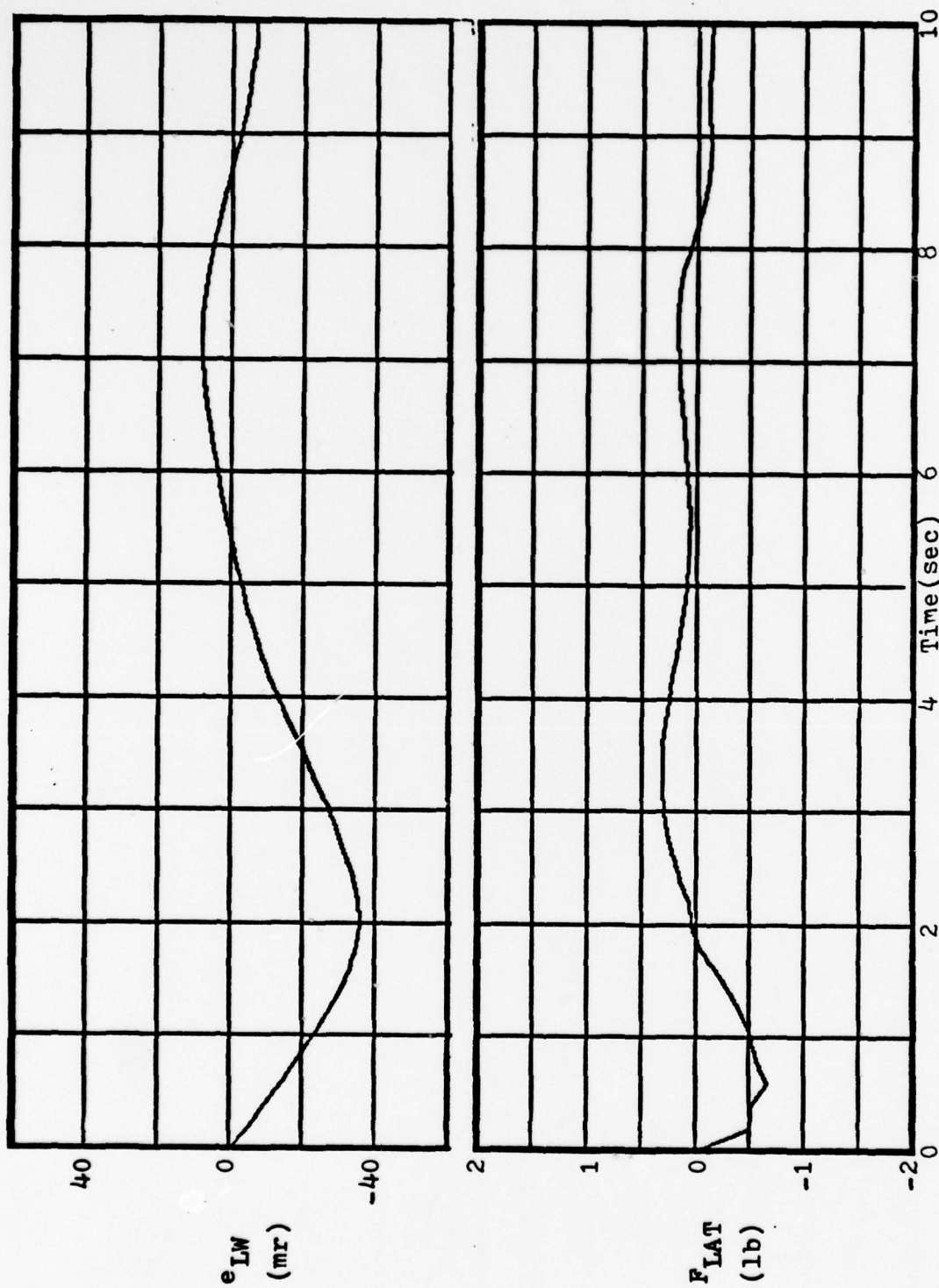
Figure 36. Traverse Tracking Error and Stick Force vs. Time for 60 Deg Bank Target/ Nominal Pilot Model Gains and Differential Bank Angle Feedback.

88
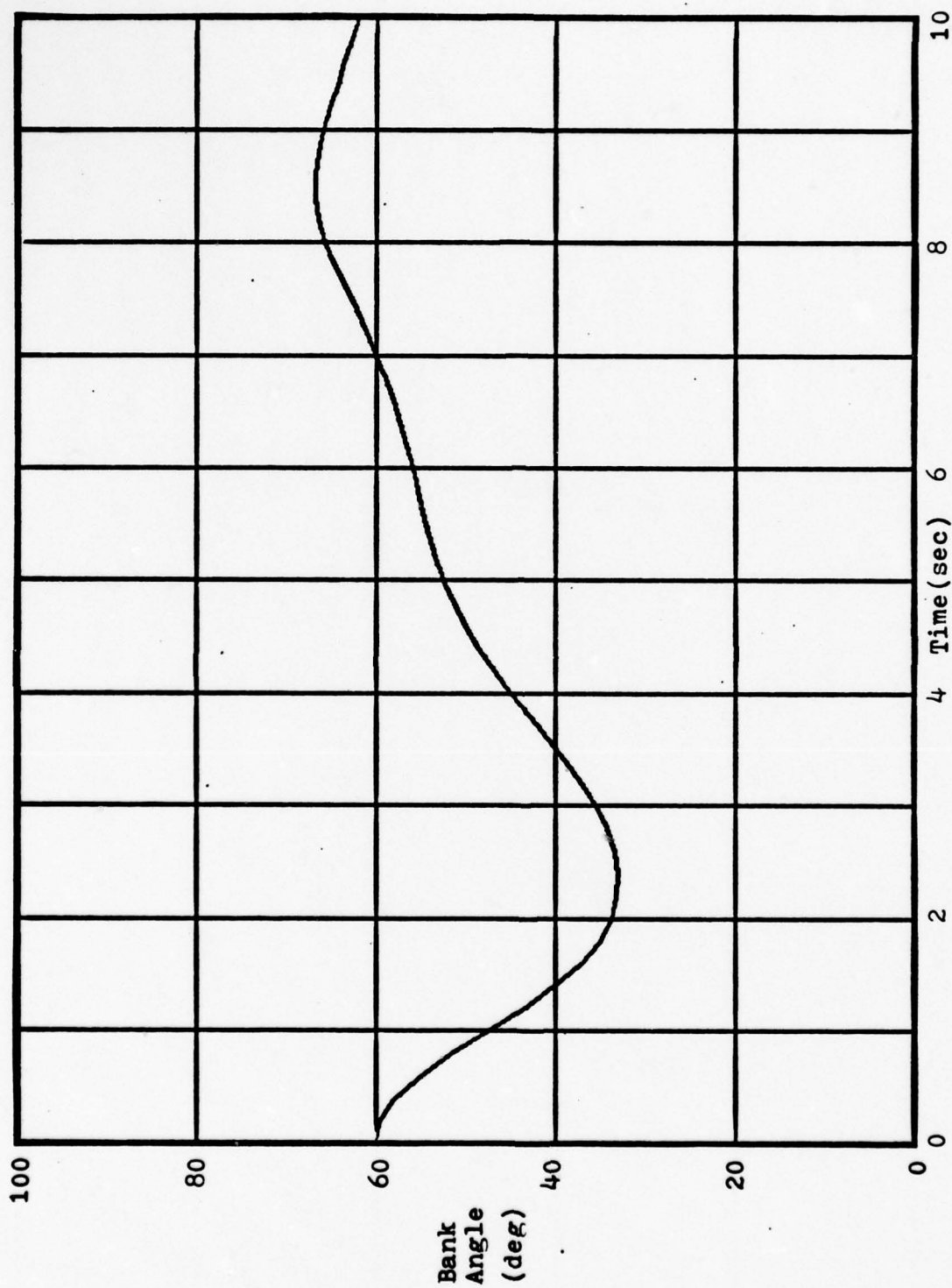
Figure 37. Attacker Bank Angle vs. Time for 60 Deg Bank Target with Differential Bank Angle Feedback.

89
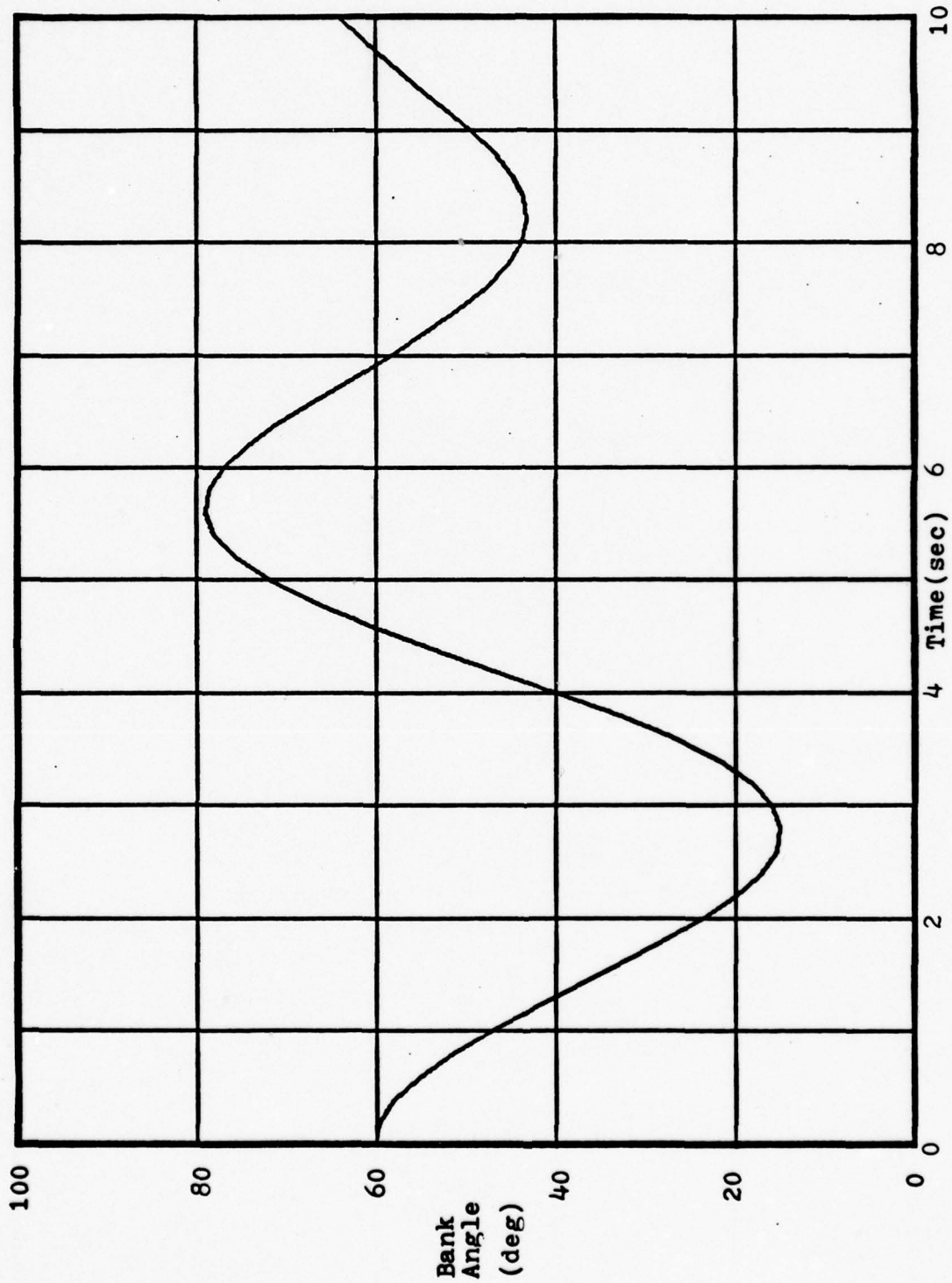
Figure 38. Attacker Bank Angle vs. Time for 60 Deg Bank Target with no Differential Bank Angle Feedback.

run are shown in Figures 39 and 40. The elevation tracking error response depicted in Figure 39 shows excellent tracking for the entire 10 second simulation. The traverse tracking error response shown in Figure 40 shows significant improvement in tracking capability. The characteristics of the tracking response in this simulation run are similar to those obtained in the TAWDS programs except that the traverse error response is more highly damped for the case simulated herein.

One final simulation run was conducted using the gain values of K_{PE} = 1.5 and K_{AIL} = 1.0, but with the lateral pilot model deadzones on traverse error rate ($DZ_{\dot{e}_{LW}}$) and differential bank angle (DZ_{φ}) removed from the model. This technique was recommended by Mr. Richard Quinlivan of General Electric Company. Mr. Quinlivan is the General Electric program manager for the Fire Fly program, and he contends that the human pilot responses do not exhibit an appreciable deadzone on either traverse tracking error rate or on differential bank angle. The results of this simulation run are shown in Figures 41 and 42. The elevation tracking error response shown in Figure 41 is essentially the same as the response obtained in the previous run. The traverse tracking error response depicted in Figure 42 shows a slight decrease in the magnitude of the tracking errors, but the response is very similar to that obtained in Figure 40 where the deadzones were not removed. Since the value of K_{φ} in this simulation run was zero, removing the deadzone
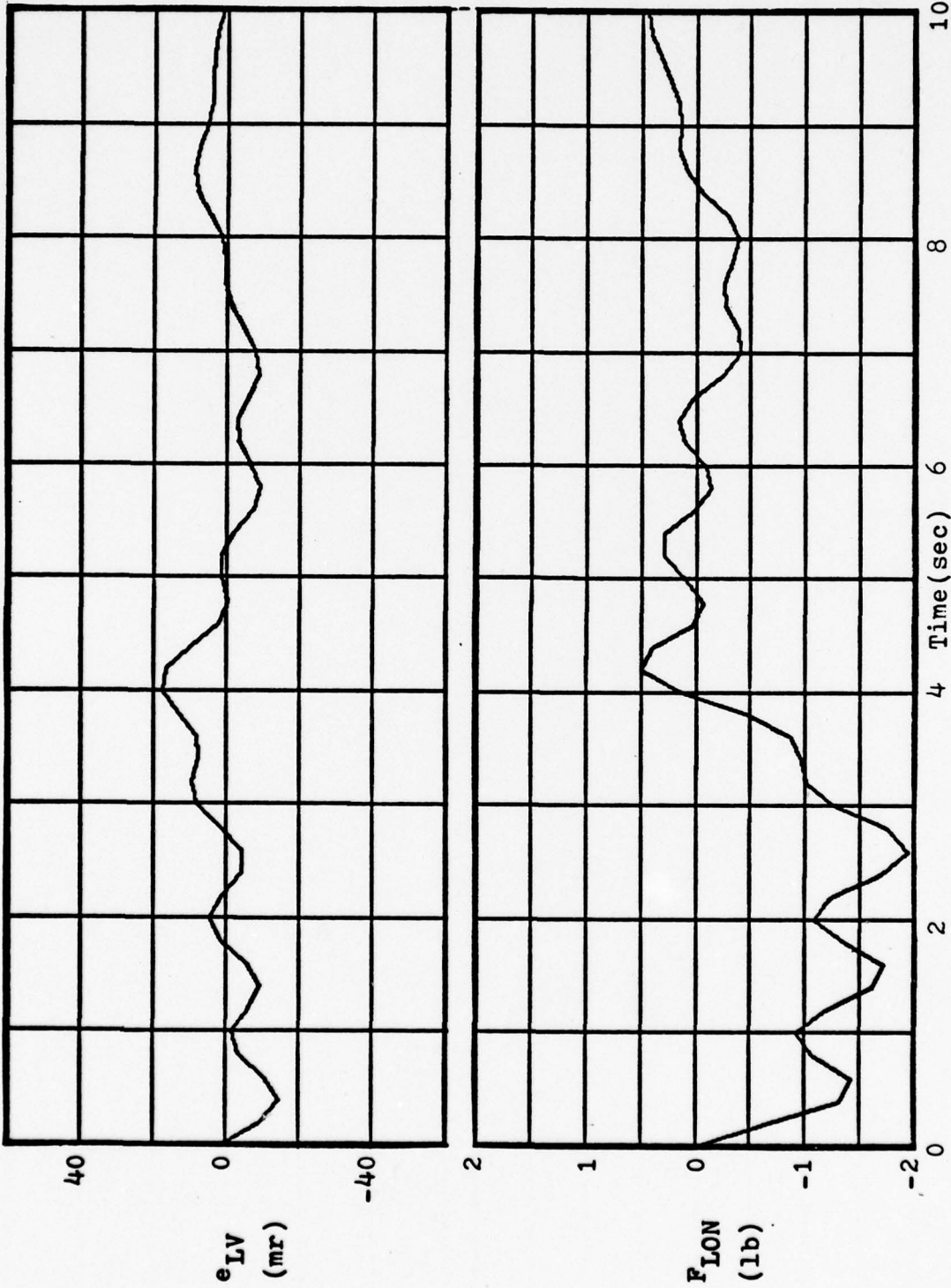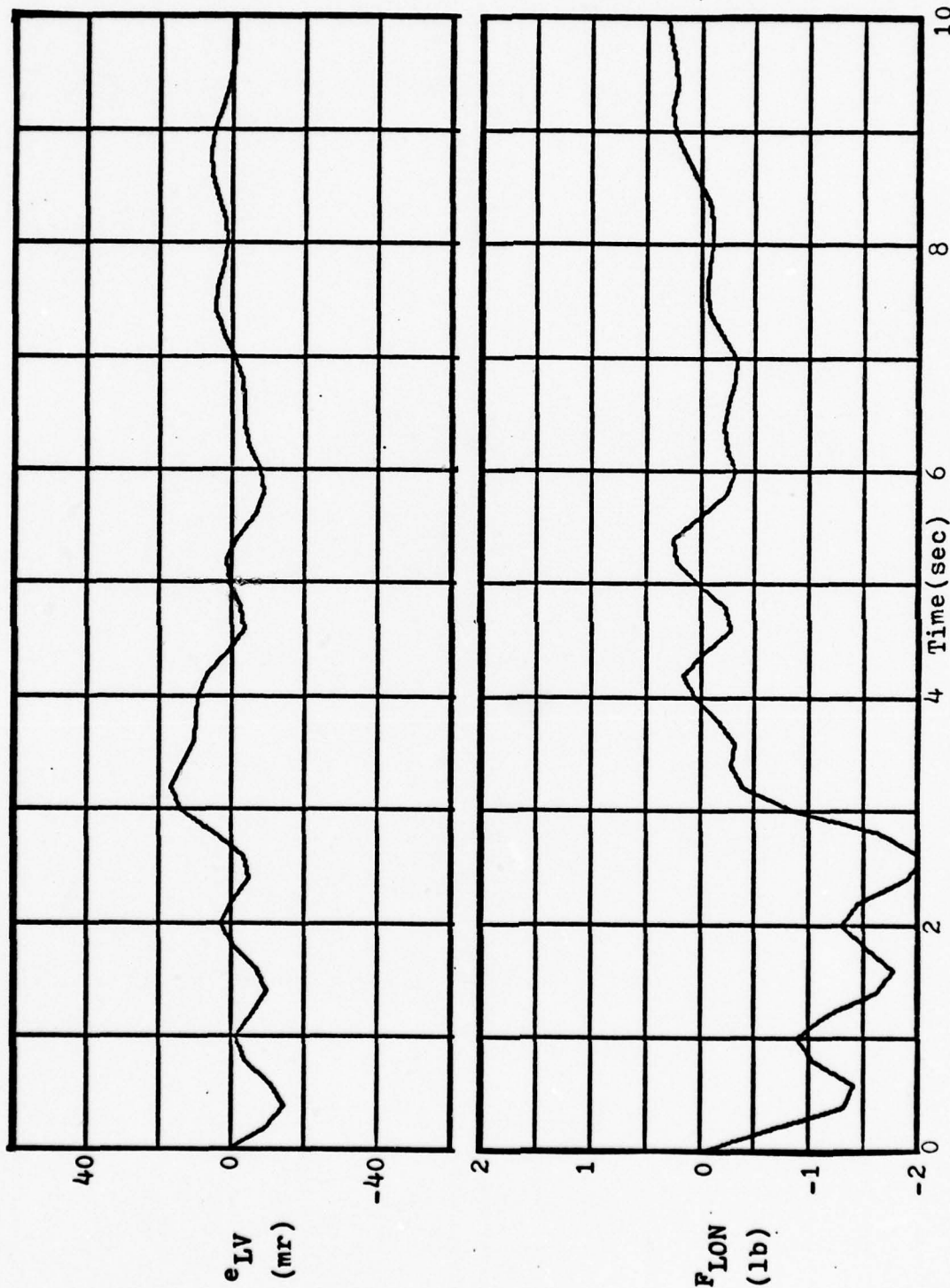
Figure 39. Elevation Tracking Error and Stick Force vs. Time for 60 Deg Bank Target/ $K_{PE} = 1.5$ and $K_{AIL} = 1.0$.
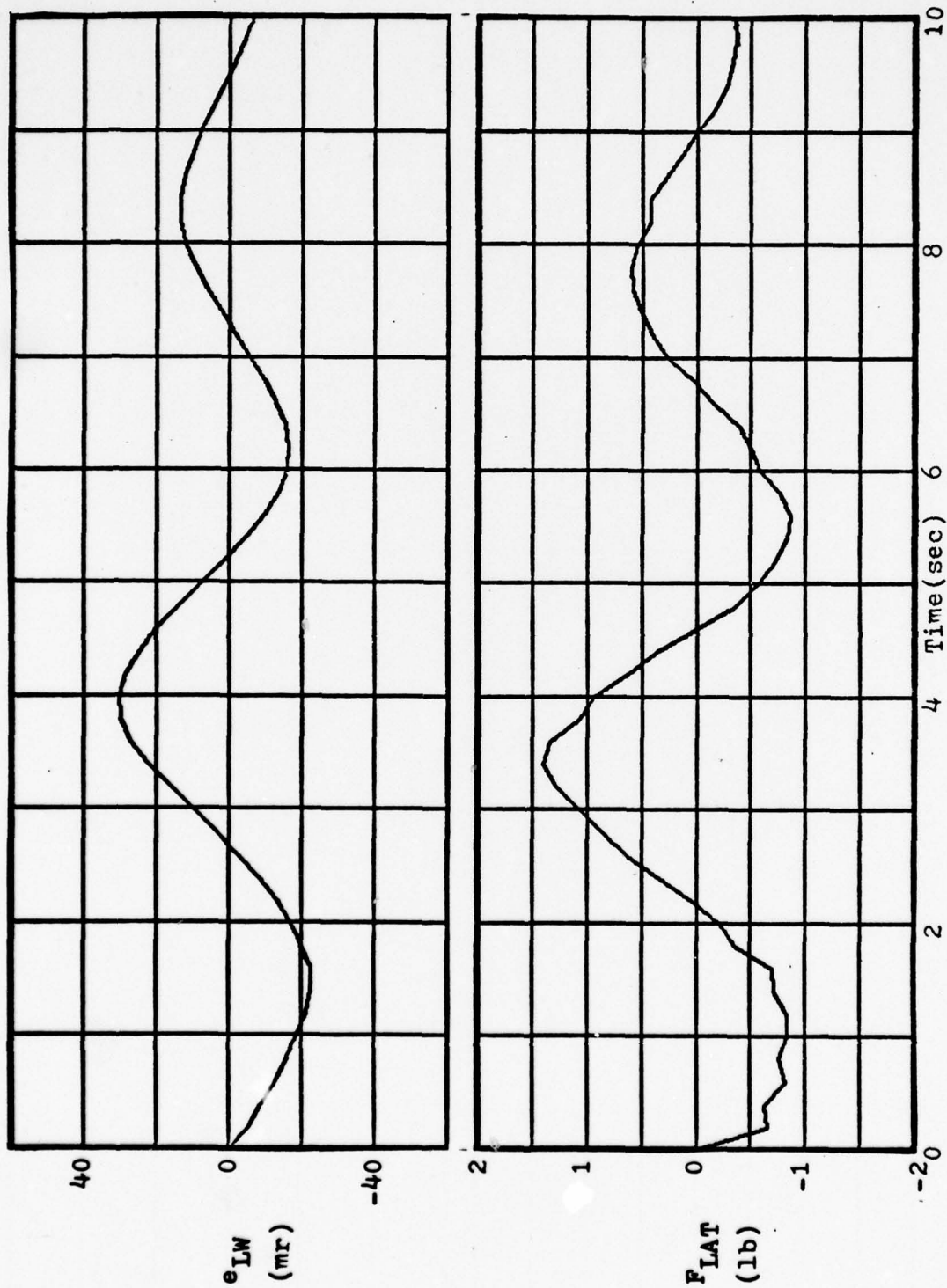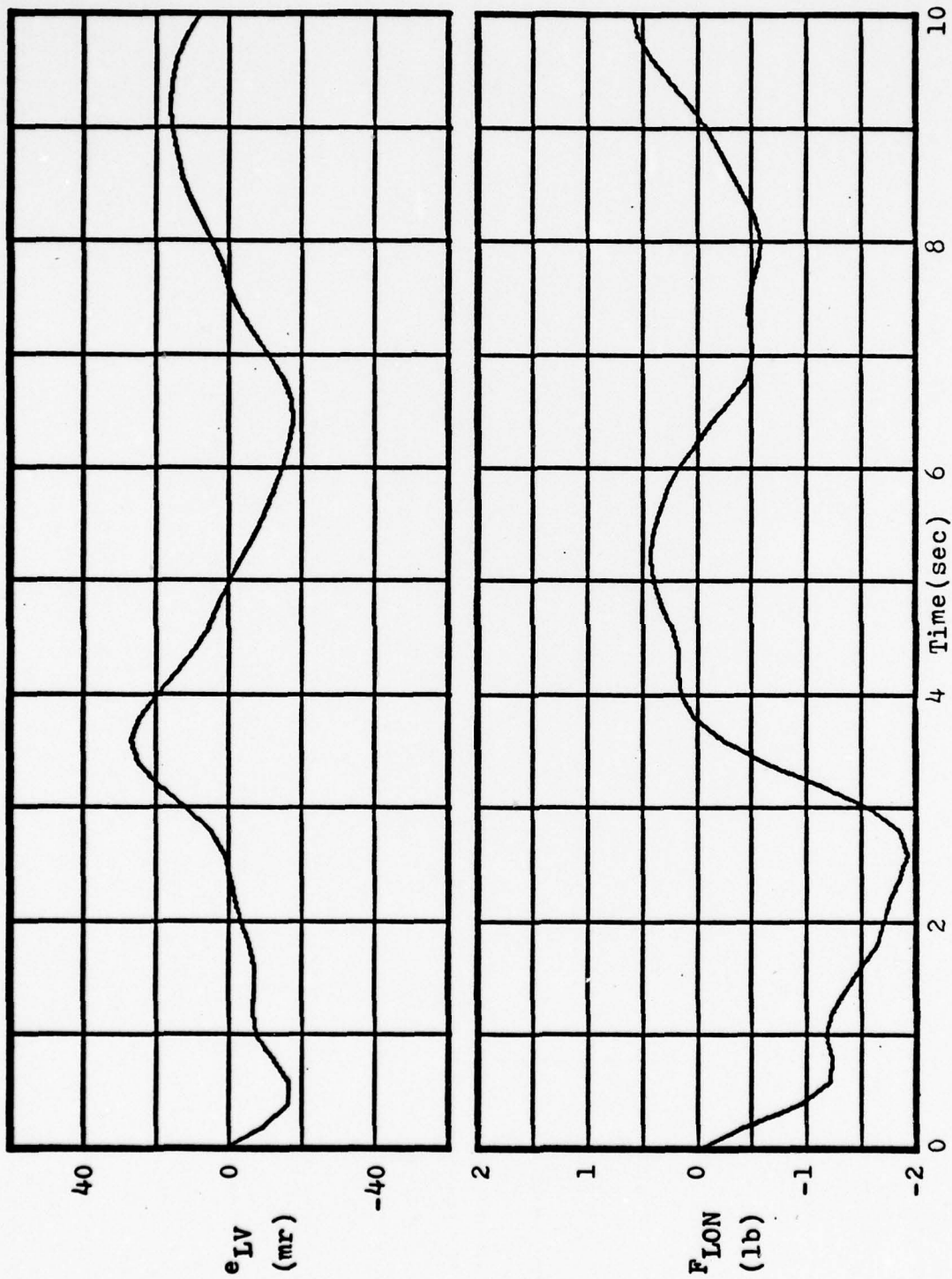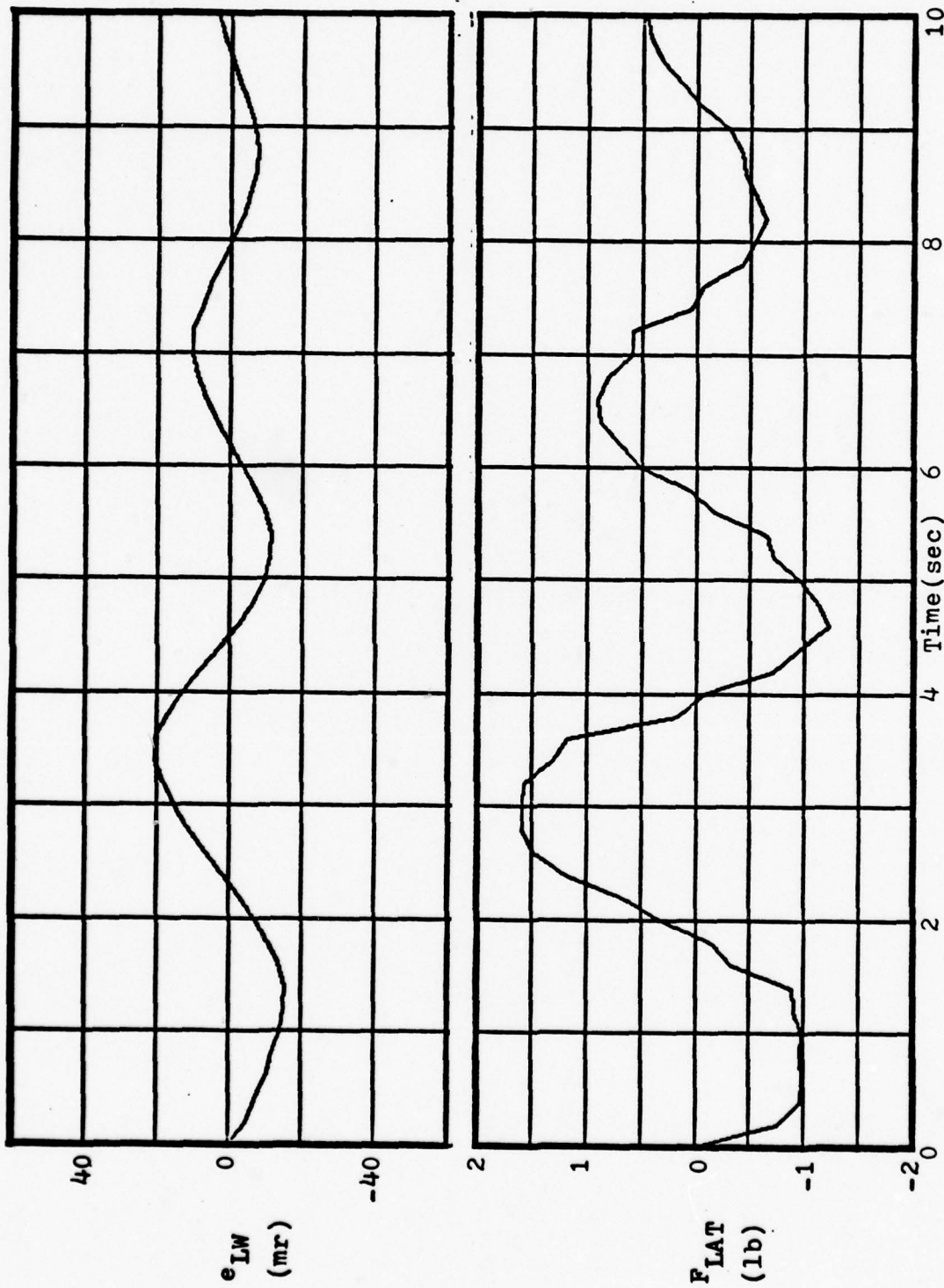
Figure 40. Traverse Tracking Error and Stick Force vs. Time for 60 Deg Bank Target/ $K_{PE} = 1.5$ and $K_{AIL} = 1.0$.

93

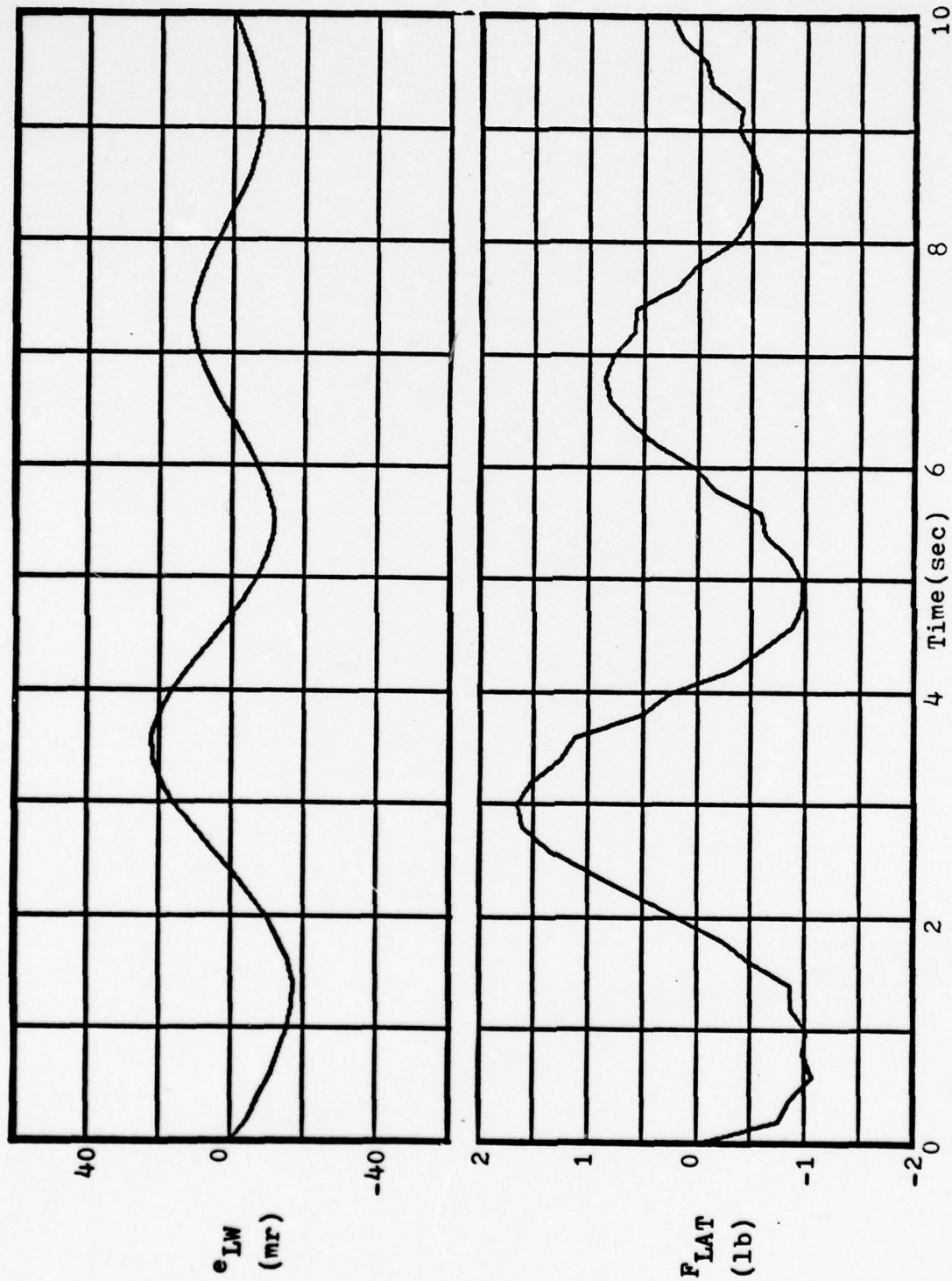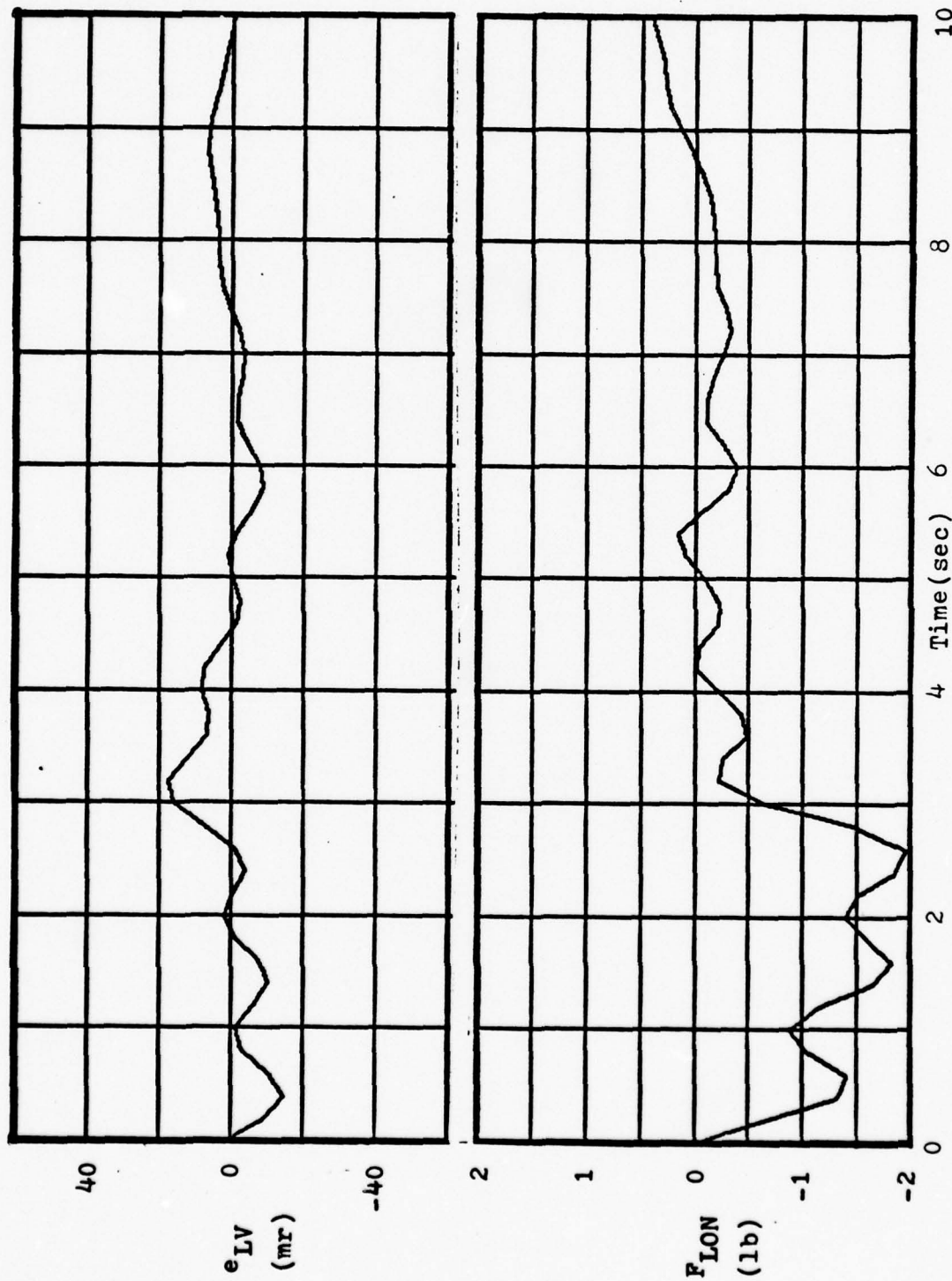**Figure 41.** Elevation Tracking Error and Stick Force vs. Time for 60 Deg Bank Target/ K_{PE} = 1.5 and K_{AIL} = 1.0/ Lateral Pilot Model Deadzones Removed.

94

e_{LW} (mr)

F_{LAT} (lb)

Time(sec)
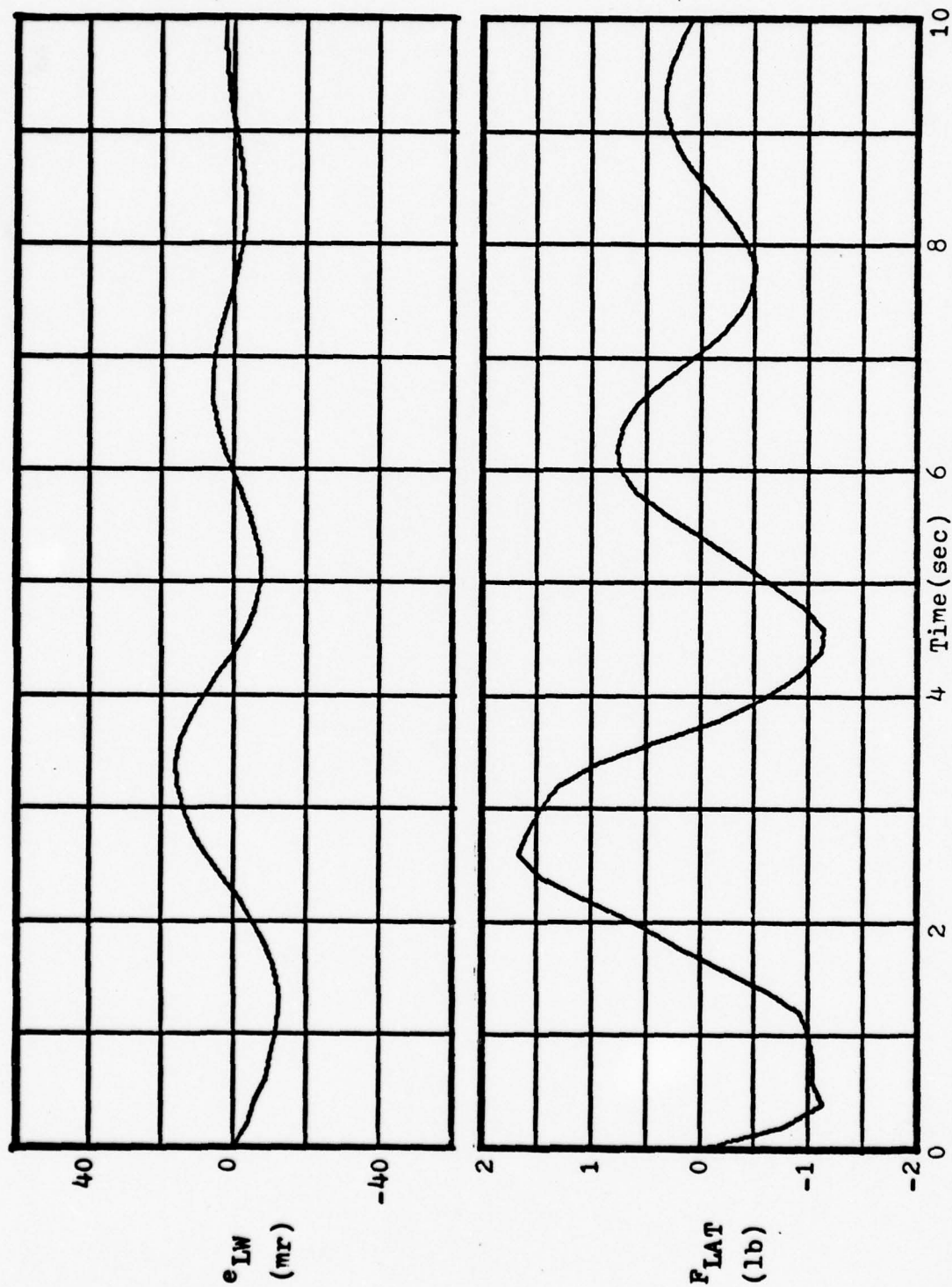
Figure 42. Traverse Tracking Error and Stick Force vs. Time for 60 Deg Bank Target/ $K_{PE} = 1.5$ and $K_{AIL} = 1.0$/ Lateral Pilot Model Deadzones Removed.

on differential bank angle had no effect on the traverse tracking error response. However, when the value of K_φ was increased to 0.1, the tracking response observed for the traverse error was essentially the same as the response shown in Figure 36 where the deadzone on differential bank angle was not removed. For the one case simulated, the effect on the traverse tracking error response of removing the lateral pilot model deadzones was not significant.

Summary of Tracking Performance

This chapter presented the results of the closed loop simulation of the F-106/Fire Fly manual director gunsight system to determine the tracking performance in the terminal phase of air-to-air gunnery. A multi-axis pilot model was adapted from the TAWDS pilot model and a nominal set of pilot model parameter values was determined. The first section of this chapter discussed the results of simulation runs against targets in straight and level flight, and in 30, 60, and 70 degree bank turns. The tracking error responses were found to have characteristics similar to those obtained from F-4 man-in-the-loop simulation studies, except that the magnitudes of the tracking errors observed in this simulation study were larger.

In the second section of the chapter, simulation results were presented from runs conducted against targets in 60 degree bank turns. In these runs, several pilot model parameter values were varied to demonstrate the effects on

the tracking error time histories. The values of the longitudinal and lateral pilot transmission gains, K_{PE} and K_{AIL}, were varied from the minimum values necessary for stable tracking, 0.5 and 0.2 respectively, to values of $K_{PE} = 1.5$ and $K_{AIL} = 1.0$. A significant decrease was noted in the magnitudes of the tracking errors as the gains were increased. The addition of rudder pedal force commands in the lateral pilot model had a negligible effect on traverse tracking error response.

The addition of differential bank angle feedback to the lateral pilot model decreased the overall magnitude of the traverse tracking errors observed, but also resulted in a marked increase in the initial time required to reach zero traverse error.

A simulation run conducted with the lateral pilot model deadzones removed showed no significant difference in the characteristics of the traverse tracking error response.

The tracking error response characteristics were shown to be highly dependent on the pilot model parameter values. To make the multi-axis pilot model used in this simulation more useful, the parameter values should be adjusted for good correspondence between the tracking error responses obtained in this simulation effort and the tracking error responses obtained from F-106/Fire Fly man-in-the-loop simulation studies.

Table III presents a set of recommended pilot model parameter values based on the simulation results presented

97

in this chapter.

Table III. Recommended Pilot Model Parameter Values for F-106/Fire Fly Manual Director Gunsight

Longitudinal Parameters	K_{PE}	K_L	K_R	τ_E	$DZ\dot{e}_{LV}$	ζ_n, ω_n
Parameter Values	1.0-1.5	1.0	1.0	0.05	5.0 mr/sec	0.6, 1.0

Lateral Parameters	K_{AIL}	K_{RTR}	K_{RUD}	K_φ	τ_T	$DZ\dot{e}_{LW}$	DZ_φ
Parameter Values	0.36-1.0	0.5-1.0	0.0	0.0	0.05	5.0 mr/sec	5.0 deg

98

VI. Conclusions and Recommendations for Further Study

Conclusions

The primary objective of this thesis effort was to evaluate the tracking performance, during the terminal phase of air-to-air gunnery, of the Fire Fly manual director gunsight system. Further objectives were to adapt the TAWDS multi-axis pilot model for use in the F-106/Fire Fly simulation, and to determine the usefulness of the EASY computer programs for modeling and analysis of six degree of freedom nonlinear weapon systems.

To accomplish the objectives outlined above, a digital computer model of the aircraft/gunsight/target/pilot closed loop system was developed using the EASY Model Generation Program. A set of nominal pilot model parameter values was selected from within the range of values recommended for the TAWDS pilot model. The tracking performance of the closed loop system was simulated using the EASY Analysis Program. Target maneuvers consisted of constant altitude, constant speed, constant rate turns at bank angles of 30, 60, and 70 degrees. After establishing that the system model could track the targets being simulated, the pilot model parameter values were varied to note the effects on the tracking error responses.

The simulation results presented in Chapter Five show that the tracking performance of the Fire Fly manual director gunsight system is stable for the target maneuvers simulated.

99

The characteristics of the tracking error responses are significantly dependent on the pilot model parameter values selected. The structure of the tracking error responses is similar to the responses obtained for the F-4 aircraft in the TAWDS simulation studies.

The multi-axis analytical pilot model used in the simulation is readily modeled using standard components of the EASY Model Generation Program. If the pilot model parameter values are selected to obtain a good correspondence between the tracking error responses presented in this simulation study and the responses obtained from F-106/Fire Fly man-in-the-loop simulations, the pilot model should prove to be a valuable tool for future simulation studies.

The EASY Model Generation and Analysis Programs provide powerful tools for modeling and analysis of complex weapon systems. The EASY Model Generation Program, with its capability for intermixing EASY standard components with user Fortran statements, gives the programmer the necessary flexibility to accurately model a six degree of freedom, nonlinear aircraft system over a wide range of flight conditions. The EASY Analysis Program provides a wide variety of tools for the design and evaluation of closed loop systems. The ease with which parameters can be changed in the model makes the program particularly useful to the control systems design engineer.

Recommendations for Further Study

The tracking performance of the Fire Fly manual director gunsight system should be evaluated against dynamically maneuvering targets. This task can be accomplished in two ways. A target subroutine could be added as a standard component of the EASY Model Generation Program and then programmed to perform the type of maneuvers desired for simulation. An alternative method is to develop a TAWDS model of the closed loop system and run simulations against the target model which now exists in the TAWDS program.

For simulations against dynamically maneuvering target models, it would be useful to explicitly model the Kalman filter and the tracking system of the Fire Fly system.

Simulation of the automatic flight control capabilities of the Fire Fly system could be performed using a model of the F-106, but an appropriate control augmentation system would have to be added. Since the Fire Fly system probably will not be implemented operationally on the F-106, it would be more useful to model an aircraft such as the F-16, which has a control augmentation system which could be utilized for analyzing the automatic control features of the Fire Fly system.

Bibliography

1. General Electric Aircraft Equipment Division. <u>Definition</u>
   <u>and Preliminary Evaluation of Integrated Automatic Flight</u>
   <u>and Fire Control Systems (Fire Fly I)</u>. Binghamton, New
   York: General Electric Company, March 1975.

2. Quinlivan, Richard P. <u>Multi-mode Flight Control Definition</u>
   <u>Study for Precision Weapon Delivery</u>. AFFDL TR 71-39.
   Wright-Patterson Air Force Base, Ohio: Air Force Flight
   Dynamics Laboratory, June 1971.

3. Hohwiesner, Capt William. <u>Principles of Airborne Fire</u>
   <u>Control</u>. United States Air Force Academy, Colorado:
   Department of Astronautics and Computer Science, December
   1975.

4. Quinlivan, Richard P., and Gene Tye. <u>Control and Display</u>
   <u>Factors in Air-to-Air Gunnery</u>. Binghamton, New York:
   General Electric Company.

5. Berg, R.L., and M.M. Sears. <u>Air-to-Air Fire Control</u>
   <u>Exposition. Phase III (EXPO III)</u>. AFAL TR 73-287.
   Wright-Patterson Air Force Base, Ohio: Air Force Avionics
   Laboratory, September 1973.

6. Berger, J.B., R.P. Meyer, and D.B. Groll. <u>Flight Control</u>
   <u>Requirements for Weapon Delivery, Volume I - Development</u>
   <u>of the Terminal Aerial Weapon Delivery Simulation (TAWDS)</u>
   <u>Programs and Their Use in Formulating Flying Qualities</u>
   <u>Guidelines for Manually Coupled Aircraft Weapon Delivery</u>
   <u>Systems</u>. AFFDL TR 76-35, Volume I. Wright-Patterson
   Air Force Base, Ohio: Air Force Flight Dynamics Laboratory,
   March 1976.

7. General Electric Company. <u>Fire Fly II User's Manual</u>.
   Contract No. F33615-75-C-3143. Binghamton, New York:
   General Electric Company, March 1977.

8. Holt, R.L. <u>F-102/F-106 Five Degree of Freedom Flight</u>
   <u>Response Program</u>. GDCA-DFM-72-001. San Diego, California:
   General Dynamics Corporation, April 1972.

9. Roskam, Jan. <u>Flight Dynamics of Rigid and Elastic Airplanes</u>,
   <u>Part One</u>. Lawrence, Kansas: Roskam Aviation and Engineering
   Corporation, 1972.

10. Blakelock, John H. <u>Automatic Control of Aircraft and</u>
    <u>Missiles</u>. New York: John Wiley and Sons, Inc., 1965.

11. McRuer, Duane, Irving Ashkenas, and Dunstan Graham.
    <u>Aircraft Dynamics and Automatic Control</u>. Princeton,
    New Jersey: Princeton University Press, 1973.

12. Boeing Computer Services, Inc. Application of the EASY
    Dynamic Analysis Program to Aircraft Modeling, User's
    Manual. Seattle, Washington: Boeing Computer Services,
    Inc., November 15,1976.

13. Teper, Gary L. Aircraft Stability and Control Data.
    STI TR 176-1. Hawthorne, California: Systems Technology,
    Inc., April 1969.

14. Berger, J.B., and R.P. Meyer. Flight Control Requirements
    for Weapon Delivery, Volume II- Background Information
    on Development of Pilot Models for Use in Evaluating
    Manually Coupled Aircraft Weapon Delivery Systems.
    AFFDL TR 76-35, Volume II. Wright-Patterson Air Force
    Base, Ohio: Air Force Flight Dynamics Laboratory, March 1976.

15. Boeing Computer Services, Inc. ECS Transient Analysis
    Volume III Integrated Computer Program (EASY). Boeing
    Document No., D180-18575-3, Seattle, Washington: Boeing
    Computer Services, Inc., June 8, 1976.

Appendix A. <u>Computer</u> <u>Modeling</u> <u>and</u> <u>Simulation</u> <u>Techniques</u>

In the first section of this appendix, a listing of the closed loop simulation model is presented. Next, the functional flow of the model is discussed. Included are block diagrams of the pilot model/control system connections. The third section discusses specific techniques used in the simulation analysis.

Computer Model

COMMANDS

> MODEL DESCRIPTICN=NONLINEAR F106 MODEL WITH PILOT MODEL+FIRE CONTROL

> ADD TABLES=DELCNB,-23,CYDA,-23,CLAT,-23,CLBT,-23,CLOT,-23,

> CMAT,-23,CMOT,-23,CNBA,-23,CNBT,-23,CNDAA,-23,CNDADE,-23,

> CYAT,-23,CYBT,-23

> ADD TABLES=CZO,68,CLB,68,CL9A,68,CL9A2,68,CL9B,58,CLDA,68,

> CLDR,68,CLP,68,CLPA2,68,CLR,68,CLPA,68,CMDE,68,CMO,68,CMQ,68,

> CNB,68,CNBA2,68,CNBR,68,CNDA,68,CNDR,68,CNP,68,CNR,68,CYB,68,

> CYBA2,68,CYBB,68,CYDA,68,CYDR,68,CYP,68,CYR,68,CZA,68,CZDE,68,

> TNP,68,CLPA,68,CDRAG1,152,CDRAG2,152,CDRAG3,152

> ADD PARAMETERS= BLTANK,XCG,YREF,YCG,ZREF,ZCG,RPD

> ADD VARIABLES=YAW,C11,C12,C13,C21,C22,C23,C31,C32,C33,RAX,RAY,RAZ

> ADD VARIABLES=C3,A,B,C,TOF,PITC,ROLL,ABV,ABW,RRV,WB,ALPH,RRW,ELV,ELW

> ADD VARIABLES=VRV,VRU,VRW,APU,ARV,APW,RTU,RTV,RTW,RA,RADOT

> ADD VARIABLES=ATX,ATY,ATZ,VTX,VTY,VTZ,AAX,AAY,AAZ,VAX,VAY,VAZ

> ADD VARIABLES=ARX,APY,ARZ,VRX,VRY,VPZ,AAU,AAV,AAW

> ADD VARIABLES=AX,AY,AZ

> LOCATION=56   AV   INPUTS=SD

> LOCATION=76   FV ·   INPUTS=SD(ALT=X),AV(MAC=X)

> LOCATION=52   MA   INPUTS=FV(X=C1),LGTT,

> LOCATION=2   EN   INPUTS=MA(X=THR)

1

> FORTRAN STATEMENTS

> CCCC

> CC   COMPUTE ACCELERATIONS IN G

> CCCC

>   G=32.2

> AX=EU AV/G

> AY=FV AV/G

> AZ=EW AV/G

> CCCC

> CC   COMPUTE LONGITUDINAL FORCE TERMS   FZ EN AND FX EN

2

105

```
C CCCC
C CCCC
C CC                    INTERPOLATE TO FIND LIFT COEFFICIENTS
C CCCC
        CLOTO= -TBLU1(MACAV,CLOT(4),CLOT(14),1,-10)
        CLATO= -TBLU1(MACAV,CLAT(4),CLAT(14),1,-10)
        CLO= -TBLU2(MACAV,ALTSO,CZO(9),CZO(4),CZO(19),1,1,-10,-5,10,5)
        CLA= -TBLU2(MACAV,ALTSO,CZA(9),CZA(4),CZA(19),1,1,-10,-5,10,5)
        CLDE=-TBLU2(MACAV,ALTSO,CZDE(9),CZDE(4),CZDE(19),1,1,-10,-5,10,5)      ⌉ 2
C CCCC
C CC                    COMPUTE LIFT,DRAG COEFFICIENTS AND BODY AXIS FORCES
C CCCC
        ELEV= X2 LA E*RPD
        ALPHA= AL AV*RPD
        CL1= CL0 + CLOTO + (CLA+CLATO)*ALPHA + CLDE*FLEV      ⌋
C CCCC
C CC                    LINEAR INTERP. OF DRAG COEFFICIENTS AT TWO MACHS      ⌉
C CCCC
        CDO1= TBLU2(X2 LA E,CL1,CDRAG2(28),CDRAG2(4),CDRAG2(33),1,1,
       1          -5,-24,5,24)
        IF(MACAV.LT. .90) GO TO 100
        CDO2= TBLU2(X2 LA E,CL1,CDRAG3(28),CDRAG3(4),CDRAG3(33),1,1,
       1          -5,-24,5,24)
        CDO= (MACAV-.90)*20.*CDO2 + (.95-MACAV)*20.*CDO1
        GO TO 200
100     CDO2= TBLU2(X2 LA E,CL1,CDRAG1(28),CDRAG1(4),CDRAG1(33),1,1,      │ 3
       1          -5,-24,5,24)
        CDO= (.90-MACAV)*10.*CDO2 + (MACAV-.80)*10.*CDO1
200     CALP= COS(ALPHA)
        SALP= SIN(ALPHA)
        FZSAV= FZ EN
        FXSAV=.FX EN
        FZ EN=-QS AV*(CL1*CALP + CDO*SALP) + FZ EN      ⌋
```

106

```
>          FX EN= QS AV*(CL1*SALP - CDO*CALP) + FX EN                    ⌐3
> CCCC
> CC    .        LOOK UP LONGITUDINAL DERIVATIVES FOR M=TY AND COMPUTE TY EN   ⌐
> CCCC
>          MO LO= TBLU2(MACAV,ALTSD,CMO(9),CMO(4),CMO(19),1,1,-10,-5,10,5)
>          MQ LO=2.*TBLU2(MACAV,ALTSD,CMQ(9),CMQ(4),CMQ(19),1,1,-10,-5,10,5)
>          MADLO=MQ LO
>          MDELO=TBLU2(MACAV,ALTSD,CMDE(9),CMDE(4),CMDE(19),1,1,-10,-5,10,5)
>          CMOTO= TBLU1(MACAV,CMOT(4),CMOT(14),1,-10)
>          CMATO= TBLU1(MACAV,CMAT(4),CMAT(14),1,-10)
>          TY EN= QS AV*C LO*(CMOTO + CMATO*ALPHA) + TY EN              4
> LOCATION=4       LO      INPUTS=AV,LA F(X=ELE),EN
>  FORTRAN STATEMENTS
> CCCC
> CC           ADD AERO-FORCE TORQUES TO M=TY2LO
> CCCC
>          TNPO=TBLU2(MACAV,ALTSD,TNP(9),TNP(4),TNP(19),1,1,-10,-5,10,5)
>          TY2LO= TY2LO + (ZREF-ZCG)*(FX2LO-FXSAV) - (TNPO*C LO-XCG)*
>      1                   (FZ2LO-FZSAV)                              ⌐
> CCCC
> CC           COMPUTE LATERAL DIRECTIONAL NONLINEAR TERMS FY1LO,TX1LO,TZ1LO  ⌐
> CCCC
> CCCC ..
> CC                 INTERPOLATE TO FIND FY DERIVATIVES
> CCCC
>          CYBTO= TBLU1(MACAV,CYBT(4),CYBT(14),1,-10)
>          CYATO= TBLU1(MACAV,CYAT(4),CYAT(14),1,-10)
>          CYBA2O= TBLU2(MACAV,ALTSD,CYBA2(9),CYBA2(4),CYBA2(19),1,1,
>      1             -10,-5,10,5)                                      5
>          CYBAO= TBLU1(MACAV,CYBA(4),CYBA(14),1,-10)
>          CYBRO= TBLU2(MACAV,ALTSD,CYBR(9),CYBR(4),CYBR(19),1,1,
>      1             -10,-5,10,5)
> CC                 COMPUTE NONLINEAR Y FORCES
```

107

```
     TERM= BLTANK*P  SO*RPO/(VT AV + VT AV)

     BETA = BE AV*RPO

     FY1LD= QS AV*(CY3TO*BETA + CYATO*TERM + BETA*(ALPHA*
    1          (CYBA2O*ALPHA + CYBAO) + CYBBO*ABS(BETA)))
CCCC
CC                   INTERPOLATE TO FIND L=TX DERIVATIVES
CCCC
     CLBTO= TBLU1(MACAV,CLBT(4),CLBT(14),1,-10)
     CLBA2O= TBLU2(MACAV,ALTSD,CLBA2(9),CLBA2(4),CLBA2(19),1,1,
    1          -10,-5,10,5)
     CLBAO=TBLU2(MACAV,ALTSD,CLBA(9),CLBA(4),CLBA(19),1,1,-10,-5,10,5)
     CLBBO=TBLU2(MACAV,ALTSD,CLBB(9),CLBB(4),CLBB(19),1,1,-10,-5,10,5)
     CLPA2O= TBLU2(MACAV,ALTSD,CLPA2(9),CLPA2(4),CLPA2(19),1,1,
    1          -10,-5,10,5)
     CLPAO=TBLU2(MACAV,ALTSD,CLPA(9),CLPA(4),CLPA(19),1,1,-10,-5,10,5)
     CLRAO=TBLU2(MACAV,ALTSD,CLRA(9),CLRA(4),CLRA(19),1,1,-10,-5,10,5)
CCCC
CC                   COMPUTE NONLINEAR L=TX TORQUES
CCCC
     CLTANK= CLBTO*BETA -(CLOTO*BLTANK + CYATO*2.33)*TERM
     CNOLIN= ((CLBA2O*ABS(ALPHA) + CLBAO)*ALPHA + CLBBO*ABS(BETA))
    1          *BETA + ((CLPA2O*ALPHA + CLPAO)*P  SD + CLRAO*R  SD)
    2          *ALPHA*B  LD*RPO/(VT AV+VT AV)
     TX1LD = QS AV*B  LD*(CLTANK + CNOLIN)
CCCC
CC                   INTERPOLATE TO FIND N=TZ DERIVATIVES
CCCC
     CNBTO= TBLU1(MACAV,CNBT(4),CNBT(14),1,-10)
     CNBA2O= TBLU2(MACAV,ALTSD,CNBA2(9),CNBA2(4),CNBA2(19),1,1,
    1          -10,-5,10,5)
     CNBAO= TBLU1(MACAV,CNBA(4),CNBA(14),1,-10)
     CNBBO=TBLU2(MACAV,ALTSD,CNBB(9),CNBB(4),CNBB(19),1,1,-10,-5,10,5)
     DELCNO= TBLU1(MACAV,DELCNB(4),DELCNB(14),1,-10)
```

5

6

7

```
>          CNDAAO= TBLU1(MACAV,CNDAA(4),CNDAA(14),1,-10)
>          COADEO= TBLU1(MACAV,CNDADE(4),CNDADE(14),1,-10)
> CCCC
> CC                    COMPUTE NONLINEAR N=TZ TORQUES
> CCCC              •
>          CNTANK= CNBTO*BETA - 0.6*TERM
>          AIL= X2 LA A*RPO
>          CNONLI= ALPHA*(CNBA2O*ALPHA + CNBAO) + BETA*(CNBBO*ABS(BETA)
>     1               + DELCNO) + (CNDAAO*ALPHA + COADEO*ELEV)*AIL
>          TZ1LO= QS AV*B LO*(CNTANK + CNONLI)
> CCCC
> CC            LOOK UP LATERAL-DIRECTIONAL LINEAR COEFFICIENTS FOR LO
> CCCC
>          YB LO=TBLU2(MACAV,ALTSO,CYB(9),CYB(4),CYB(19),1,1,-10,-5,10,5)
>          YP LO=TBLU2(MACAV,ALTSO,CYP(9),CYP(4),CYP(19),1,1,-10,-5,10,5)
>          YR LO=TBLU2(MACAV,ALTSO,CYR(9),CYR(4),CYR(19),1,1,-10,-5,10,5)
>          YDALO=TBLU2(MACAV,ALTSO,CYDA(9),CYDA(4),CYDA(19),1,1,-10,-5,10,5)
>          YDRLO=TBLU2(MACAV,ALTSO,CYDR(9),CYDR(4),CYDR(19),1,1,-10,-5,10,5)
>          LP LO=TBLU2(MACAV,ALTSO,CLP(9),CLP(4),CLP(19),1,1,-10,-5,10,5)
>          LR LO=TBLU2(MACAV,ALTSO,CLR(9),CLR(4),CLR(19),1,1,-10,-5,10,5)
>          LB LO=TBLU2(MACAV,ALTSO,CLB(9),CLB(4),CLB(19),1,1,-10,-5,10,5)
>          LDALO=TBLU2(MACAV,ALTSO,CLDA(9),CLDA(4),CLDA(19),1,1,-10,-5,10,5)
>          LDRLO=TBLU2(MACAV,ALTSO,CLDR(9),CLDR(4),CLDR(19),1,1,-10,-5,10,5)
>          NB LO=TBLU2(MACAV,ALTSO,CNB(9),CNB(4),CNB(19),1,1,-10,-5,10,5)
>          NDALO=TBLU2(MACAV,ALTSO,CNDA(9),CNDA(4),CNDA(19),1,1,-10,-5,10,5)
>          NDRLO=TBLU2(MACAV,ALTSO,CNDR(9),CNDR(4),CNDR(19),1,1,-10,-5,10,5)
>          NP LO=TBLU2(MACAV,ALTSO,CNP(9),CNP(4),CNP(19),1,1,-10,-5,10,5)
>          NR LO=TBLU2(MACAV,ALTSO,CNR(9),CNR(4),CNR(19),1,1,-10,-5,10,5)
> LOCATION=26     LO     INPUTS=AV,LO,LA A(X=AIL),LA R(X=RUO)
> FORTRAN STATEMENTS
> CCCC
> CC          ADD AERO-FORCE TORQUES TO L=TX2LO AND N=TZ2LO
> CCCC       •
```

109

```
        TX2LO= TX2LO + (YREF-YCG)*(FZ2LO-FZSAV) - (ZREF-ZCG)*FY2LO
        TZ2LO= TZ2LO +(TNPO*C  LO-XCG)*FY2LO -(YREF-YCG)*(FX2LO-FXSAV)     9
  LOCATION=9      SO      INPUTS=LO,LO
 LOCATION=40?,AFAX
 LOCATION=404,LAAX,INPUTS=AFAX                        •
 LOCATION=40S,AFAY
 LOCATION=40¬,LAAY,INPUTS=AFAY
 LOCATION=422,AFAZ
 LOCATION=42¬,LAAZ,INPUTS=AFAZ
 LOCATION=420,AFVX
 LOCATION=44C,AFVY
 LOCATION=46C,AFVZ                                                         10
 FORTRAN STATEMENTS
 CCCC
 C     COMPUTE TARGET VELOCITIES AND ACCEL IN X,Y,Z
 CCCC
       ATX=X2 LAAX
       ATY=X2 LAAY
       ATZ=X2 LAAZ
       VTX=X1 AFVX
       VTY=X1 AFVY
       VTZ=X1 AFVZ
 CCCC
 C     TRANSFORMATION MATRICES
 CCCC
       YAW=YAWSO*RPD
       PITC=PITSO*RPD
       ROLL=ROLSO*RPD
       C11=COS(YAW)*COS(PITC)                                             11
       C12=SIN(YAW)*COS(PITC)
       C13=-SIN(PITC)
       C21=COS(YAW)*SIN(PITC)*SIN(ROLL)-SIN(YAW)*COS(ROLL)
       C22=SIN(YAW)*SIN(PITC)*SIN(ROLL)+COS(YAW)*COS(ROLL)
```

110

```
        C23=COS(PITC)*SIN(ROLL)

        C31=COS(YAW)*SIN(PITC)*COS(ROLL)+SIN(YAW)*SIN(ROLL)          ⌉

        C32=SIN(YAW)*SIN(PITC)*COS(ROLL)-COS(YAW)*SIN(ROLL)          │ 11

        C33=COS(PITC)*COS(ROLL)                                      ⌋

  CCCCC

  C       COMPUTE ATTACKER ACCELERATIONS IN U,V,W,AXES               �

  CCCCC

        AAU=U0 LO-EU AV-32.2*SIN(PITC)

        AAV=V0 LO-EV AV+32.2*COS(PITC)*SIN(ROLL)

        AAW=W0 LO-EW AV+32.2*COS(PITC)*COS(ROLL)

  CCCC

  C       COMPUTE ATTACKER VELOCITIES AND ACCEL IN X,Y,Z

  CCCC

        AAX=C11*AAU+C21*AAV+C31*AAW

        AAY=C12*AAU+C22*AAV+C32*AAW

        AAZ=C13*AAU+C23*AAV+C33*AAW

        VAX=C11*U  SD+C21*V  SD+C31*W  SD

        VAY=C12*U  SD+C22*V  SD+C32*W  SD                            │ 12

        VAZ=C13*U  SD+C23*V  SD+C33*W  SD

  CCCC

  C       COMPUTE RELATIVE ACCEL AND VELOCITIES IN X,Y,Z

  CCCC

        ARX=ATX-AAX

        ARY=ATY-AAY

        ARZ=ATZ-AAZ

        VRX=VTX-VAX

        VRY=VTY-VAY

        VRZ=VTZ-VAZ

  CCCC

  C       COMPUTE RELATIVE ACCEL AND VELOCITIES IN BODY AXES

  CCCC

        ARU=C11*ARX+C12*ARY+C13*ARZ

        ARV=C21*ARX+C22*ARY+C23*ARZ
```

```
ARW=C31*ARX+C32*ARY+C33*ARZ
VRU=C11*VRX+C12*VRY+C13*VRZ
VRV=C21*VRX+C22*VRY+C23*VRZ
VRW=C31*VRX+C32*VRY+C33*VRZ
CCCC
C       COMPUTE RANGE RATE
CCCC
RADOT=SORT(VTX**2+VTY**2+VTZ**2) -SORT(VAX**2+VAY**2+VAZ**2)
X1 ITRX=VRX
X1 ITRY=VRY
X1 ITRZ=VRZ
LOCATION=436,ITRX
LOCATION=439,MARX,INPUTS=ITRX
LOCATION=456,ITRY
LOCATION=458,MARY,INPUTS=ITRY
LOCATION=476,ITRZ
LOCATION=478,MARZ,INPUTS=ITRZ
FORTRAN STATEMENTS
CCCC
C       COMPUTE RANGE COMPONENTS IN FIXED COORDINATES
CCCC
RAX=X2 MARX
RAY=X2 MARY
RAZ=X2 MARZ
CCCC
C       COMPUTE RANGE MAGNITUDE
CCCC
RA=SORT(RAX**2+RAY**2+RAZ**2)
CCCC
C       TRANSFORM RANGE COMPONENTS TO BODY AXES
CCCC
RTU=C11*RAX+C12*RAY+C13*RAZ
RTV=C21*RAX+C22*RAY+C23*RAZ
```

12

13

112

```
>        RTW=C31*RAX+C32*RAY+C33*RAZ
> CCCC
> C        COMPUTE BULLET TIME OF FLIGHT
> CCCC
>        CB=C.00625*SIGAV*SQRT(VT AV+3350.)
>        A=CB*(VT AV*RADOT-13.4)
>        B=CB*BA+RADOT-3341.
>        C=RA
>        TOF=(-B-SQRT(B**2.-4.*A*C))/(2.*A)
> CCCC
> C        COMPUT RANGE COMPONENTS REQUIRED FOR HIT
> CCCC
>        ABV=VD LD-EV AV
>        RRV=-TOF*(VRV+0.5*TOF*(ABV+ARV))
>        HB=1/(1+CB*TOF)
>        ABW=WD LD-EW AV
>        ALPH=AL AV*RPO
>        RRW=-TOF*(HB*3350.*(-.04362)+VRW+0.5*TOF*(ABW+ARW)
>        1 +TOF*HB*CB*VT AV*SIN(ALPH))
> CCCC
> C        COMPUTE ERROR SIGNALS TO DRIVE PILOT MODEL
> CCCC
>        ELV=(RRW-RTW)/RA
>        ELW=-(RRV-RTV)/RA
>        C2 MAPP=ELV
>        C2 MAPP=ELW
> LOCATION=542,MAPP,INPUTS=ITLP(X=X)
> LOCATION=534,MALL,INPUTS=MAPP
> LOCATION=536,ITLP,INPUTS=MALL
> LOCATION=557,TFLP,INPUTS=ITLP
> LOCATION=515,SALP,INPUTS=MALL
> LOCATION=538,MALP,INPUTS=ITLP,SALP(X=C2)
> LOCATION=560,MCLP,INPUTS=MALP,TFLP
```

13

14

15

```
.> LOCATION=580,ITAI,INPUTS=MCLP
·> LOCATION=641,MADD,INPUTS=ITLO(X=X)
·> LOCATION=633,MADL,INPUTS=MADD
·> LOCATION=635,ITLO,INPUTS=MADL
·> LOCATION=615,SADD,INPUTS=MADL
·> LOCATION=637,MCDD,INPUTS=SADD,ITLO
·> LOCATION=602,MCBA,INPUTS=SD(ROL=X)
·> LOCATION=604,SALD,INPUTS=MCBA
·> LOCATION=639,MCLD,INPUTS=SALD,MCDD
·> LOCATION=657,MAD2,INPUTS=MCDD
·> LOCATION=659,MAD1,INPUTS=MCLD
```

15

```
·> LOCATION=102      FUTQ      INPUTS=AV(SIG=X)
·> LOCATION=142      FUKQ      INPUTS=AV(SIG=X)
·> LOCATION=122      LE Q      INPUTS=SD(Q=X),FUTQ(X=PO),FUKQ(X=GAI)
·> LOCATION=124      SA Q      INPUTS=LE Q,
·> LOCATION=144      LA Q      INPUTS=SA Q,
·> LOCATION=164,MC E,INPUTS=LA Q,ITAI,LGET(X=C4)
·> LOCATION=166      SA E      INPUTS=MC E,
>  LOCATION=168      LA E      INPUTS=SA E,
>  LOCATION=223      FU A      INPUTS=AV(OC=X)
>  LOCATION=201,MAAI,INPUTS=LGAT(X=C2),MAD1(X=X)
·> LOCATION=203,MA A,INPUTS=FU A(X=C1),MAAI
>  LOCATION=207      LA A      INPUTS=MA A,
·> LOCATION=233      LE R      INPUTS=SD(R=X)
>  LOCATION=253      FU P      INPUTS=AV(OC=X)
>  LOCATION=255      LE P      INPUTS=SD(P=X),FU P(X=GAI)
>  LOCATION=235      MC R      INPUTS=MA A,LE R,LE P,LGRT(X=C4)
>  LOCATION=237,MA R,INPUTS=MAD2,MC R(X=C2)
>  LOCATION=239,LA R,INPUTS=MA R
```

16

```
>  LOCATION=312,MAAT,INPUTS=SD(ROL=X)
>  LOCATION=332,LGAT,INPUTS=MAAT,
>  LOCATION=314,MART,INPUTS=AV  (EV=X)
>  LOCATION=334,LGRT,INPUTS=MART,
```

17

114

```
>    LOCATION=317,MAET,INPUTS=SO    (ALT=X)

>    LOCATION=337,LGET,INPUTS=MAET,

>    LOCATION=320,MATT,INPUTS=AV    (MAC=X)

>    LOCATION=340,LGTT,INPUTS=MATT,

>    END OF MODEL



>  PRINT
```

17

Discussion of the Computer Model

The EASY computer source program for the closed loop F-106/Fire Fly gunsight system was presented above. This source program contains standard components of the EASY Model Generation Program intermixed with Fortran statements. A listing of the EASY standard component names used in this program and their description is presented in Table IV.

Table IV. EASY Standard Components (from Ref 12: 22-23)

Standard Component Name	Description
AF	Analytic Function Generator
AV	Aerodynamic Variables from States
EN	Engine Model
FU, FV	Tabular Function Generators, One Input, Two Inputs
IT	Integrator
LA	Lag Transfer Function (Time Constant Form)
LD	Lateral Aerodynamic Model
LE	Lead Lag Transfer Function (Pole-Zero Form)
LG	Lag Transfer Function (Pole Form)
LO	Longitudinal Aerodynamic Model
MA	Multiply and Add (2 inputs)
MC	Multiply and Add (4 inputs)
SA	Saturation Function
SD	Six Degree of Freedom Rigid Body Dynamics
TF	Transfer Function (First Order Numerator - Second Order Denominator)

In naming EASY standard components and the physical quantities associated with each component, the following character assignments are specified (Ref 12: 15):
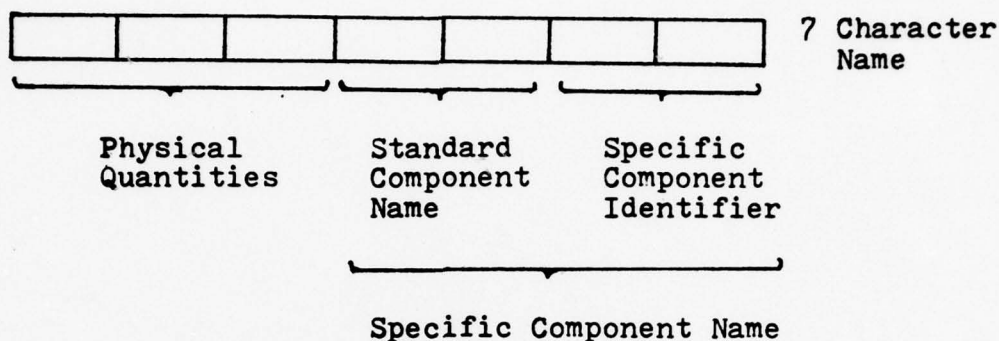
Thus, a lag transfer function in pole form, LG, could be identified simply as LG. If more than one lag transfer function is needed in the model, separate lag transfer functions would be identified using the character specific component identifier. Hence, LGET identifies a lag transfer function used for elevator trim, and LGRT identifies a lag used for rudder trim. The three character physical quantity name aids in making connections between components and in specifying parameter values. For example, ALTSD is the output state which identifies the aircraft altitude as computed in the six degree of freedom rigid body dynamics standard component. GAILAAX identifies the gain parameter for the lag transfer function in time constant form, LAAX.

The use of EASY standard components allows the programmer to model most of the basic aircraft equations and flight control system components simply by specifying input and output connections for the components and by specifying

the component parameters. The use of Fortran statements allows flexibility in the use of table look-up functions for aero-coefficients and in the specification of nonlinear stability derivatives.

The EASY model program used in the simulation is divided into sections as indicated by the numbers along the right hand side of the program listing. In Section One, the basic connections between the aerodynamic variables component (AV) and the engine model component (EN) are specified. The component FV is a two dimensional table look-up function which is used to determine a nominal thrust level as a function of altitude (ALTSD), and Mach number (MACAV). This nominal thrust value is multiplied (MA) by an incremental thrust value which is determined by the thrust trim component LGTT. The resulting required thrust level (THREN) is fed into the engine component (Ref 12: 117).

Section Two, written in Fortran, provides interpolation functions to determine the lift coefficients from tables of data. The general form of the table interpolation function can be found in Reference 12. Then the equation to determine the total lift coefficient, CL1, is specified.

In Section Three the drag coefficients are determined by interpolation and the total drag(CDO) is determined. Then the total longitudinal force equations (FZ EN and FX EN) are specified.

In Section Four, the pitching moment coefficients (C_{m_o}, C_{m_q}, C_{m_α}, and $C_{m_{\delta_E}}$) are determined by interpolation of tabular

118

values and the tank pitching derivatives ($C_{m_{o_T}}$ and $C_{m_{\alpha_T}}$) are added to the engine pitching moment to yield the total external moment TYEN. Next, the standard component for the longitudinal aerodynamic model (LO) is specified which determines the linear pitching moment equation. The aircraft neutral point (TNP) is found by interpolation and used in the equation for the total pitching moment TY2LO (Ref 12: 119).

In Section Five, the nonlinear side force derivatives ($C_{y_{\beta_T}}$, $C_{y_{\alpha_T}}$, $C_{y_{\beta_\alpha 2}}$, $C_{y_{\beta_\alpha}}$, and $C_{y_{\beta|\beta|}}$) are determined by interpolation and used to determine the nonlinear side force FY1LD. In Section Six, the nonlinear rolling moment derivatives ($C_{\ell_{\beta_T}}$, $C_{\ell_{\beta_\alpha 2}}$, $C_{\ell_{\beta_\alpha}}$, $C_{\ell_{\beta|\beta|}}$, $C_{\ell_{P_\alpha 2}}$, $C_{\ell_{P_\alpha}}$, and $C_{\ell_{R_\alpha}}$) are found by interpolation and used to determine the nonlinear rolling moment TX1LD.

Section Seven determines the nonlinear yawing moment derivatives ($C_{n_{\beta_T}}$, $C_{n_{\beta_\alpha 2}}$, $C_{n_{\beta_\alpha}}$, $C_{n_{\beta|\beta|}}$, ΔC_{n_β}, $C_{n_{\delta_A \alpha}}$, and $C_{n_{\delta_A \delta_E}}$) by interpolation and uses the values to determine the nonlinear yawing moment TZ1LD. In Section Eight, the linear lateral side force coefficients (C_{y_β}, C_{y_P}, C_{y_R}, $C_{y_{\delta_A}}$, and $C_{y_{\delta_R}}$), the linear rolling moment coefficients (C_{ℓ_P}, C_{ℓ_R}, C_{ℓ_β}, $C_{\ell_{\delta_A}}$, and $C_{\ell_{\delta_R}}$), and the linear yawing moment coefficients (C_{n_β}, $C_{n_{\delta_A}}$, $C_{n_{\delta_R}}$, C_{n_P}, and C_{n_R}) are determined by interpolation and then

the lateral directional aerodynamic model standard component
(LD) is specified. In Section Nine, the total rolling and
yawing moments TX2LD and TZ2LD are determined by adding the
moments due to the cg moment arms. Then, to complete the
basic aircraft model, the standard component SD is specified
to determine the equations of the six degree of freedom rigid
body dynamics.

Section 10 specifies the target acceleration and velocity
components in inertially-fixed coordinates $\overline{X}\overline{Y}\overline{Z}$. The AF
functions specify analytic equations for the acceleration
and velocity of the target. For the simulation, the target
maneuvers are constant speed, constant altitude, constant
rate turns. Thus, the target acceleration vector is given by

$$\overline{A}_t = -A \sin(\omega_t t) \overline{X} + A \cos(\omega_t t) \overline{Y} \tag{75}$$

where A is the magnitude of the target acceleration and ω_t
is the target turn rate. The fixed coordinate system $\overline{X}\overline{Y}\overline{Z}$
has its origin at the center of mass of the attacker and is
directed so that at time t = 0, $\overline{X}$ is out the nose of the
attacker, $\overline{Y}$ is out the right wing, and $\overline{Z}$ is determined by the
right hand rule.

Similarly, the target velocity vector is given by

$$\overline{V}_t = V \cos(\omega_t t) \overline{X} + V \sin(\omega_t t) \overline{Y} \tag{76}$$

where V is the magnitude of the target velocity.

The components AFAX, AFAY, and AFAZ are the $\bar{X}$, $\bar{Y}$, and $\bar{Z}$ components of the target acceleration vector. The components LAAX, LAAY, and LAAZ are simple lag transfer functions which simulate the time delay in the processing of target acceleration information by the Kalman filter in the Fire Fly system. The components AFVX, AFVY, and AFVZ are the $\bar{X}$, $\bar{Y}$, and $\bar{Z}$ components of the target velocity vector. The components of target acceleration and velocity are then renamed for convenience.

In Section 11, the components of the transformation matrix to transform between fixed coordinates $\bar{X}\bar{Y}\bar{Z}$ and aircraft body coordinates $\overline{uvw}$ are specified in terms of the Euler angles, YAW, PITC, and ROLL. The parameter RPD converts the Euler angles from degrees to radians. In Section 12, the attacker acceleration components are computed in body-fixed coordinates and transformed to fixed coordinates. The attacker velocity components in body-fixed coordinates are also transformed to fixed coordinates. Then the components of relative acceleration (ARX, ARY, and ARZ) and the components of relative velocity (VRX, VRY, and VRZ) are computed and transformed back to body axes.

In Section 13, the range rate (RADOT) is computed. The equation for RADOT is strictly valid only if the attacker and target velocity vectors are collinear. In the terminal phase of tracking considered here, the velocity vectors remain essentially collinear, and thus the given equation is used. The relative velocity components in fixed coordinates are

121

integrated and added to the initial range components (specified in MARX, MARY, and MARZ) to give the present range in fixed coordinates. The present range components are used to compute the present range magnitude and are then transformed to yield the present range components in body-fixed coordinates (RTU, RTV, and RTW).

Section 14 computes the bullet time-of-flight (TOF) and the range components required for a hit (RRV and RRW). The required range components are compared to the present range components to yield the elevation and traverse error signals to be fed to the pilot model.

Section 15 specifies the multi-axis pilot model in terms of EASY standard components. Figures 43 and 44 are block diagrams which show the connections of the longitudinal and lateral pilot models with the longitudinal and lateral flight control systems. In parentheses near each component are the EASY acronyms which represent each component in the model. The parameter values shown are the nominal values which were used in the simulation.

The standard components in Section 17 are used for trimming the aircraft at the beginning of each simulation run. After an initial trim condition is reached, the output states of the lag components for aileron trim (LGAT), rudder trim (LGRT), elevator trim (LGET), and thrust trim (LGTT) are held constant. These trim components are included in Figures 43 and 44 and are outlined by dashed lines.
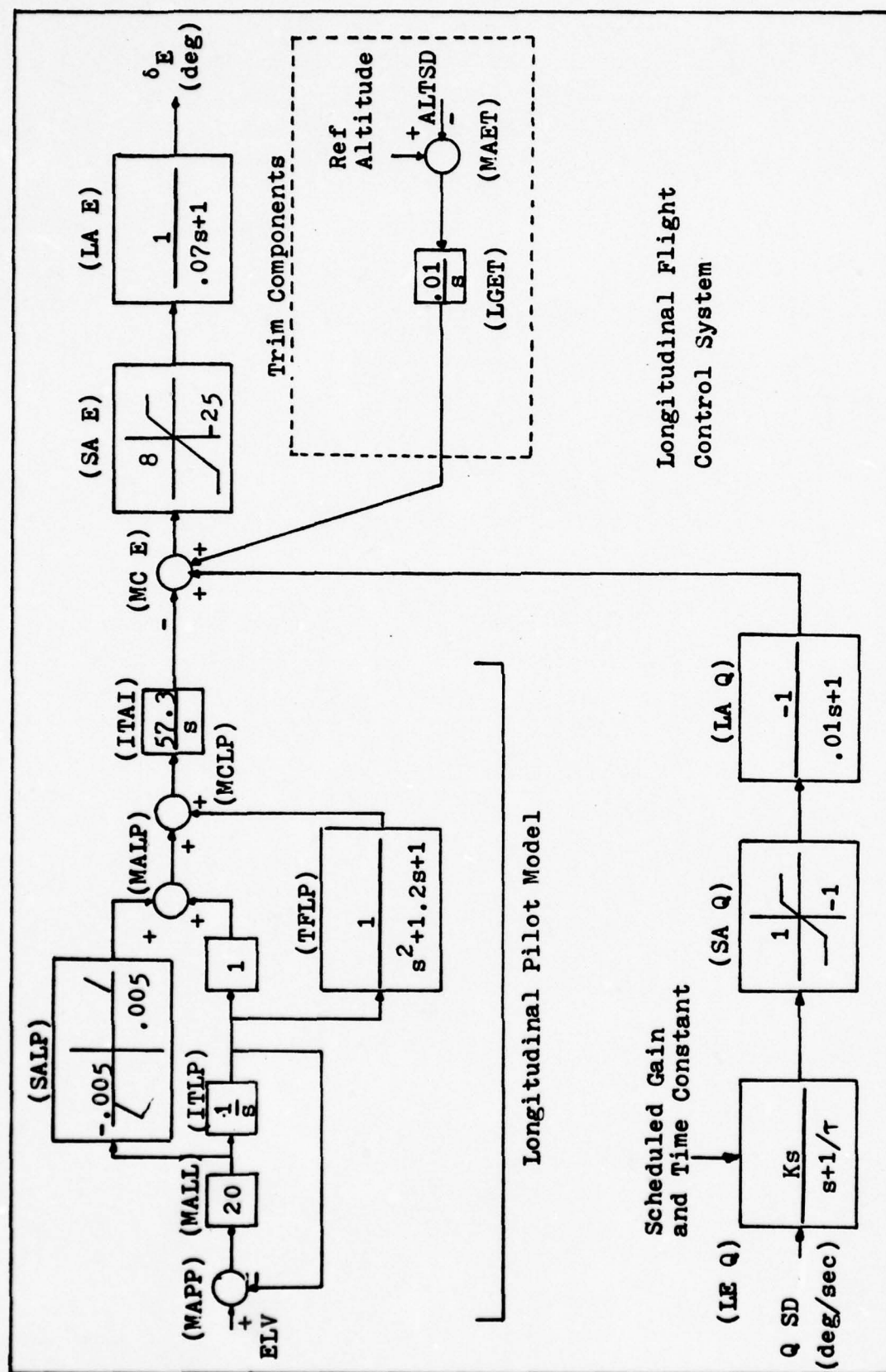
Figure 43. EASY Model - Longitudinal Pilot Model and Longitudinal Flight Control System.

123
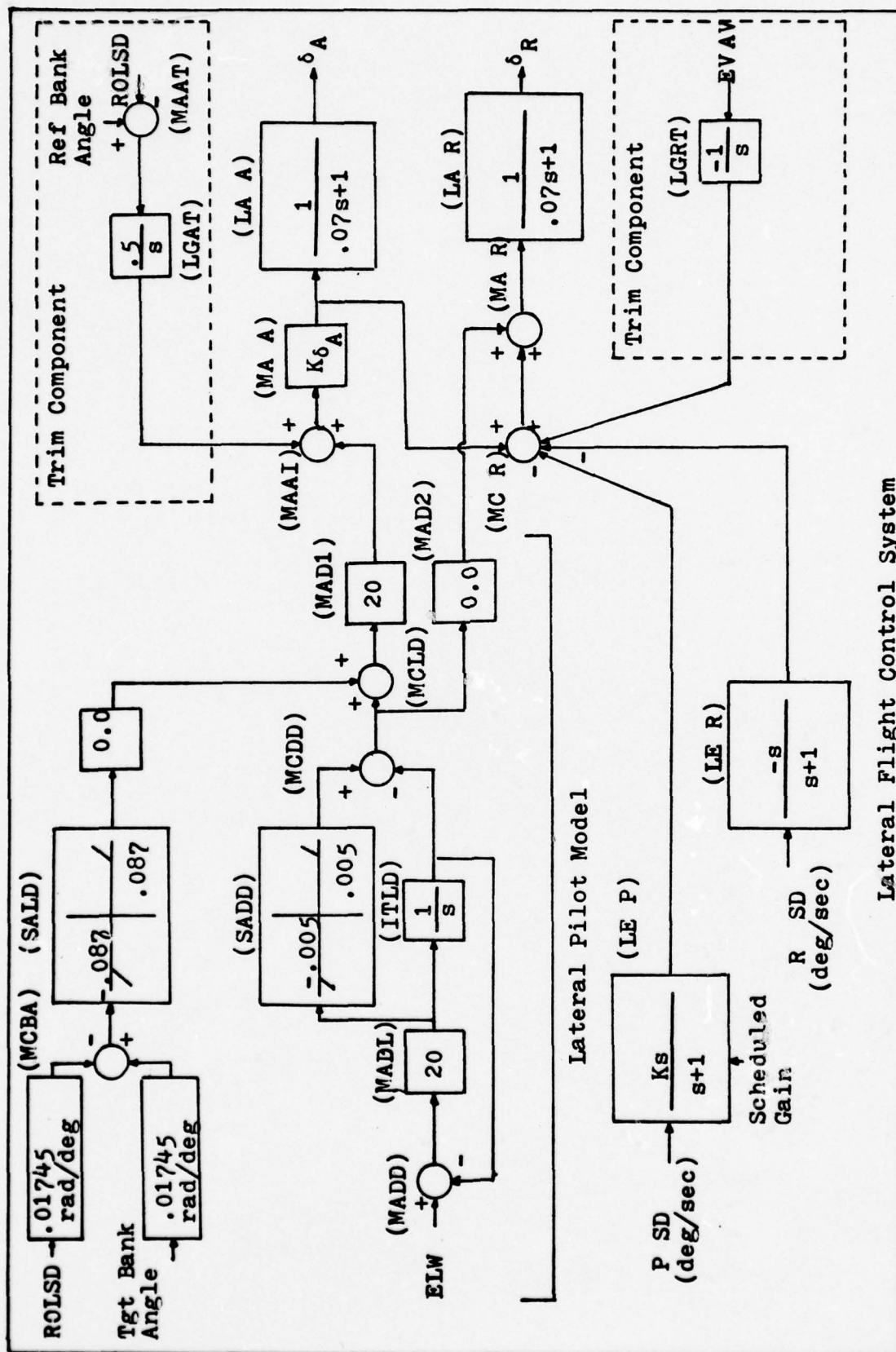
Figure 44. EASY Model - Lateral Pilot Model and Lateral Flight Control System.

Discussion of Simulation Techniques

This section presents some of the specific techniques used in the simulation program. For more complete information on the use of the EASY Analysis Program the reader is referred to References 12 and 15. Included in this section is an outline of the procedures used for a typical simulation run, and a discussion of some of the sensitive parameters in the model and how the parameter values can affect computer run costs.

A typical simulation run begins with the specification of all the parameter values and tables. Next, initial conditions are specified to define an operating point. Typically, these initial conditions include initial altitude, airspeed, and bank angle. Next, the steady state command is used to specify values of the states at the desired trim point. The operating point state values are then loaded into an initial condition vector for initializing a time simulation.

The computer simulation time is very sensitive to the arrangement of the model components. Derivative operations in the forward loop, such as in the pilot model, cause computer run time for a ten second real time simulation to be near 400 octal seconds. By eliminating the specific derivative operations, simulation computer run time is decreased by almost a factor of ten. In the model used for the simulations, the pilot model requires as inputs the derivatives of the tracking errors in elevation and traverse. Rather than trying to specifically take the derivatives of the errors,

125

simple lag feedback circuits were modeled and the error rates were picked off just ahead of the integrators. This concept is illustrated in Figures 43 and 44. Care must be exercised in the selection of the time constants used in the feedback circuits. These time constants (τ_E and τ_T) represent the pilot's lag in response to the observed elevation and traverse tracking errors. Making the values of τ_E and τ_T too small causes the same type of computer run time problems as discussed above. For example, a value of $\tau_E = \tau_T = .001$ results in simulation run times of about 350 octal seconds for a ten second real time simulation. Increasing the values to $\tau_E = \tau_T = 0.05$ results in a simulation run time of 45 octal seconds. Since the recommended range of values of τ_E and τ_T for the TAWDS pilot model is 0.0 to 0.05, increasing the values to 0.05 keeps the parameters within the recommended range.

Two other considerations for the use of the EASY programs are in order. First, the setting of error controls for the integrator states has an effect on the accuracy of results and also on the integration efficiency. The default value for error controls is 0.1, but this value is not appropriate for all the states. The values of the state outputs vary widely; for instance, the altitude state output might be 10,000 feet while the output of a control system state might be 0.1 degrees. A more appropriate integrator error control value is 0.1 percent of the estimated maximum value of the state. The second consideration is the type of integration routine to use. Three integration methods are available in

126

EASY: Fixed-Step Euler, Runga-Kutta, and Variable-Order Gear. For dynamic simulation of nonlinear systems, the Fixed Step Euler method is inappropriate because of computation errors. Runga-Kutta and Variable Order Gear can both be used. Runga-Kutta with a maximum step size of 0.2 seconds was used in the simulation because the Runga-Kutta method proved to be more efficient due to the nonlinearities in the model.

Appendix B. Parameter Values and Aerodynamic Data

Appendix B presents a listing of the constant parameters and tabular aerodynamic data used in the digital simulation. This data was provided by the Air Force Flight Dynamics Laboratory. The tabular data for the aerodynamic coefficients was obtained by curve fitting flight test data.

The weapon delivery constants are presented in the first section. The second section presents F-106B airframe constants. The third section presents the F-106B flight control system gain schedules. The remaining sections present the tabular data in essentially the same order that the data are used in the digital computer program. The EASY program acronyms for each table are listed in parentheses at the end of the table titles.

Weapon Delivery Constants

Bullet time-of-flight equation constants:

Ballistic Coefficient, k_o = 0.00625

Constants assumed to represent second order effects,

$$C_1 = 19.4$$
$$C_2 = 3341$$

Gun angle with respect to aircraft $\bar{u}$ axis,

$$E_{LG} = 2.5 \text{ degrees (depressed gun)}$$

Bullet Muzzle Velocity, V_m = 3350 ft/sec

F-106B Airframe Constants

Wing Reference Area, S = 695 sq ft

Wingspan, b = 38.13 ft

Mean Aerodynamic Chord, c = 23.755 ft

Aircraft Mass, m = 924.7 slugs

Moments of Inertia: I_x = 18,634 slug-ft^2

I_y = 177,858 slug-ft^2

I_z = 191,236 slug-ft^2

Product of Inertia: I_{xz} = 5539 slug-ft^2

Distance from aircraft cg to origin of the thrust vector:

In the $\bar{u}$ direction, x_o = -11.8 ft

In the $\bar{w}$ direction, z_o = 0

Tank Buttock Line, $(BL)_T$ = 9.37 ft

X_{cg} = -5.09 ft Y_{cg} = 0 Z_{cg} = -.76 ft

Y_{ref} = 0 Z_{ref} = -.83 ft

Flight Control System Gain Schedules

Table V. Pitch Rate Feedback Gain (K_q)

Air Density Ratio ρ/ρ_o	0	.05	.35	1
Gain K_q	-.4	-.4	-.2	-.1

Table VI. Pitch Damper Washout Circuit Time Constant (τ_q)

Air Density Ratio ρ/ρ_o	0	.07	.2	1
Time Constant τ_q	.5	.5	.25	.05

Table VII. Differential Elevon-to-Rudder Crossfeed Gain (K_{δ_A})

$\bar{q}$ (lb/ft^2)	0	100	150	200	300	400	500	600	800
Gain K_{δ_A}	3	3	1.25	.6	-.2	-.7	-1.1	-1.25	-1.5

Table VIII. Roll Rate Feedback Gain (K_P)

$\bar{q}$ (lb/ft^2)	0	100	150	200	300	400	500	600	800
Gain K_P	.2	.155	.13	.11	.08	.065	.05	.042	.033

Thrust Required

Table IX. Nominal Thrust Values (lb)

Mach No.	Altitude (ft)						
	5000	10000	15000	20000	25000	30000	35000
0.40	9500	8700	7768	6802	5836	5032	4390
0.88	10300	9350	8515	7565	6615	5742	4870
0.90	10400	9450	8584	7624	6664	5794	4924

Lift Coefficients

Table X. Lift Coefficient at $\alpha=0$, C_{L_o} (-CZO)

Mach No.	Altitude (ft)				
	0	15000	30000	45000	55000
0.20	-.0425	-.0425	-.0425	-.0425	-.0425
0.50	-.0485	-.0586	-.0487	-.0488	-.0490
0.80	-.0560	-.0573	-.0580	-.0584	-.0588
0.90	-.0600	-.0628	-.0654	-.0665	-.0669
1.00	-.0575	-.0637	-.0686	-.0719	-.0738
1.10	-.0380	-.0452	-.0510	-.0553	-.0570
1.20	-.0262	-.0324	-.0375	-.0414	-.0426
1.50	-.0139	-.0185	-.0221	-.0255	-.0269
1.80	-.0127	-.0166	-.0203	-.0230	-.0243
2.00	-.0127	-.0164	-.0196	-.0222	-.0235

Table XI. Lift Curve Slope, C_{L_α} (-CZA)

Mach No.	Altitude (ft)				
	0	15000	30000	45000	55000
0.20	2.500	2.500	2.500	2.500	2.500
0.50	2.560	2.565	2.570	2.575	2.580
0.80	2.720	2.759	2.780	2.798	2.802
0.90	2.860	2.930	2.970	3.000	3.018
1.00	3.079	3.195	3.290	3.385	3.420
1.10	2.910	3.040	3.170	3.270	3.310
1.20	2.680	2.800	2.940	3.040	3.095
1.50	2.145	2.260	2.370	2.480	2.525
1.80	1.800	1.892	1.989	2.081	2.125
2.00	1.625	1.695	1.800	1.865	1.912

Table XII. Lift Coefficient Due to Elevator Deflection, $C_{L_{\delta_E}}$ (-CZDE)

Mach No.	Altitude (ft)				
	0	15000	30000	45000	55000
0.20	.899	.892	.900	.884	.888
0.50	.830	.882	.903	.921	.929
0.80	.680	.792	.871	.923	.941
0.90	.536	.679	.799	.870	.897
1.00	.271	.488	.590	.715	.761
1.10	.200	.309	.431	.540	.598
1.20	.156	.240	.332	.421	.460
1.50	.080	.120	.179	.231	.262
1.80	.045	.069	.103	.149	.170
2.00	.034	.050	.082	.111	.130

Table XIII. Lift Coefficient at $\alpha=0$ Due to Tanks, $C_{L_{o_T}}$ (-CLOT)

Mach No.	0.20	0.50	0.80	0.90	1.0
$C_{L_{o_T}}$	.000463	.000289	.000054	.000144	.000226

Mach No.	1.1	1.2	1.5	1.8	2.0
$C_{L_{o_T}}$	.000235	.000224	.000210	.000194	.000183

Table XIV. Lift Curve Slope Due to Tanks, $C_{L_{\alpha_T}}$ (-CLAT)

Mach No.	0.20	0.50	0.80	0.90	1.0
$C_{L_{\alpha_T}}$	.000272	.000253	.000226	.000207	.000189

Mach No.	1.1	1.2	1.5	1.8	2.0
$C_{L_{\alpha_T}}$	.000180	.000185	.000180	.000180	.000180

Table XV. C_{D_1} (CDRAG2)

C_L	δ_E (deg)				
	-15	-10	-5	-2.5	0
-0.25	.0395	.0350	.0312	.0312	.0340
-0.20	.0355	.0300	.0254	.0254	.0271
-0.15	.0320	.0264	.0210	.0210	.0219
-0.10	.0292	.0237	.0176	.0176	.0177
-0.075	.0281	.0228	.0165	.0165	.0165
-0.05	.0272	.0219	.0157	.0154	.0154
-0.025	.0266	.0214	.0152	.0145	.0145
0.0	.0262	.0210	.0149	.0139	.0139
0.025	.0262	.0209	.0147	.0135	.0135
0.05	.0265	.0210	.0149	.0135	.0134
0.075	.0280	.0215	.0152	.0138	.0136
0.10	.0304	.0228	.0159	.0145	.0140
0.125	.0333	.0248	.0168	.0154	.0148
0.15	.0375	.0276	.0183	.0168	.0157
0.175	.0425	.0311	.0206	.0185	.0170
0.20	.0480	.0361	.0236	.0204	.0189
0.225	.0535	.0416	.0280	.0230	.0208
0.25	.0600	.0478	.0330	.0266	.0235
0.275	.0660	.0540	.0384	.0312	.0266
0.30	.0730	.0611	.0440	.0368	.0305
0.35	.0874	.0762	.0565	.0485	.0410
0.40	.1028	.0925	.0706	.0614	.0535
0.45	.1185	.1037	.0854	.0760	.0684
0.50	.1340	.1256	.1003	.0906	.0840

Table XVI. C_{D_2} (Mach ≥ 0.9), (CDRAG3)

C_L	δ_E (deg)				
	-15	-10	-5	-2.5	0
-0.25	.0466	.0400	.0339	.0329	.0348
-0.20	.0421	.0350	.0285	.0270	.0280
-0.15	.0339	.0305	.0240	.0221	.0226
-0.10	.0354	.0272	.0205	.0185	.0185
-0.075	.0340	.0259	.0193	.0171	.0171
-0.05	.0331	.0250	.0181	.0159	.0159
-0.025	.0324	.0242	.0167	.0154	.0154
0.0	.0324	.0238	.0165	.0149	.0149
0.025	.0326	.0238	.0166	.0147	.0144
0.05	.0334	.0242	.0167	.0149	.0144
0.075	.0350	.0248	.0172	.0151	.0145
0.10	.0428	.0303	.0205	.0175	.0166
0.125	.0466	.0336	.0227	.0189	.0178
0.15	.0517	.0383	.0255	.0210	.0194
0.175	.0580	.0430	.0289	.0238	.0214
0.20	.0635	.0482	.0336	.0275	.0237
0.225	.0703	.0536	.0383	.0316	.0267
0.25	.0762	.0600	.0438	.0365	.0303
0.275	.0903	.0731	.0556	.0476	.0404
0.30	.1050	.0880	.0685	.0607	.0516
0.35	.1192	.1035	.0830	.0755	.0656
0.40	.1331	.1188	.0980	.0910	.0806
0.45	.1331	.1188	.0980	.0910	.0806
0.50	.1331	.1188	.0980	.0910	.0806

Table XVII. C_{D_2} (Mach < 0.9), (CDRAG1)

δ_E (deg)

C_L	-15	-10	-5	-2.5	0
-0.25	.0323	.0294	.0263	.0275	.0335
-0.20	.0285	.0254	.0223	.0234	.0264
-0.15	.0254	.0216	.0189	.0196	.0212
-0.10	.0230	.0191	.0160	.0167	.0175
-0.075	.0220	.0182	.0149	.0156	.0162
-0.05	.0215	.0175	.0139	.0145	.0150
-0.025	.0212	.0172	.0134	.0139	.0140
0.0	.0210	.0171	.0130	.0134	.0134
0.025	.0212	.0171	.0128	.0132	.0132
0.05	.0216	.0174	.0132	.0132	.0132
0.075	.0231	.0181	.0136	.0136	.0136
0.10	.0250	.0191	.0147	.0141	.0141
0.125	.0276	.0213	.0160	.0151	.0151
0.15	.0319	.0241	.0174	.0162	.0161
0.175	.0368	.0294	.0191	.0176	.0174
0.20	.0425	.0334	.0215	.0194	.0184
0.225	.0485	.0393	.0250	.0214	.0209
0.25	.0550	.0454	.0296	.0245	.0234
0.275	.0613	.0520	.0354	.0290	.0264
0.30	.0682	.0590	.0416	.0345	.0302
0.35	.0825	.0735	.0549	.0466	.0402
0.40	.0977	.0890	.0700	.0615	.0529
0.45	.1130	.1045	.0862	.0785	.0677
0.50	.1234	.1196	.1040	.0975	.0852

Pitching Moment Coefficients

Table XVIII. Pitching Moment Coefficient for $\alpha=0$, C_{m_o} (CMO)

Mach No.	Altitude (ft)				
	0	15000	30000	45000	55000
0.20	.00410	.00410	.00410	.00410	.00410
0.50	.00487	.00483	.00487	.00492	.00496
0.80	.00632	.00636	.00640	.00644	.00648
0.90	.00802	.00820	.00835	.00840	.00845
1.00	.00972	.01055	.01099	.01131	.01162
1.10	.01088	.01181	.01251	.01295	.01316
1.20	.00805	.00908	.00955	.00990	.01009
1.50	.00245	.00302	.00359	.00390	.00161
1.80	.00028	.00079	.00121	.00149	.00161
2.00	-.00091	-.00045	-.00005	.00019	.00042

Table XIX. Pitch Moment Due to Pitch Rate, C_{m_q} (CMQ)

Mach No.	Altitude (ft)				
	0	15000	30000	45000	55000
0.20	-.8100	-.8800	-.9000	-.9300	-.9600
0.50	-.5600	-.6600	-.7000	-.7300	-.7500
0.80	-.5400	-.7100	-.8000	-.8600	-.8800
0.90	-.5900	-.8200	-.9200	-1.000	-1.030
1.00	-.4900	-.6800	-.7500	-.8400	-.8900
1.10	-.3500	-.4900	-.5900	-.6200	-.6400
1.20	-.3600	-.5000	-.5900	-.6400	-.6700
1.50	-.2900	-.4100	-.4800	-.5300	-.5400
1.80	-.2600	-.3800	-.4300	-.4700	-.4800
2.00	-.2600	-.3800	-.4200	-.4500	-.4700

137

Table XX. Pitch Moment Due to Elevator Deflection $C_{m_{\delta_E}}$ (CMDE)

	Altitude (ft)				
Mach No.	0	15000	30000	45000	55000
0.20	-.3350	-.3300	-.3370	-.3320	-.3322
0.50	-.3224	-.3375	-.3425	-.3475	-.3482
0.80	-.3019	-.3225	-.3500	-.3600	-.3650
0.90	.02785	-.3150	-.3400	-.3625	-.3700
1.00	-.2287	-.2837	-.3285	-.3607	-.3770
1.10	-.1725	-.2137	-.2512	-.2800	-.2950
1.20	-.1362	-.1650	-.1950	-.2212	-.2312
1.50	-.0758	-.0950	-.1137	-.1300	-.1375
1.80	-.0475	-.0600	-.0750	-.0875	-.0938
2.00	-.0362	-.0456	-.0555	-.0675	-.0745

Table XXI. Pitch Moment at $\alpha=0$ Due to Tanks $C_{m_{o_T}}$ (CMOT)

Mach No.	0.20	0.50	0.80	0.90	1.0
$C_{m_{o_T}}$	-.001142	-.001151	-.001169	-.001151	-.000941

Mach No.	1.0	1.2	1.5	1.8	2.0
$C_{m_{o_T}}$	-.000987	-.001042	-.001094	-.001096	-.001096

Table XXII. Pitch Moment Curve Slope Due to Tanks $C_{m_{\alpha_T}}$ (CMAT)

Mach No.	0.20	0.50	0.80	0.90	1.0
$C_{m_{\alpha_T}}$	.000158	.000159	.000159	.000159	.000160

Mach No.	1.0	1.2	1.5	1.8	2.0
$C_{m_{\alpha_T}}$	.000160	.000159	.000161	.000165	.000166

Table XXIII. Aircraft Neutral Point, N.P. (TNP)

Mach No.	Altitude (ft)				
	0	15000	30000	45000	55000
0.20	-.351	-.351	-.351	-.351	-.351
0.50	-.354	-.354	-.354	-.354	-.354
0.80	-.363	-.365	-.367	-.369	-.369
0.90	-.377	-.382	-.386	-.388	-.389
1.00	-.409	-.420	-.427	-.434	-.436
1.10	-.430	-.442	-.451	-.460	-.462
1.20	-.440	-.453	-.463	-.470	-.474
1.50	-.444	-.456	-.466	-.475	-.479
1.80	-.435	-.446	-.457	-.465	-.469
2.00	-.426	-.439	-.450	-.458	-.462

Nonlinear Side Force Coefficients

Table XXIV. Effect of Tanks on C_{y_β}, $C_{y_{\beta_T}}$ (CYBT)

Mach No.	0.20	0.50	0.80	0.90	1.0
$C_{y_{\beta_T}}$	-.00164	-.00156	-.00155	-.00183	-.00211

Mach No.	1.1	1.2	1.5	1.8	2.0
$C_{y_{\beta_T}}$	-.00216	-.00212	-.00198	-.00185	-.00180

Table XXV. Effect of Tanks on C_{y_α}, $C_{y_{\alpha_T}}$ (CYAT)

Mach No.	0.20	0.50	0.80	0.90	1.0
$C_{y_{\alpha_T}}$	.001103	.001021	.000994	.001111	.001473

Mach No.	1.1	1.2	1.5	1.8	2.0
$C_{y_{\alpha_T}}$	.001600	.001609	.001545	.001491	.001446

Table XXVI. Second Order Effect of α on C_{y_β}, $C_{y_{\beta_\alpha}2}$ (CYBA2)

Mach No.	Altitude (ft)				
	0	15000	30000	45000	55000
0.20	-.000018	-.000018	-.000018	-.000018	-.000018
0.50	-.000105	-.000105	-.000105	-.000105	-.000105
0.80	-.000197	-.000197	-.000197	-.000197	-.000197
0.90	-.000265	-.000265	-.000265	-.000265	-.000265
1.00	-.000235	-.000235	-.000235	-.000235	-.000235
1.10	-.000103	-.000103	-.000103	-.000103	-.000103
1.20	-.000036	-.000036	-.000036	-.000036	-.000036
1.50	-.000320	-.000330	-.000334	-.000341	-.000337
1.80	-.000382	-.000438	-.000461	-.000467	-.000463
2.00	-.000295	-.000378	-.000418	-.000431	-.000429

Table XXVII. Second Order Effect of β on C_{y_β}, $C_{y_{\beta|\beta|}}$ (CYBB)

Mach No.	Altitude (ft)				
	0	15000	30000	45000	55000
0.20	-.00483	-.00483	-.00483	-.00483	-.00483
0.50	-.00881	-.00881	-.00881	-.00881	-.00881
0.80	-.01400	-.01420	-.01426	-.01432	-.01438
0.90	-.01559	-.01569	-.01579	-.01589	-.01599
1.00	-.01409	-.01420	-.01441	-.01460	-.01478
1.10	-.01138	-.01171	-.01206	-.01220	-.01234
1.20	-.00939	-.00963	-.00975	-.00987	-.00999
1.50	-.00505	-.00509	-.00512	-.00516	-.00519
1.80	-.00197	-.00191	-.00185	-.00177	-.00171
2.00	-.00075	-.00063	-.00050	-.00038	-.00025

<u>Table</u> <u>XXVIII</u>. <u>Effect</u> <u>of</u> α <u>on</u> C_{y_β}, $C_{y_{\beta_\alpha}}$ (<u>CYBA</u>)

Mach No.	0.20	0.50	0.80	0.90	1.0
$C_{y_{\beta_\alpha}}$	.0051	.0086	.0142	.0174	.0198
Mach No.	1.1	1.2	1.5	1.8	2.0
$C_{y_{\beta_\alpha}}$	.0198	.0182	.0126	.0084	.0074

<u>Nonlinear</u> <u>Rolling</u> <u>Moment</u> <u>Coefficients</u>

<u>Table</u> <u>XXIX</u>. <u>Effect</u> <u>of</u> <u>Tanks</u> <u>on</u> C_{ℓ_β}, $C_{\ell_{\beta_T}}$ (<u>CLBT</u>)

Mach No.	0.20	0.50	0.80	0.90	1.0
$C_{\ell_{\beta_T}}$	.000101	.000097	.000096	.000113	.000131
Mach No.	1.1	1.2	1.5	1.8	2.0
$C_{\ell_{\beta_T}}$	.000134	.000131	.000122	.000114	.000111

<u>Table</u> <u>XXX</u>. <u>Second</u> <u>Order</u> <u>Effect</u> <u>of</u> α <u>on</u> C_{ℓ_β}, $C_{\ell_{\beta_{\alpha^2}}}$ (<u>CLBA2</u>)

| Mach No. | Altitude (ft) | | | | |
	0	15000	30000	45000	55000
0.20	.000156	.000156	.000156	.000156	.000156
0.50	.000152	.000153	.000153	.000154	.000154
0.80	.000144	.000145	.000146	.000147	.000148
0.90	.000113	.000115	.000117	.000119	.000121
1.00	.000089	.000092	.000094	.000096	.000096
1.10	.000138	.000142	.000146	.000150	.000154
1.20	.000180	.000188	.000196	.000201	.000204
1.50	.000226	.000227	.000227	.000227	.000228
1.80	.000235	.000216	.000201	.000190	.000186
2.00	.000204	.000176	.000153	.000138	.000129

Table XXXI. Effect of α on C_{ℓ_β}, $C_{\ell_{\beta_\alpha}}$ (CLBA)

Mach No.	Altitude (ft)				
	0	15000	30000	45000	55000
0.20	-.00859	-.00859	-.00859	-.00859	-.00859
0.50	-.00870	-.00872	-.00874	-.00877	-.00879
0.80	-.00871	-.00882	-.00890	-.00900	-.00909
0.90	-.00858	-.00877	-.00892	-.00901	-.00911
1.00	-.00800	-.00832	-.00861	-.00878	-.00889
1.10	-.00695	-.00726	-.00755	-.00777	-.00786
1.20	-.00582	-.00611	-.00638	-.00656	-.00669
1.50	-.00322	-.00340	-.00357	-.00369	-.00379
1.80	-.00085	-.00098	-.00102	-.00107	-.00111
2.00	-.00041	.00044	.00047	.00050	.00052

Table XXXII. Second Order Effect of β on C_{ℓ_β}, $C_{\ell_{\beta|\beta|}}$ (CLBB)

Mach No.	Altitude (ft)				
	0	15000	30000	45000	55000
0.20	-.00078	-.00078	-.00078	-.00078	-.00078
0.50	-.00143	-.00143	-.00144	-.00144	-.00144
0.80	-.00219	-.00222	-.00224	-.00225	-.00225
0.90	-.00231	-.00236	-.00239	-.00242	-.00243
1.00	-.00199	-.00204	-.00210	-.00215	-.00216
1.10	-.00152	-.00161	-.00165	-.00170	-.00172
1.20	-.00113	-.00119	-.00123	-.00127	-.00129
1.50	-.00021	-.00022	-.00023	-.00024	-.00024
1.80	.00041	.00043	.00044	.00045	.00047
2.00	.00060	.00064	.00067	.00069	.00070

Table XXXIII. Second Order Effect of α on C_{ℓ_p}, $C_{\ell_{p_\alpha 2}}$ (CLPA2)

Altitude (ft)

Mach No.	0	15000	30000	45000	55000
0.20	.000285	.000286	.000287	.000288	.000289
0.50	.000300	.000307	.000310	.000312	.000315
0.80	.000337	.000359	.000373	.000382	.000387
0.90	.000397	.000430	.000457	.000459	.000478
1.00	.000584	.000644	.000696	.000740	.000758
1.10	.000513	.000576	.000633	.000677	.000697
1.20	.000430	.000486	.000536	.000577	.000597
1.50	.000257	.000295	.000330	.000360	.000374
1.80	.000173	.000199	.000227	.000248	.000260
2.00	.000137	.000161	.000187	.000204	.000212

Table XXXIV. Effect of α on C_{ℓ_p}, $C_{\ell_{p_\alpha}}$ (CLPA)

Altitude (ft)

Mach No.	0	15000	30000	45000	55000
0.20	-.00174	-.00176	-.00176	-.00176	-.00176
0.50	-.00176	-.00179	-.00183	-.00184	-.00185
0.80	-.00184	-.00195	-.00204	-.00209	-.00212
0.90	-.00200	-.00216	-.00229	-.00238	-.00242
1.00	-.00246	-.00272	-.00294	-.00311	-.00318
1.10	-.00227	-.00252	-.00278	-.00296	-.00306
1.20	-.00202	-.00228	-.00253	-.00273	-.00281
1.50	-.00149	-.00172	-.00194	-.00211	-.00219
1.80	-.00117	-.00136	-.00155	-.00171	-.00178
2.00	-.00102	-.00119	-.00137	-.00151	-.00158

Table XXXV. Effect of α on C_{ℓ_R}, $C_{\ell_{R_\alpha}}$ (CLRA)

Mach No.	Altitude (ft)				
	0	15000	30000	45000	55000
0.20	.01455	.01459	.01464	.01467	.01470
0.50	.01480	.01510	.01540	.01550	.01560
0.80	.01615	.01706	.01775	.01820	.01835
0.90	.02058	.02230	.02310	.02410	.02485
1.00	.02135	.02326	.02520	.02670	.02730
1.10	.01429	.01588	.01780	.01892	.01944
1.20	.01100	.01238	.01370	.01482	.01558
1.50	.00755	.00865	.00970	.01056	.01097
1.80	.00609	.00708	.00802	.00881	.00920
2.00	.00548	.00640	.00730	.00808	.00843

Nonlinear Yawing Moment Coefficients

Table XXXVI. Effect of Tanks on C_{n_β}, $C_{n_{\beta_T}}$ (CNBT)

Mach No.	0.20	0.50	0.80	0.90	1.0
$C_{n_{\beta_T}}$	-.000300	-.000282	-.000264	-.000219	-.000180

Mach No.	1.1	1.2	1.5	1.8	2.0
$C_{n_{\beta_T}}$	-.000140	-.000115	-.000077	-.000084	-.000086

Table XXXVII. Second Order Effect of α on C_{n_β}, $C_{n_{\beta_{\alpha^2}}}$ (CNBAA)

Mach No.	Altitude (ft)				
	0	15000	30000	45000	55000
0.20	-.000056	-.000056	-.000056	-.000056	-.000056
0.50	-.000066	-.000066	-.000066	-.000066	-.000066
0.80	-.000115	-.000114	-.000113	-.000112	-.000111
0.90	-.000147	-.000146	-.000145	-.000144	-.000143
1.00	-.000137	-.000137	-.000137	-.000137	-.000137
1.10	-.000058	-.000058	-.000058	-.000058	-.000058
1.20	-.000016	-.000016	-.000016	-.000016	-.000016
1.50	-.000242	-.000242	-.000242	-.000242	-.000234
1.80	-.000380	-.000380	-.000377	-.000377	-.000375
2.00	-.000435	-.000399	-.000385	-.000380	-.000385

Table XXXVIII. Second Order Effect of β on C_{n_β}, $C_{n_{\beta|\beta|}}$ (CNBB)

Mach No.	Altitude (ft)				
	0	15000	30000	45000	55000
0.20	.00235	.00235	.00235	.00235	.00235
0.50	.00420	.00422	.00425	.00427	.00430
0.80	.00650	.00656	.00659	.00662	.00665
0.90	.00665	.00670	.00680	.00685	.00690
1.00	.00580	.00590	.00605	.00617	.00621
1.10	.00420	.00430	.00440	.00445	.00450
1.20	.00260	.00267	.00274	.00282	.00290
1.50	-.00130	-.00128	-.00125	-.00122	-.00120
1.80	-.00370	-.00375	-.00380	-.00385	-.00390
2.00	-.00460	-.00465	-.00470	-.00475	-.00480

Table XXXIX. Effect of α on C_{n_β}, $C_{n_{\beta_\alpha}}$ (CNBA)

Mach No.	0.20	0.50	0.80	0.90	1.0
$C_{n_{\beta_\alpha}}$	-.00303	-.00259	-.00195	-.00165	-.00310
Mach No.	1.1	1.2	1.5	1.8	2.0
$C_{n_{\beta_\alpha}}$	-.00293	-.00311	-.00318	-.00267	-.00239

Table XL. Effect of α on $C_{n_{\delta_A}}$, $C_{n_{\delta_A}\alpha}$ (CNDAA)

Mach No.	0.20	0.50	0.80	0.90	1.0
$C_{n_{\delta_A}\alpha}$	.00074	.00053	-.00017	-.00029	.00094
Mach No.	1.1	1.2	1.5	1.8	2.0
$C_{n_{\delta_A}\alpha}$	.00179	.00250	.00241	.00144	.00108

Table XLI. Effect of δ_E on $C_{n_{\delta_A}}$, $C_{n_{\delta_A}\delta_E}$ (CNDADE)

Mach No.	0.20	0.50	0.80	0.90	1.0
$C_{n_{\delta_A}\delta_E}$	.00149	.00165	.00200	.00236	.00394
Mach No.	1.1	1.2	1.5	1.8	2.0
$C_{n_{\delta_A}\delta_E}$	.00358	.00294	.00204	.00147	.00120

Linear Lateral Coefficients

Table XLII. C_{y_β} (CYB)

Altitude (ft)

Mach No.	0	15000	30000	45000	55000
0.20	-.6060	-.6060	-.6060	-.6060	-.6060
0.50	-.6286	-.6294	-.6303	-.6312	-.6320
0.80	-.6445	-.6494	-.6510	-.6529	-.6548
0.90	-.6600	-.6672	-.6729	-.6765	-.6780
1.00	-.6461	-.6590	-.6700	-.6780	-.6819
1.10	-.6320	-.6500	-.6659	-.6760	-.6812
1.20	-.6188	-.6390	-.6562	-.6675	-.6729
1.50	-.5920	-.6118	-.6286	-.6420	-.6471
1.80	-.5680	-.5865	-.6034	-.6150	-.6206
2.00	-.5550	-.5719	-.5840	-.6000	-.6058

Table XLIII. C_{y_P} (CYP)

Altitude (ft)

Mach No.	0	15000	30000	45000	55000
0.20	-.00770	-.00775	-.00612	-.00625	-.00637
0.50	-.00475	-.00550	-.00600	-.00625	-.00637
0.80	-.00087	-.00325	-.00475	-.00600	-.00625
0.90	.00225	-.00150	-.00400	-.00575	-.00625
1.00	.00900	.00300	-.00150	-.00475	-.00600
1.10	.01375	.00575	.00015	-.00400	-.00550
1.20	.01570	.00745	.00120	-.00325	-.00500
1.50	.01850	.00950	.00225	-.00250	-.00475
1.80	.02010	.01070	.00325	-.00175	-.00400
2.00	.02070	.01110	.00350	-.00137	-.00375

Table XLIV. C_{y_R} (CYR)

Altitude (ft)

Mach No.	0	15000	30000	45000	55000
0.20	.8960	.8960	.8960	.8960	.8960
0.50	.9150	.9160	.9170	.9190	.9200
0.80	.9490	.9560	.9610	.9640	.9650
0.90	.9660	.9650	.9740	.9800	.9830
1.00	.7650	.7920	.8050	.8140	.8230
1.10	.7250	.7480	.7670	.7800	.7860
1.20	.7560	.7800	.8000	.8170	.8250
1.50	.6820	.7050	.7280	.7460	.7540
1.80	.5950	.6140	.6320	.6470	.6540
2.00	.5540	.5710	.5880	.6020	.6090

Table XLV. $C_{y_{\delta A}}$ (CYDA)

Altitude (ft)

Mach No.	0	15000	30000	45000	55000
0.20	.2040	.2050	.2060	.2070	.2080
0.50	.2220	.2280	.2320	.2330	.2330
0.80	.2200	.2440	.2590	.2640	.2680
0.90	.1960	.2320	.2630	.2760	.2840
1.00	.1360	.2020	.2530	.2830	.3030
1.10	.1020	.1650	.2240	.2580	.2810
1.20	.0600	.1240	.1740	.2060	.2280
1.50	.0140	.0380	.0580	.0690	.0760
1.80	.0070	.0180	.0300	.0350	.0390
2.00	.0070	.0160	.0260	.0310	.0340

Table XLVI. $C_{y_{\delta_R}}$ (CYDR)

Altitude (ft)

Mach No.	0	15000	30000	45000	55000
0.20	.1148	.1148	.1150	.1150	.1150
0.50	.1063	.1100	.1120	.1131	.1140
0.80	.0896	.0987	.1046	.1080	.1098
0.90	.0743	.0852	.0930	.0973	.0996
1.00	.0449	.0572	.0681	.0745	.0782
1.10	.0317	.0419	.0515	.0588	.0607
1.20	.0250	.0340	.0420	.0480	.0508
1.50	.0149	.0218	.0279	.0330	.0345
1.80	.0100	.0159	.0211	.0256	.0279
2.00	.0081	.0140	.0193	.0238	.0254

Table XLVII. C_{ℓ_P} (CLP)

Altitude (ft)

Mach No.	0	15000	30000	45000	55000
0.20	-.1650	-.1670	-.1666	-.1670	-.1670
0.50	-.1638	-.1670	-.1700	-.1711	-.1720
0.80	-.1601	-.1693	-.1762	-.1809	-.1826
0.90	-.1616	-.1630	-.1830	-.1900	-.1929
1.00	-.1670	-.1834	-.1975	-.2088	-.2139
1.10	-.1599	-.1781	-.1954	-.2082	-.2140
1.50	-.1403	-.1612	-.1802	-.1957	-.2030
1.80	-.1299	-.1505	-.1700	-.1862	-.1939
2.00	-.1234	-.1438	-.1639	-.1801	-.1875

Table XLVIII. C_{ℓ_R} (CLR)

Altitude (ft)

Mach No.	0	15000	30000	45000	55000
0.20	.1384	.1384	.1384	.1384	.1384
0.50	.1333	.1333	.1333	.1333	.1333
0.80	.1172	.1177	.1178	.1179	.1180
0.90	.1119	.1123	.1123	.1124	.1125
1.00	.0885	.0893	.0901	.0909	.0917
1.10	.1112	.1159	.1198	.1224	.1234
1.20	.1084	.1126	.1163	.1194	.1203
1.50	.0933	.0965	.0995	.1014	.1022
1.80	.0832	.0862	.0884	.0901	.0908
2.00	.0795	.0822	.0845	.0851	.0877

Table XLIX. C_{ℓ_β} (CLB)

Altitude (ft)

Mach No.	0	15000	30000	45000	55000
0.20	-.0280	-.0280	-.0280	-.0280	-.0280
0.50	-.0279	-.0278	-.0276	-.0275	-.0274
0.80	-.0202	-.0196	-.0187	-.0183	-.0180
0.90	-.0188	-.0178	-.0156	-.0165	-.0160
1.00	-.0291	-.0284	-.0279	-.0272	-.0266
1.10	-.0524	-.0544	-.0559	-.0571	-.0580
1.20	-.0588	-.0618	-.0645	-.0656	-.0663
1.50	-.0562	-.0583	-.0610	-.0624	-.0632
1.80	-.0483	-.0507	-.0528	-.0539	-.0542
2.00	-.0404	-.0425	-.0444	-.0450.	-.0454

Table L. $C_{\ell_{\delta_A}}$ (CLDA)

Altitude (ft)

Mach No.	0	15000	30000	45000	55000
0.20	-.1140	-.1180	-.1200	-.1200	-.1200
0.50	-.1080	-.1160	-.1200	-.1230	-.1250
0.80	-.0830	-.0980	-.1120	-.1200	-.1250
0.90	-.0590	-.0810	-.0980	-.1080	-.1140
1.00	-.0190	-.0400	-.0600	-.0740	-.0830
1.10	-.0090	-.0230	-.0390	-.0530	-.0620
1.20	-.0070	-.0190	-.0320	-.0440	-.0510
1.50	-.0040	-.0120	-.0230	-.0330	-.0390
1.80	-.0010	-.0080	-.0160	-.0240	-.0290
2.00	-.0010	-.0050	-.0120	-.0180	-.0220

Table LI. $C_{\ell_{\delta_R}}$ (CLDR)

Altitude (ft)

Mach No.	0	15000	30000	45000	55000
0.20	.0209	.0209	.0209	.0206	.0206
0.50	.0190	.0197	.0202	.0206	.0208
0.80	.0156	.0175	.0188	.0196	.0200
0.90	.0125	.0148	.0165	.0175	.0179
1.00	.0066	.0094	.0116	.0133	.0140
1.10	.0046	.0068	.0089	.0102	.0109
1.20	.0034	.0054	.0072	.0086	.0091
1.50	.0018	.0032	.0046	.0056	.0062
1.80	.0009	.0022	.0034	.0046	.0049
2.00	.0006	.0019	.0030	.0040	.0045

Table LII. C_{n_β} (CNB)

	Altitude (ft)				
Mach No.	0	15000	30000	45000	55000
0.20	.1090	.1090	.1090	.1090	.1090
0.50	.1148	.1151	.1154	.1157	.1160
0.80	.1210	.1235	.1250	.1264	.1270
0.90	.1237	.1268	.1299	.1324	.1325
1.00	.1408	.1477	.1538	.1570	.1590
1.10	.1490	.1580	.1660	.1720	.1740
1.20	.1428	.1526	.1617	.1685	.1704
1.50	.1164	.1262	.1350	.1405	.1437
1.80	.0949	.1036	.1112	.1173	.1200
2.00	.0834	.0915	.0994	.1049	.1074

Table LIII. $C_{n_{\delta_A}}$ (CNDA)

	Altitude (ft)				
Mach No.	0	15000	30000	45000	55000
0.20	-.0720	-.0720	-.0730	-.0730	-.0730
0.50	-.0730	-.0750	-.0760	-.0770	-.0780
0.80	-.0760	-.0830	-.0880	-.0900	-.0920
0.90	-.0710	-.0870	-.0970	-.1020	-.1050
1.00	-.0560	-.0850	-.1100	-.1240	-.1340
1.10	-.0400	-.0730	-.0990	-.1150	-.1260
1.20	-.0280	-.0540	-.0780	-.0920	-.1020
1.50	-.0070	-.0170	-.0250	-.0320	-.0360
1.80	-.0030	-.0090	-.0140	-.0170	-.0190
2.00	-.0040	-.0080	-.0120	-.0140	-.0160

Table LIV. $C_{n_{\delta_R}}$ (CNDR)

Altitude (ft)

Mach No.	0	15000	30000	45000	55000
0.20	-.0570	-.0570	-.0570	-.0570	-.0570
0.50	-.0535	-.0550	-.0560	-.0565	-.0570
0.80	-.0463	-.0505	-.0534	-.0552	-.0556
0.90	-.0405	-.0457	-.0495	-.0517	-.0527
1.00	-.0278	-.0347	-.0400	-.0436	-.0453
1.10	-.0203	-.0259	-.0307	-.0346	-.0359
1.20	-.0160	-.0210	-.0250	-.0288	-.0298
1.50	-.0100	-.0137	-.0171	-.0196	-.0209
1.80	-.0076	-.0104	-.0134	-.0158	-.0170
2.00	-.0063	-.0091	-.0120	-.0145	-.0155

Table LV. C_{n_P} (CNP)

Altitude (ft)

Mach No.	0	15000	30000	45000	55000
0.20	.0073	.0073	.0073	.0074	.0074
0.50	.0068	.0070	.0073	.0075	.0075
0.80	.0055	.0066	.0074	.0079	.0081
0.90	.0045	.0063	.0076	.0082	.0086
1.00	.0021	.0052	.0075	.0091	.0096
1.10	.0004	.0041	.0071	.0090	.0098
1.20	-.0006	.0034	.0066	.0088	.0097
1.50	-.0019	.0024	.0058	.0082	.0092
1.80	-.0028	.0016	.0051	.0075	.0085
2.00	-.0032	.0012	.0046	.0071	.0082

Table LVI. C_{n_R} (CNR)

Altitude (ft)

Mach No.	0	15000	30000	45000	55000
0.20	-.378	-.378	-.378	-.378	-.378
0.50	-.400	-.402	-.402	-.403	-.403
0.80	-.430	-.433	-.436	-.438	-.439
0.90	-.443	-.448	-.453	-.456	-.458
1.00	-.374	-.384	-.392	-.395	-.398
1.10	-.356	-.367	-.377	-.383	-.387
1.20	-.369	-.382	-.394	-.402	-.406
1.50	-.338	-.349	-.361	-.368	-.372
1.80	-.299	-.309	-.318	-.324	-.328
2.00	-.281	-.290	-.297	-.304	-.307

VITA

David Lee Frostman was born on 30 April 1949 in Superior, Wisconsin. He graduated from high school in Superior, Wisconsin in 1967 and attended the United States Air Force Academy from which he received the degree of Bachelor of Science in Electrical Engineering in June 1971. Upon graduation, he received his commission in the USAF and entered pilot training at Laughlin AFB, Texas. After receiving his wings in July 1972, he served as a KC-135 pilot in the 46th Air Refueling Squadron, K.I. Sawyer AFB, Michigan. In May 1976 he received the degree of Master of Science in Business Administration from Michigan Technological University. He entered the School of Engineering, Air Force Institute of Technology, in June 1976.

> Permanent address: 1522 East Third Street
> Superior, Wisconsin   54880

SECURITY CLASSIFICATION OF THIS PAGE *(When Data Entered)*

REPORT DOCUMENTATION PAGE	READ INSTRUCTIONS BEFORE COMPLETING FORM

1. REPORT NUMBER AFIT/GGC/EE/77-5	2. GOVT ACCESSION NO.	3. RECIPIENT'S CATALOG NUMBER

4. TITLE *(and Subtitle)* AN INVESTIGATION OF THE TRACKING PERFORMANCE OF THE FIRE FLY MANUAL DIRECTOR GUNSIGHT FOR AIR-TO-AIR GUNNERY.	5. TYPE OF REPORT & PERIOD COVERED MS Thesis
	6. PERFORMING ORG. REPORT NUMBER

7. AUTHOR(s) David L. Frostman	8. CONTRACT OR GRANT NUMBER(s)

9. PERFORMING ORGANIZATION NAME AND ADDRESS Air Force Institute of Technology (AFIT-EN) Wright-Patterson AFB, Ohio 45433	10. PROGRAM ELEMENT, PROJECT, TASK AREA & WORK UNIT NUMBERS

11. CONTROLLING OFFICE NAME AND ADDRESS Air Force Flight Dynamics Lab/FGL Wright-Patterson AFB OH 45433	12. REPORT DATE December 1977
	13. NUMBER OF PAGES 177

14. MONITORING AGENCY NAME & ADDRESS(if different from Controlling Office)	15. SECURITY CLASS. *(of this report)* Unclassified
	15a. DECLASSIFICATION/DOWNGRADING SCHEDULE

16. DISTRIBUTION STATEMENT *(of this Report)*

Approved for public release; distribution unlimited

17. DISTRIBUTION STATEMENT *(of the abstract entered in Block 20, if different from Report)*

18. SUPPLEMENTARY NOTES

Approved for public release; IAW AFR 190-17

JERRAL F. GUESS, Captain, USAF
Director of Information

19. KEY WORDS *(Continue on reverse side if necessary and identify by block number)*

Air-to-Air Gunnery
Pilot Modeling
Fire Control Systems

20. ABSTRACT *(Continue on reverse side if necessary and identify by block number)*

The tracking performance of the Fire Fly manual director gunsight is evaluated during the terminal phase of air-to-air gunnery using the F-106 aircraft as the test bed. A digital simulation of the closed loop tracking task is performed using the EASY Dynamic Analysis programs developed by Boeing Computer Services, Inc. The multi-axis pilot model, developed for the Terminal Aerial Weapon Delivery Simulation (TAWDS) program by

DD FORM 1473 EDITION OF 1 NOV 65 IS OBSOLETE
1 JAN 73

SECURITY CLASSIFICATION OF THIS PAGE *(When Data Entered)*

McDonnell Aircraft Company, is adapted for use in the F-106/Fire Fly gunsight simulation. A set of nominal pilot model parameter values, determined by root locus analysis, is used in simulating the tracking performance of the Fire Fly gunsight against targets in constant altitude, constant airspeed, constant rate turns at bank angles of 30,60, and 70 degrees. The tracking error responses are found to have characteristics similar to those observed in the tracking responses obtained from man-in-the-loop simulation studies conducted by McDonnell Aircraft Company. The dependence of the tracking error responses on the pilot model parameter values is demonstrated by simulation runs in which several pilot model parameter values are varied.